Cranfield University

Farahnaz Ansari

The Use of Magnetic Nanoparticles to Enhance Biodesulfurization

School of Applied Sciences
Microsystems & Nanotechnology Centre

PhD

Cranfield University

School of Applied Science
Microsystems & Nanotechnology Centre

PhD THESIS

2008

Farahnaz Ansari

The Use of Magnetic Nanoparticles to Enhance Biodesulfurization

Supervisor: Prof. J.J. Ramsden

Academic Year 2005 to 2008

This thesis is submitted in partial fulfilment of the requirements for the degree of PhD

(NB. This section can be removed if the award of the degree is based solely on examination of the thesis)

The Use of Magnetic Nanoparticles to Enhance Biodesulfurization

ABSTRACT

Biodesulfurization (BDS) is an alternative to hydrodesulfurization (HDS) as a method to remove sulfur from crude oil. Dibenzothiophene (DBT) was chosen as a model compound for the forms of thiophenic sulfur found in fossil fuels; up to 70% of the sulfur in petroleum is found as DBT and substituted DBTs; these compounds are however particularly recalcitrant to hydrodesulfurization, the current standard industrial method. My thesis deals with enhancing BDS through novel strains and through nanotechnology. Chapter highlights are:

Chapter 2. My first aim was to isolate novel aerobic, mesophilic bacteria that can grow in mineral media at neutral pH value with DBT as the sole sulfur source. Different natural sites in Iran were sampled and I enriched, isolated and purified such bacteria. Twenty four isolates were obtained that could utilize sulfur compounds. Five of them were shown to convert DBT into HBP. After preliminary characterization, the five isolates were sent to the Durmishidze Institute of Biotechnology in Tbilisi for help with strain identification. Two isolates (F2 and F4) were identified as *Pseudomonas* strains, F1 was a *Flavobacterium* and F3 belonged to the strain of *Rhodococcus*. The definite identification of isolate F5 was not successful but with high probability it was a known

strain. Since no new strains were apparently discovered, I did not work further in this direction.

Chapter 3. In a second approach I studied the desulfurization ability of *Shewanella putrefaciens* strain NCIMB 8768, because in a previous investigation carried out at Cranfield University, it had been found that it reduced sulfur odour in clay. I compared its biodesulfurization activity profile with that of the widely studied *Rhodococcus erythropolis* strain IGTS8. However, *S. putrefaciens* was not as good as *R. erythropolis*.

Chapter 4 and 5. I then turned to nanotechnology, which as a revolutionary new technological platform offers hope to solve many problems. There is currently a trend toward the increasing use of nanotechnology in industry because of its potentially revolutionary paths to innovation. I then asked how nanotechnology can contribute to enhancing the presently poor efficiency of biodesulfurization. Perhaps the most problematic difficulty is how to separate the microorganisms at the end of the desulfurization process. To make BDS more amenable, I explored the use of nanotechnology to magnetize biodesulfurizing bacteria. In other words, to render desulfurizing bacteria magnetic, I made them magnetic by decorating their outer surfaces with magnetic nanoparticles, allowing them to be separated using an external magnet. I used the best known desulfurizing bacterial strain, *Rhodococcus erythropolis* IGTS8.

The decoration and magnetic separation worked very well. Unexpectedly, I found that the decorated cells had a 56% higher desulfurization activity compared to the nondecorated cells. I proposed that this is due to permeabilization of the bacterial membrane, facilitating the entry and exit of reactant and product respectively. Supporting evidence for enhanced permeabilization was obtained by Dr Pavel Grigoriev, Institute of Cell Biophysics, Russian Academy of Sciences, Pushchino.

In **Chapter 6,** to optimize attachment of the nanoparticles to the surface of the bacteria I created thin magnetic nanofilms from the nanoparticles and measured the attachment of the bacteria using a uniquely powerful noninvasive optical technique (Optical Waveguide Lightmode Spectroscopy, OWLS) to quantify the attachment and determine how the liquid medium and other factors influence the process.

Keywords:

Biodesulfurization; Dibenzothiophene; Shewanella putrefaciens; biodesulfurization; dibenzothiophene; Rhodococcus erythropolis; magnetic Fe_3O_4; *nanoparticles, black lipid membrane; optical waveguide lightmode spectroscopy; monolayer; polyethylene glycol; adsorption.*

ACKNOWLEDGEMENTS

I am deeply indebted to my supervisor, Professor Jeremy Ramsden for his support and his encouragement and assistance throughout the research and in the preparation of this thesis. Sincere thanks to Dr Pavel Grigoriev from Institute of Cell Biophysics, the Russian Academy of Sciences in Pushchino, Dr Mimi Hill from the University of Liverpool, Dr George Kvesitadze from the Durmishidze Institute of Biochemistry and Biotechnology, Tbilisi and Dr Robert Horvath for their assistance in the analytical section and their helpful advice and comments during the work. I am also grateful to Dr Robert Wright, Jane Hubble, Matthew Kershaw and Christine Kimpton for their help with technical issues over the course of my work. I would also like to thank all of my friends and colleagues at Cranfield from the bottom of my heart for making my time at Cranfield much brighter, especially all the Ramsden group members whose interest overlapped with mine, Amir, Mohammad, Julie, Yun-Peng, James and Gergely.

Heartfelt indebtedness belongs to my husband Masoud who have always been patient, understanding and supportive. Finally, thanks to my daughters, Newsha and Mojan, for their loving tolerance of a mother who is at the same time a research student.

TABLE OF CONTENTS

Chapter 6 : A novel assay for optimizing nanoparticle-bacterium interactions 124

LIST OF SCHEMES

TABLE OF FIGURES

TABLE OF TABLES

LIST OF PUBLICATIONS

Journals:

- **Ansari, F.,** Grigoriev, P. A., Libor, S., Tothill, I. and Ramsden, J.J. DBT degradation enhancement by decorating *Rhodococcus erythropolis* IGST8 with magnetic Fe_3O_4 nanoparticles. *Biotechnology Bioengineering,* Vol. 102, No. 5: 1505–1512 (2009).

- **Ansari, F.,** Kavosh, M., Horvath, R. and Ramsden, J.J. Kinetics of PEG-Fe_3O_4 hybrid nanoparticles self-assembled on Si(Ti)O_2. *Langmuir,* Submitted (2009).

- **Ansari, F**., Kavosh**,** M. Horvath, R., and Ramsden, J.J. Kinetics of bacterial adsorption onto thin Fe_3O_4 nanofilms. *Nanoletter,* Submitted (2009).

- **Ansari, F**., Kavosh**,** M. Horvath, R., and Ramsden, J.J. Tuning the charge of magnetic Fe3)4 nanoparticles on the kinetics of adsorption. In preparation (2009).

- **Ansai, F**., Libor, S. and Ramsden, J.J., Fabrication and characterization of magnetic Fe_3O_4 nanoparticles. *Cranfield University publication*, in press (2008).

- **Ansari, F**., Prayuenyong, P. and Tothill, I. Biodesulfurization of dibenzothiophene by *Shewanella putrefaciens* NCIMB 8768. *Journal of Biological Physics and Chemistry*, Vol. 7, 75–78 (2007).

- **Ansari, F.** and Parivar, K. Effect of electromagnetic fields on serum proteins, liver and spleen tissue of female Balb/c mice. *Journal of Science of Tehran University*, 28, 167-181 (2002).

- **Ansari, F.,** Parivar, K. and Golestanian, N. Effect of Electromagnetic Fields on Cells. *Iranian Biomedical Journal*, 4, 138-139 (2000).

Conferences:

- **Ansari, F**., Aref, A., Libor, S., Horvath, R. and Ramsden' J.J. Adsorption kinetics of bacteria onto a thin Fe_3O_4 magnetic nanofilm. (Oral) *11th Annual Nanotechnology Conference and Trade Show, Boston, Massachusetts*, U.S.A., June 1-5 (2008). http://www.nsti.org/Nanotech2008/showabstract.html?absno=140

- Aref, A., Horvath, R., **Ansari, F.** and Ramsden, J. J. Attachment and spreading of human embryonal carcinoma stem cells on nanosurfaces using optical waveguides. (Oral) *11th Annual Nanotechnology Conference and Trade Show*, *Boston, Massachusetts*, U.S.A., June 1-5 (2008). http://www.nsti.org/Nanotech2008/showabstract.html?absno=141

- **Ansari, F.,** Horvath, R., Aref, A. and Ramsden, J.J. Fabrication of a thin Fe_3O_4 magnetic nanofilm on silica titania for bioapplications. (Oral) *7th International Conference on the Scientific and Clinical Applications of Magnetic Carriers University of British Columbia (UBC)*, Vancouver, Canada, May 20-24, 2008. http://www.magneticmicrosphere.com/meetings/meet2008/MagMeet2008_posters.pdf

- **Ansari, F.**, Libore, S. and Ramsden, J.J. Fabrication and characterization of magnetic Fe_3O_4 nanoparticles. (Oral) *Cranfield Multi-Strand Conference: Wealth Through Research and Innovation (CMC)*, England, May 6-7 (2008).

- **Ansari, F.** and Ramsden, J.J. Biodesulfurization / Biodegradation. *Research Poster Conference of Cranfield University*, 28th June, UK (2007).

- **Ansari, F.,** Yeh, Y. P., and Ramsden, J. J. Biodesulfurization by coated bacteria with Fe_3O_4 nanoparticles. *The 9th annual meeting, Design Surfaces to Direct Cell Behaviour*, 13-14 Sep., Manchester, England (2007).

SYMBOLS & ABBREVIATIONS

AFM	Atomic Force Microscopy
API	American Petroleum Institute
Atm. Pres.	= 101325 Pa. = 101.325 KPa. = 0.1 MPa
ATCC	American Type Culture Collection
BDS	Biodesulfurization
BP	Boiling Point (°C)
BT	Benzothiophene
CFU	Colony Forming Unit
C_x-DBT	Alkyl DBT
DBT	Dibenzothiophene
DBT-Mo	DBT monooxygenase
DBTO	Dibenzothiophene sulfoxide
$DBTO_2$	Dibenzothiophene sulfone
$DBTO_2$-Mo	DBT sulfone monooxygenase
$DBTSO_3$	DBT sulfonate
ELM	Ellipsometry
EPA	Environmental Protection Agency
FCC	Fluid Catalytic Cracking
FMN	Flavin mono nucleotide
$FMNH_2$	Reduced flavin mononucleotide
FTIR	Fourier transform infrared spectroscopy
GC	Gas Chromatography
GC/MS	Gas Chromatography/Mass Spectroscopy
HBP	Hydroxybiphenyl
HBPS	2- (2- hydroxybiphenyl) benzenesulfinate
HDS	Hydrodesulfurization
HPLC	High Pressure Liquid Chromatography
IR	Infrared
IRMS	Isotopic Ratio Mass Spectrometry
LCO	Light Cycle Oil

mL	millilitre (approx. 1 cubic centimetre, 1 cm^3)
MNP, MNPs	Magnetic nanoparticle, Magnetic nanoparticles
M	Molar = moles per litre
MPa	Megapascal = 10^6 Pascal
MW	Molecular weight ($g\ mol^{-1}$)
NADH	Nicotinamide adenine dinucleotide
NNI	National Nanotechnology Institute
NP, NPs	Nanoparticle, Nanoparticles
OWLS	Optical Waveguide Lightmode Spectroscopy
$PASH_2$	Polyaromatic sulfur heterocycles
PBS	2- phenylbenzene sulfinate
ppm	Parts per million
QCM	Quartz crystal microbalance
RI	Refractive index
rpm	revolutions per minute
SEM	Scanning Electron Microscopy
SFC	Supercritical Fluid Chromatography
SMNP	Superparamagnetic nanoparticle
SO_x	Sulfur Oxides
SPR	Surface Plasmon Resonance
SRB	Sulfate Reducing Bacteria
T	Thiophene
TEM	Transmission Electron Microscopy
TLC	Thin Layer Chromatography
UV	Ultra violet
Vol %	Volume percent
w/v	Weight per volume (e.g. grams per millilitre)
Wt %	Weight percent
XRD	X-Ray Diffraction
χ	Magnetic susceptibility; it indicates how responsive a material is to an applied magnetic field.

Chapter 1 : Introduction and literature review

1.1 The need for enhancement of biodesulfurization

Clean fuels research including desulfurization has become an important subject of environmental catalysis studies worldwide. Sulfur content in diesel fuel is an environmental concern because sulfur is converted to (sulfur oxides) SO_x during combustion, which not only contributes to acid rain, but also poisons the catalytic converter for exhaust emission treatment. The problem of sulfur removal has become more apparent due to the increasing high sulfur contents in remaining reservoirs of crude oils and the low limit of sulfur content required in finished fuel products by regulations specified by the authorities. It is impossible to have clean atmospheric air, or in particular to reduce air pollution from the transport sector, without removing sulfur from fuels. No significant air pollution reduction strategy can work successfully without reducing sulfur to near-zero level. The Environmental Protection Agency of the United States (EPA) has set a target to reduce the sulfur content of diesel from 500 ppm (2006 regulation) to 15 ppm for the year 2012 (EPA 2005) .

Hydrodesulfurization (HDS) involves the catalytic reaction of hydrogen and the organic matter in the feed, at pressures ranging from 5 up to 10 MPa and temperatures between 300 and 350 °C, depending on the oil fraction and the required level of desulfurization (Gary et al., 2001; Shafi et al., 2000). Due to the high costs and inherent chemical limitations associated with HDS, alternatives for this technology are of great interest to the petroleum industry. The benefits of sulfur reduction would be more important than the costs, even though required refinery investments continue to be significant. The U.S.

EPA found human health benefits and environmental profits due to sulfur reduction ten times higher than the costs (Blumberg et al., 2003). Furthermore, a European study showed that ultralow sulfur fuels significantly reduce total fuel costs by increasing fuel economy—from which the considerable potential for greenhouse gas emission reductions adds further payback to the health, environmental, and social benefits of sulfur reduction.

The global refining industry has spent about $37 billion on new desulfurization equipment and an additional $10 billion on annual operating expenditures for sulfur removal through the last 10 years to meet the new sulfur regulations. More than 70 million barrels of crude are worldwide produced each day, of which half is considered to be "high sulfur" (>1%). This concern will become more serious owing to the decreasing availability of low-sulfur fuels (Monticello, 1998).

So in many areas of the world industry needs new technologies to reduce sulfur to the ultralow levels now acceptable in use. Current costs might be reasonable; the refining industry continues to develop more active catalysts and novel processes for the removal of sulfur in order to reduce costs even more.

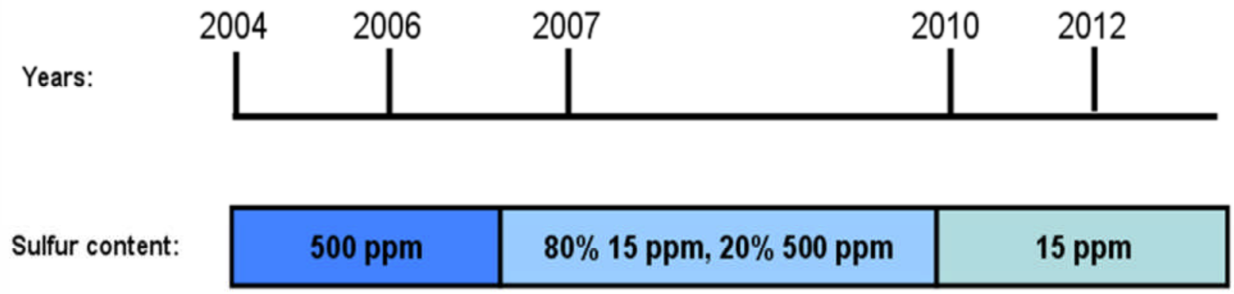

Figure 1.1: Evolution of permissible sulfur content of diesel fuel (Keaveney 2008).

1.2 Sulfur

Sulfur has been used in small quantities for thousands of years and known as brimstone, "the stone that burns". By 2000 before Christ, the Egyptians began using sulfur in linen textile bleaching. The Greeks used burning sulfur and pitch in order to produce suffocating gases. The Romans combined brimstone with tar, pitch, and other combustible materials in order to produce the first incendiary weapons. Sulfur is a necessary ingredient in gunpowder, which was developed in China in the 10th century. Introduction of gunpowder into Europe led to its use in warfare in the 14th century and made sulfur an important mineral product (Wilburn et al., 2005).

Sulfur is nearly ubiquitous in fossil fuels, where it arises both as inorganic (e.g., elemental sulfur, hydrogen sulfide and pyrites) and as organic sulfur (e.g., sulfur atom or moiety present in a wide variety of hydrocarbon molecules, including for example, mercaptans, disulfides, sulfones, thiols, thioethers, thiophenes, and other more complex forms) that can account for near to 100% of the total sulfur content of petroleum liquids, such as crude oil and many petroleum distillate fractions. Crude oils can typically range from close to about 5 wt % down to about 0.1 wt % organic sulfur (Monticello, 1995).
The presence of sulfur in oil has been related to the corrosion of pipeline, pumping, and refining equipment, and with premature breakdown of combustion engines. Sulfur also contaminates many catalysts which are used in the refining and combustion of fossil fuels. Burning of gasoline and diesel emits sulfur dioxide (SO_2) or sulfate particulate matter leading to acid rain, which has harmful effects on aquatic and forest ecosystems, as well as on agricultural areas (Monticello, 1998).

Any reduction in fuel sulfur straightaway reduces these sulfur compounds and leads to benefits including reduction in total pollutant emissions. There were several reasons why this reduction became attractive:

(i) Hydrogen sulfide is an odorous and toxic substance for which incidental human contact should be limited;

(ii) Hydrogen sulfide, if left during the refining operation, causes corrosion and produces foul smelling products;

(iii) The general increase in gasoline consumption increases the need for lower sulfur levels in the final product in order to keep pollution at an acceptable level.

1.2.1 Sulfur compounds in oil

The sulfur content and types of sulfur compounds vary significantly within a crude supply. With the increase of density in the crude oil, sulfur levels and the difficulty of sulfur removal also tend to increase. Generally, refineries are built to process either premium priced “sweet” (with lower sulfur content), or “sour” (with higher sulfur content) crude oil. While refiners gain some advantage in using higher quality crude, the price premium more than cancels the cost advantage for low-sulfur fuel refining (Blumberg et al., 2003).

Since there are many different sulfur-containing compounds in petroleum-derived fuels, the sulfur content is usually expressed as the weight percent (wt%) of sulfur in the fuel and ranges from 0.03 wt% to values as high as 8 wt% (demonstrated on 78 different crude oil types (Rall et al., 1972). As mentioned before, the most important constituents are organic sulfur compounds, but inorganic sulfur can also be present. An overview of the range of organic sulfur contents in crude oils found in different countries over the world is given in Figure 1.2.

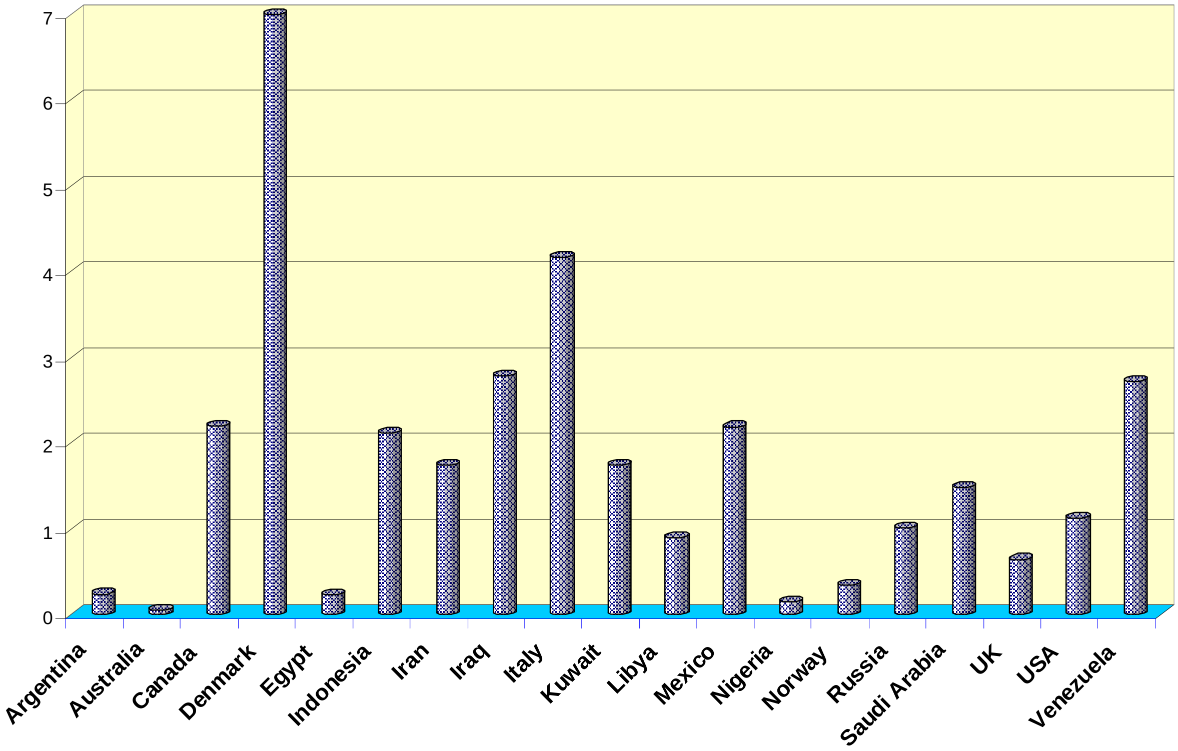

Figure 1.2: Average organic sulfur contents in crude oils (Marcelis, 2003).

Sulfur compounds in crude oil include thiols, sulfides, polysulfides, thiophenic and alkyl-substituted isomers of thiophenic compounds containing a variety of aromatic rings (i. e. polycyclic aromatic sulfur heterocycles such as thiophene, benzothiophene, dibenzothiophene, and benzonaphthothiophene) which are carcinogenic (Monot et al., 2002). The molecular structures of some of these sulfur components are presented in Scheme 1.1.

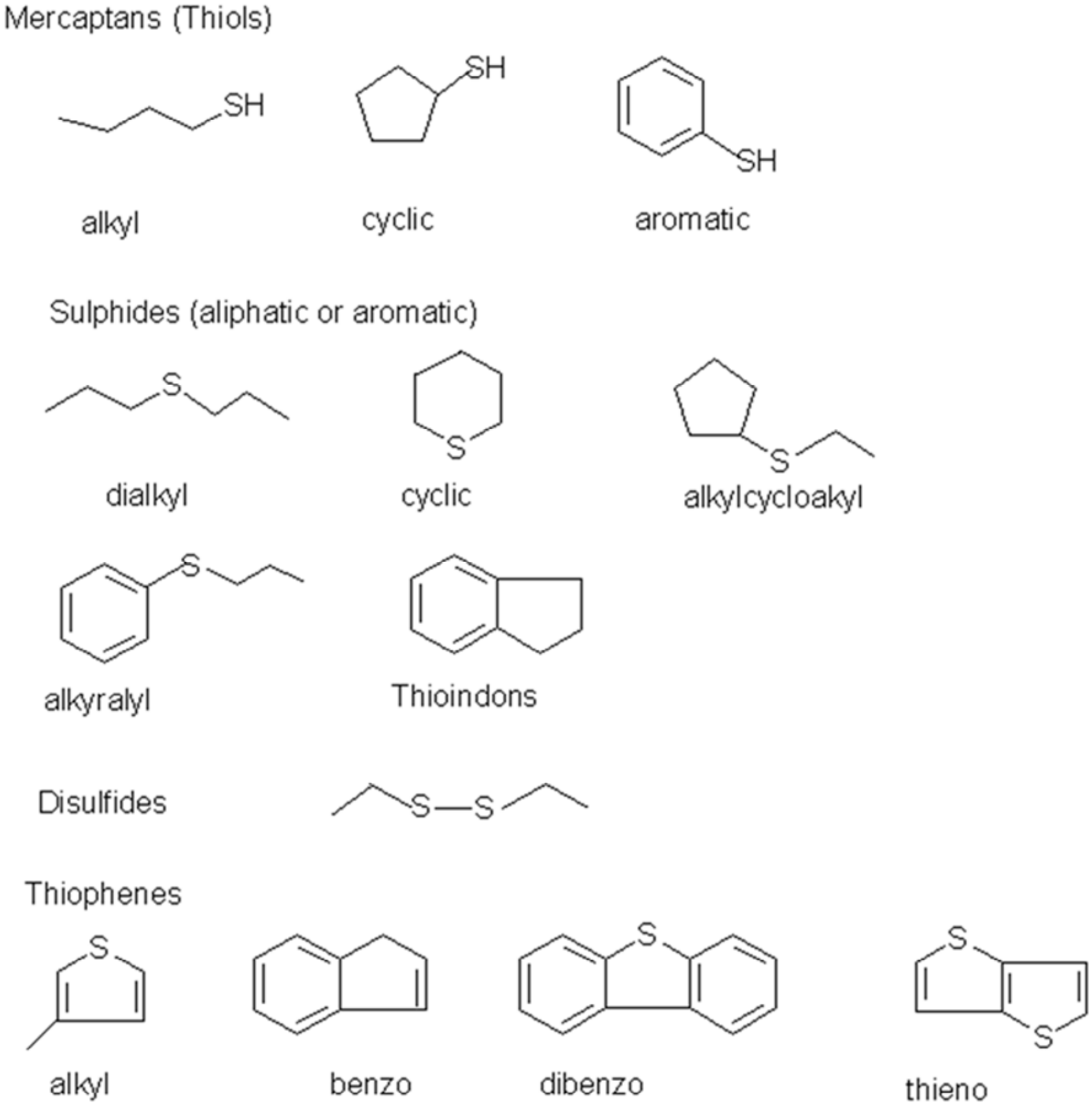

Scheme 1.1: Types of sulfur-containing organic compound identified in crude oils

The distribution and amount of organic sulfur compounds reflect the reservoir and maturity of the oil. Chemically immature oils are rich in sulfur and often have a high content of non-thiophenic sulfur compounds (Schulz et al., 1999). Mercaptans in crude oils are generally of low molecular weight (less than eight carbon atoms). They are readily removed from crude oil during refinery processing and are negligible in petroleum products. Aliphatic sulfides (cyclic or acyclic) are major components of the sulfur-containing fraction of petroleum products, e.g. diesel fuels and heating oils. Aromatic sulfides are of lower concentration in the heavier cuts. Thiophenic sulfur is normally the most plentiful form but as mentioned before, depending on the reservoir history of the oil, other sulfur compounds are often present in appreciable quantities. The unsaturated five member heterocyclic ring, thiophenes, is an important constituent of high-sulfur oils and its derivatives are the most abundant sulfur compound in distillates and residues, including heavy fuel oils and bitumens.

1.3 Hydrodesulfurization processes

The ability of refiners to reduce the sulfur levels depends on a number of factors: the refinery organization and amount of excess desulfurization equipment on hand, the sulfur level in the fuels currently produced, the quality of crude oil being used, and the quality and types of products being produced.

Hydrodesulfurization (HDS) is a physico-chemical technology based on a reductive chemical change to remove organic-bound sulfur to specified levels. The removal of sulfur present in gas/oil is conventionally performed by hydrotreatment with co-current flow of hydrogen gas and hydrocarbon over a catalyst bed. Although many different hydrotreater designs are in use, they all work according to the same principle. Figure 1.3 presents a typical process layout of this technique.

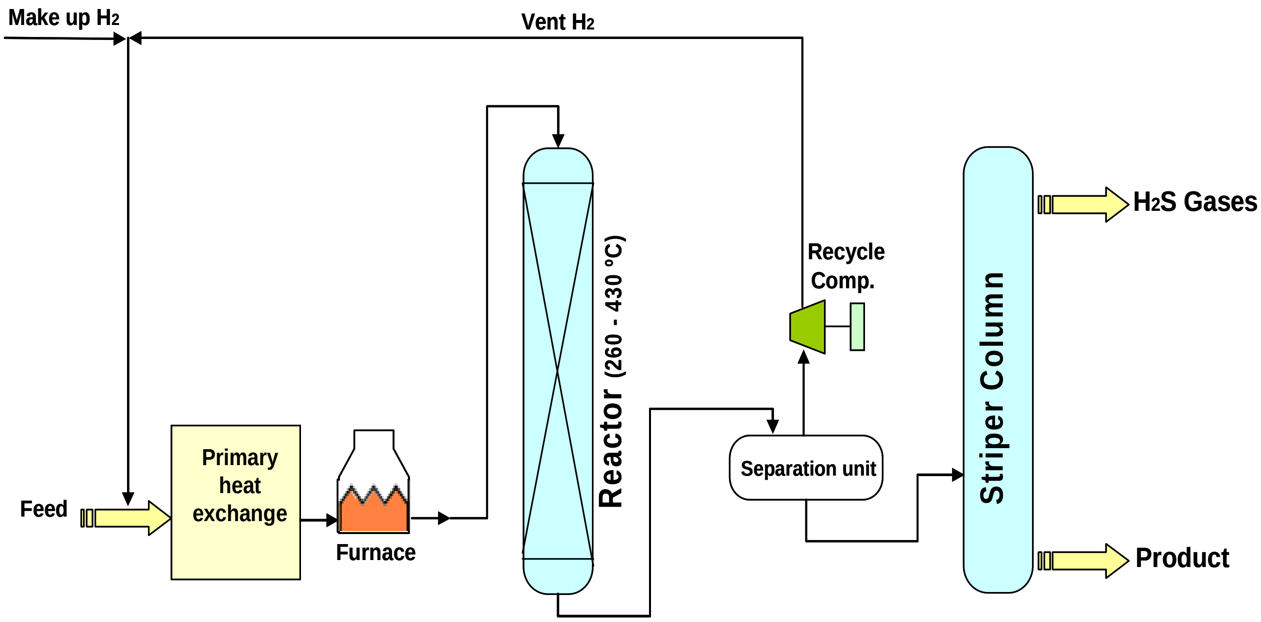

Figure 1.3: Typical hydrodesulfurization plan of refining technology showing the desulfurization processing sequence.

The feed stream is mixed with hydrogen and heated to a temperature between 260-430 ºC and pressures from 5 up to 10 MPa, depending on the desulfurization degree required. The gas mixture is made to flow over a catalyst bed of metal oxides (mostly cobalt or molybdenum oxides on different metal carriers). The catalysts help the hydrogen to react with sulfur and nitrogen to form hydrogen sulfide (H_2S) and ammonia. The reaction product leaves the reactor and is then cooled, and the oil feed and gas mixture is then separated in a stripper column. H_2S is a corrosive gaseous product, which is removed from the fossil fuel by stripping. By elevating the levels of H_2S in the reactor, it inactivates or poisons the chemical HDS catalyst and complicates the desulfurization of high-sulfur fossil fuels (Cyr, 2000).

For particular types of fossil fuels, the efficiency of HDS treatment varies due to the broad chemical diversity of hydrocarbons (Worrell et al., 2005). Some classes of organic sulfur molecules can be readily desulfurized by HDS because of instability, which includes the classes of organic molecules consisting of mercaptans, thioethers, and disulfides, but this technique is not suitable to get deep desulfurization levels and separate some of the sulfur molecules in oil, particularly the polyaromatic sulfur heterocyclies (PASHs) found in the heavier fractions, and which are the main class of HDS-refractory organic sulfur-containing molecules. Up to 70% of sulfur in fuels is found as refractory molecules like dibenzothiophene (DBT) and substituted DBTs (Monticello, 2000). HDS is capable of removing these refractory molecules only at temperatures and pressures so extreme that valuable hydrocarbons in the fossil fuel would be damaged in the process (Monticello, 1995). As the HDS units are expensive to build and control, therefore the application of novel catalyst types and innovations on HDS process configurations are needed to achieve desired levels. Therefore researchers are attempting to move to biological methods, which present many advantages.

1.4 Biodesulfurization

Since 1935, when an early account of microbial desulfurization of crude oil was published (Maliyantz, 1935; Shennan, 1996), there have been expended lots of interest in applying biodesulfurization (BDS) processes in the oil industry to demonstrate this ability of microorganisms. In the early 1950s, a series of U.S. patents were issued covering the use of bacteria to reduce the sulfur content of petroleum. However, early attempts were not fount to work because of inability to control the bacteria (Monticello, 1998). From 1970s to 1980s, the U.S. Department of Energy (DOE) and other organisations have sponsored work to explore this technology. The isolated bacteria were not appropriate for commercial BDS technologies at that time, because they attack the hydrocarbon portion (Kodama et al., 1973). In the late 1980s, bacteria that could liberate sulfur from DBT (as the model sulfur compound) without attacking the hydrocarbon were identified (Kilbane, 1990; Campbell, 1993). During these decades significant contributions have been made to construct and operate a large scale oil biodesulfurization process that involve many challenges and in order to develop biological desulfurization processes numerous attempts have been made up until the present time.

Biological processes require relatively mild conditions (low pressures and low temperatures), which could be a major advantage of BDS. It can be noticed that biocatalytic desulfurization offers the petroleum industry several benefits over hydrodesulfurization (HDS) processes: capital cost savings, operating cost saving, flexibility to handle a wide range of petroleum streams, more rapid engineering and construction time, safer and milder conditions. Testimonies of Naser (1999) have indicated that by BDS technology, the small refinery at Woodlands (Texas) achieved capital cost savings of approximately 50 percent and operating cost saving of 10-20 percent. In addition to cost savings, BDS will result in up to 80 percent less greenhouse gas emissions over HDS, because bioprocess operates at essentially room temperature and pressure.

The scheme of the biocatalytic desulfurization process is presented in Figure 1.4. The biocatalyst is mixed with water/media and transferred to the bioreactor. The biocatalyst slurry and petroleum containing sulfur compounds are mixed with oxygen and stirred continuously in a tank reactor. The petroleum is desulfurized and separated from the aqueous/biocatalyst output stream. The biocatalyst and water are separated and the sufur by-product is removed from the process in the aqueous phase as sulfate, which can be disposed of sodium sulfate or ammonium sulfate. After the spent biocatalyst is removed the biocatalyst/water mixture is recycled to the bioreactor.

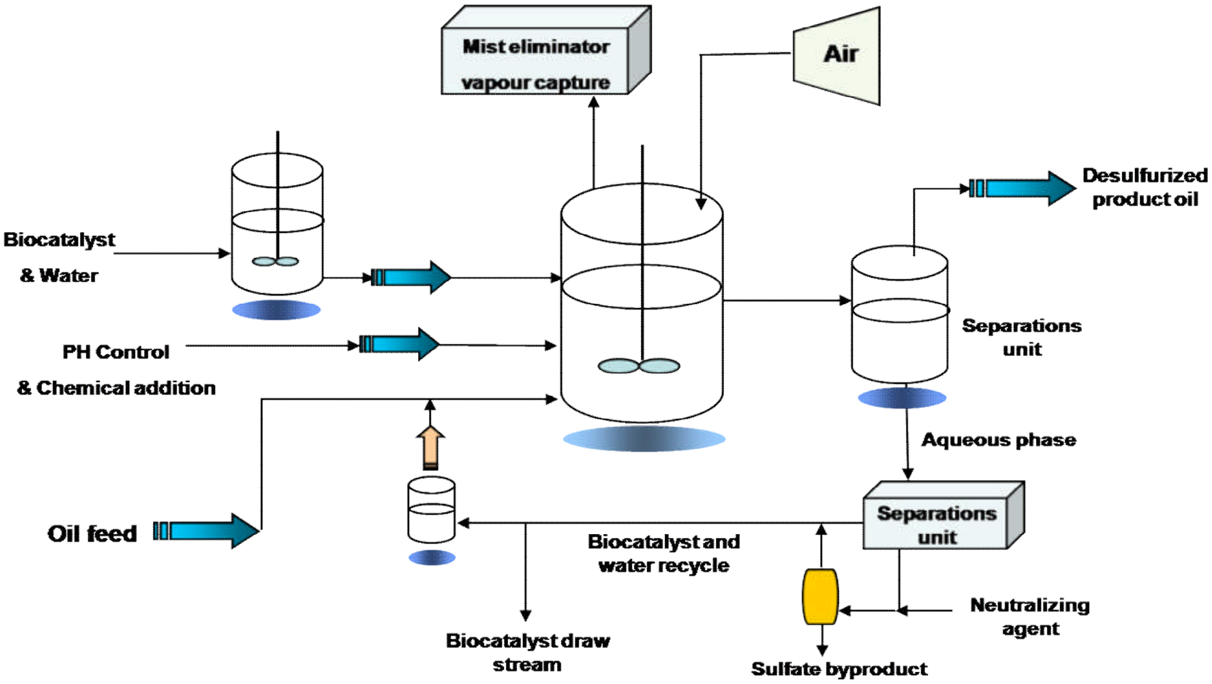

Figure 1.4: Scheme of oil biodesulfurization process (Monticello, 1998).

Basic microbiological researches have been done on the BDS mechanisms which have made a lot of progress in the recent years. Whereas significant removal of organic sulfur compounds from oil has not been demonstrate to date. To enable technological applications, to improve in knowledge on this field, the flux through this pathway must be enlarged considerably on activity, selectivity and stability of microorganisms applied in the process. For commercial applications, mixtures of microorganisms may be needed (Marcelis, 2003). Therefore, currently genetic and metabolic engineering efforts are applied by researchers. They tried to identify and clone the genes involved in the sulfur removal pathway, therefore efficiency of biological process could be enhanced by increasing the number of copies of the genes, altering the gene to produce a more active or efficient product and increasing the amount of expression from each gene. (Arensdorf et al., 2002; Hirasawa et al., 2001; Matsui et al., 2001a; Kertesz and Wietek 2001; Li et al., 1996). For example recombinants of *Rhodococcus erythropolis* containing multiple copies of the dsz-genes were used to study the conversion of sulfur compound (Kobayashi et al., 2001; Folsom et al., 1999).

1.4.1 Microbial reaction pathways

It seems that bacteria can be considered promising candidates for microbial enhanced oil recovery and improve the quality of fuel without changing the calorific value. Algae, moulds, yeasts, and protozoa are not suitable due to their size or inability to grow under the conditions present in reservoirs. Many petroleum reservoirs have high concentrations of NaCl and it seems that bacteria are able to tolerate these conditions by autoproduction of biosurfactants and polymers (Van Hamme et al., 2003).

Research on the reaction mechanism of BDS has concentrated on the study of the desulfurization of model compound like dibenzothiophene (DBT). DBT constitutes a major fraction of the residual post-HDS sulfur in fuel products and is refractory to HDS treatment. Alkyl-substituted DBT derivatives (Scheme 1.2) are even more refractory to HDS treatment, and even by repeated HDS processing cannot be removed. DBT is ubiquitous in almost all crude oils. In Texas it accounts for 70% of total sulfur compounds, and in the Middle East it accounts for more than 40% (Krishna, 2001). Hence DBT is considered as model refractory sulfur compound of a large group of heterocyclic compounds in the development of new desulfurization methods (Monticello, 1998), the microbial desulfurization of DBT can be considered to represent the degradation pattern of other such compounds. Therefore initial attention has focused on removal of sulfur from DBT to represent a major proportion of thiphenic sulfur found in most fuels.

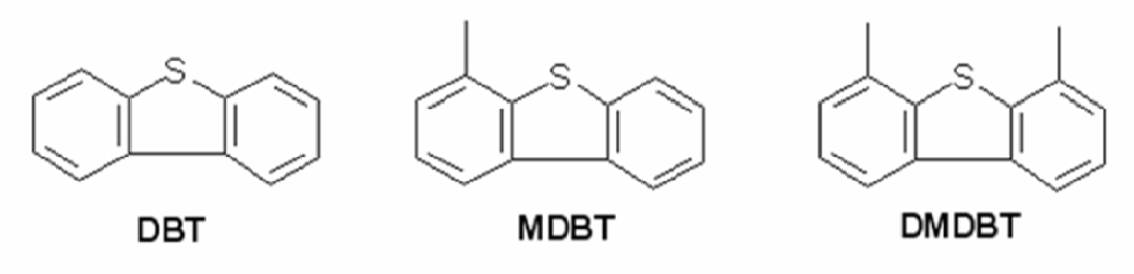

Scheme 1.2: Structural formulas of refractory dibenzothiophene (DBT) and methylated dibenzothiophenes, methyldibenzothiophene (MDBT) and dimethyldibenzothiophene (DMDBT).

From extensive investigations two alternative pathways have emerged as contender for the biodesulfurization. Kodama pathway is the first reported pathway for biodesulfurization of DBT (McFarland et al., 1998). It involves initial oxidative attack and ring cleavage of one of the aromatic rings of DBT, and in some cases the formation of sulfoxide or sulfone (Kodama et al., 1973) which leads to a reduced caloric value of the fuel and is therefore unacceptable. In addition, formyl benzothiophene remains as a dead end metabolite and a specific sulfur release is not found at the end of reaction

(Scheme 1.3). In addition, a specific sulfur release is not found since formyl benzothiophene remains as a dead end metabolite (McFarland et al., 1998).

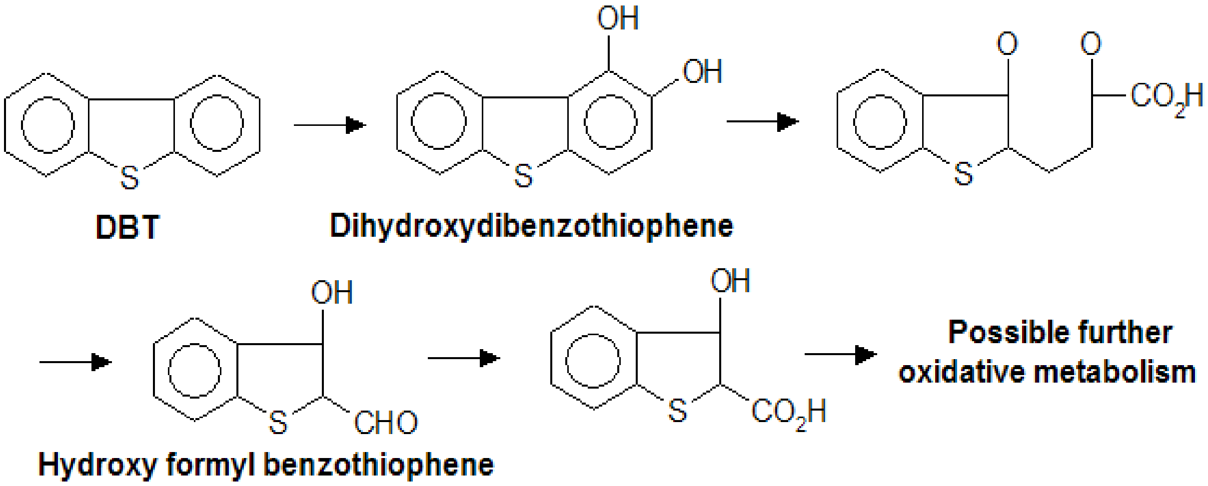

Scheme 1.3: Kodama pathway for the degradation of DBT. The product, hydroxyl formyl benzothiophene, retains the sulfur moiety (Kodama et al., 1973), so should properly not be considered a biodesulfurization mechanism.

In 1990 Kilbane proposed a sulfur specific pathway, sometimes called 4S pathway by which bacteria selectively oxidise the sulfur atom in DBT without cleavage of C-C bonds and therefore preserves the fuel value and has therefore been explored for the purpose of biodesulfurization of petroleum products (Bressler et al., 1998).

4S pathway is a sulfur-selective oxidative pathway involving the sequential oxidation of the sulfur moiety followed by cleavage of the carbon–sulfur bond to form 2-hydroxy biphenyl (HBP), leaving the carbon skeleton intact (Labana et al., 2005). This pathway involves four sequential enzymatic steps and is therefore called the 4S pathway; the enzymes selectively attack the sulfur fraction of the fuel and leave the hydrocarbon fraction unchanged. The whole reaction is presented in Scheme 1. 4. DBT is desulfurized using three enzymes DszA, DszB and DszC. This reaction can be divided into three stages: (i) activation of the thiophene ring for cleavage by oxidation of the sulfur moiety; (ii) cleavage of the thiophene ring to give an aromatic sulfinate, and (iii) removal of the sulfinate group. The end products, HBP and sulfate, (McFarland, 1998 and Gray et al., 2003), which are released in the cytoplasm and assimilated. HBP is not further metabolised by *R. erythropolis* and this compound accumulates in the medium when *R. erythropolis* is grown with DBT as the sole source of sulfur.

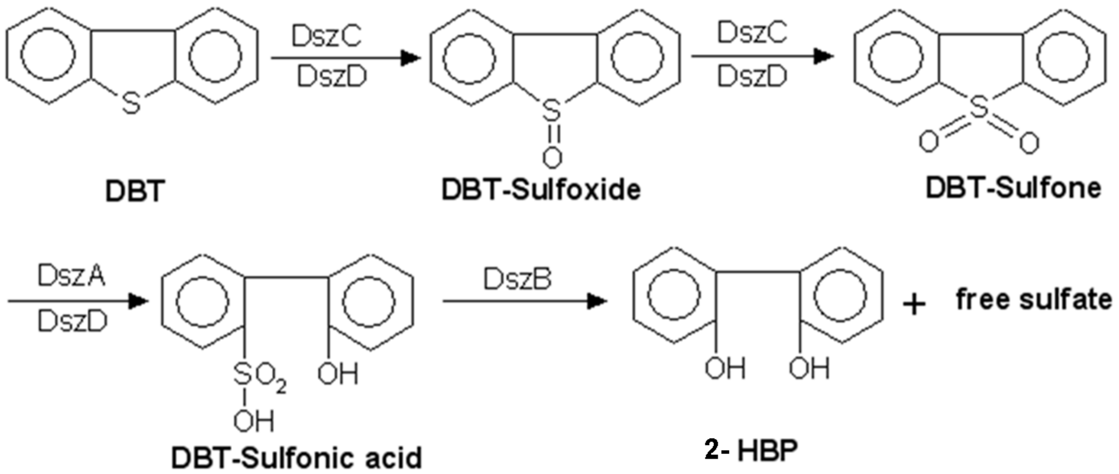

Scheme 1.4: Proposed (so called 4S) pathway for DBT desulfurization by *R. erythropolis* IGTS8.

The DBT desulfurization pathway results in the formation of 2-hydroxybiphenyl (2-HBP) and sulfate; via the Dsz enzymes (cf. Van Hamme et al., 2003). A mono-oxygenase (DszC) catalyses the stepwise S-oxidation of DBT, first to dibenzothiophene 5-oxide (DBTO) and then to dibenzothiophene 5,5-dioxide (DBTO2). The second mono-oxygenase (DszA), catalyses the conversion of DBTO2 to 2- (2’-hydroxyphenyl) benzene sulfinate (HBPS). The last step is catalyzed by a sulfinase (DszB) and yields 2-HBP and sulfate as the end products.

1.5 Degradation pathway

The first and rate-limiting step in the oxidative desulfurization of DBT and other sulfur compounds in living organisms is apparently transfer of DBT from the oil to the cell (Setti et al., 1999). In support of this, Folsom et al. (1999) found that the overall rate kinetics was affected by the concentration and distribution of the DBT. It is then oxidized to HBP in several steps by desulfurizing (Dsz) enzymes as illustrated in Scheme 1.4. These enzymes are soluble and presumably found in the cytoplasm (Marcelis, 2003).

On the other hand, there is no evidence that the DBT molecules are actively transported into the cell (Monticello, 2000). Patel et al. (1997) attributed the mass transfer of the very hydrophobic DBT to the hydrophobic nature of the *Rhodococcus erythropolis* IGTS8 surface, because of their finding that desulfurization activity is correlated to the external surface hydrophobicity of the IGTS8 wall/membrane. It might therefore be supposed that at least some of the enzymes are located in the wall/membrane region[1].

It is not presently known how the product, HBP, leaves the cells (Monticello, 2000) — assuming it is produced in the cytoplasm, not on the bacterial surface. At any rate the

---

[1] This suggests that some of the desulfurization enzymes should function in nonaqueous solvents, which consequently would facilitate contact with the oil phase and enhance mass transfer during biodesulfurization. In the other words, the *Rhodococcus* strains should be able to access to DBT directly from the oil (Monticello, 2000). This is consistent with the large body of work reporting growth of *R. erythropolis* IGTS8 on hydrocarbons such as hexadecane (Solano et al., 1999).

HBP released into the oil maintains fuel value (Gray et al., 1996). However, this compound is toxic to bacterial cells; hence growth and biodesulfurization activity become inhibited by its accumulation (Zhang et al., 2005). The sulfate formed during the 4S pathway remains in the aqueous phase and will combine with any ions — e.g. sodium, ammonium, calcium — that are present in the medium **(**McFarland et al., 1998), and might be assimilated by other microorganisms (Kilbane and Bielaga, 1990).

1.6 BDS as a complementary technique to HDS

HDS is not effective in desulfurizing all classes of sulfur compounds present in fossil fuels. Thiols, sulfides and thiophenes are readily removed by HDS. However, BT, DBT and especially derivatives bearing alkyl substitutions are considerably more resistant to HDS and represent a significant barrier to obtain very low sulfur levels in fuels because of steric hindrance (Marcelis 2003). Hence HDS alone is unable to achieve targets for deep desulfurization levels, but a separate BDS could reach this target. Bacteria do well in the water phase, consequently the organic sulfur compounds, *e.g.* benzo- and dibenzothiophenes, must be transferred from the oil bulk phase to the oil/water interface (Wilborn et al., 2005).

Because of the mild process conditions (low pressure and temperature), BDS is considered as an environmentally benign process. Therefore, with respect to these advantages, placing the BDS unit downstream of an HDS unit can be considered to use as a complementary process, after the main bulk sulfur is removed using HDS techniques. Monticello (1996) suggested a multistage process in order to desulfurise oil products. Moreover Fang et al., (2006) showed that by combination of BDS and HDS the sulfur content of catalytic diesel oil could reach to ≈20 µg/g.

1.7 Methods for identifying oil hydrocarbons and other compounds

The current techniques used for analysis of petroleum hydrocarbons can be generally grouped by their measurement outcome: the concentration of different groups of hydrocarbons; total amount of petroleum hydrocarbons; or the concentration of a specific target. Compound-specific methods frequently require samples to be diluted to keep the most concentrated analytes within the calibration range, or to protect the detectors from difficult-to-remove contamination. These requirements often cause low concentration analytes to fall below detection limits. Remedies for this problem may include analyzing the sample at more than one concentration or choosing a detection method with a wider dynamic range. In some cases, the detection limit problem cannot be resolved without risking potential contamination of the instrumentation (Weisman 1998).

A wide variety of specific and non- specific techniques are currently used in the analysis of oil hydrocarbons, including gas chromatography (GC), gas chromatography-mass spectrometry (GC-MS), high-performance liquid chromatography (HPLC), infrared spectroscopy (IR), supercritical fluid chromatography (SFC), thin-layer chromatography (TLC), ultraviolet (UV) fluorescence spectroscopy, gravimetric methods and isotopic ratio mass spectrometry (IRMS) (Wang et al., 1999; Alimi et al., 2003).

Each technique has advantages and disadvantages. UV spectrometries are very sensitive to aromatic hydrocarbons, but results may be influenced by the presence of other compounds e.g. lipids. IR-based methods have been widely used in the past because they are simple, quick and inexpensive. However, their use is currently decreasing due to the worldwide ban on Freon production (needed for sample extraction and measurement), the poor accuracy and precision and also a clean-up procedure which must be carried out preliminarily with great care to avoid contamination (the potential risk). Gravimetric-based methods are also simple, quick, and inexpensive, but they suffer from the same limitations as IR-based methods. Gravimetric-based methods are not suitable for measurement of light hydrocarbons but they may be useful for very oily sludge, which present analytical difficulties for other more sensitive methods. Immunoassay methods are gaining popularity for field testing because they offer a simple, quick technique for *in situ* quantification (Weisman, 1998; Brassington, 2007).

In recent years, GC/selective detector, HPLC, or GC/MS technique has been widely used in petroleum analysis. GC and HPLC techniques identify hydrocarbons based on their retention times which can be subject to interferences. The retention time is a time which a compound spends on a specific column and it is characteristic of a compound under given experimental parameters and specified column. As the separated components elute from the column, they are detected (Swallow et al., 1988). The detector signal is proportional to the amount of compound present. So these techniques involve use of selective detectors. GC techniques typically require a second column confirmation. GC/MS provides confirmation of the identity of an analyte through both its retention time and unique mass spectral pattern (Weisman, 1998).

Techniques such as GC-based methods may require additional technical skills/experience compared to other available methods and also requires that samples are volatile at the operating temperature of the column (Dean, 1995). Such techniques can not quantify hydrocarbons below C6. Also petroleum hydrocarbons are made up of many isomers that often have very similar/the same boiling point and thus they have very similar retention times within a GC column.

Gas chromatography coupled with mass spectrometry detection (GC-MS) can identify and measure the concentration of targeted individual petroleum hydrocarbons. These methods have a high level of selectivity, with the ability to confirm compound identity though the use of retention time and unique spectral patterns. However GC-MS requires relatively complex operation and interpretation of the data output, as such GC-MS methods tend to be a more expensive and time consuming technique for identifying the individual petroleum hydrocarbons (Brassington et al., 2005).

1.7.1 High performance liquid chromatography (HPLC)

HPLC is used to measure concentrations of target semivolatile and nonvolatile petroleum constituents. Unlike GC systems that require complete volatilization of the sample so that it can then pass into the chromatograph, HPLC systems only require that the sample be dissolved in a solvent compatible with those used in the separation. The HPLC detector most often used in petroleum environmental analysis is the fluorescence detector. A UV detector is used to measure compounds that do not fluoresce. Many modern detectors can tune excitation and emission wavelengths to maximize sensitivity and/or selectivity for each analyte during a chromatographic run.

HPLC methods measure any compounds that elute in the appropriate retention time range and which fluoresce at the targeted emission wavelength(s) as compounds are identified based on their retention times and the excitation wavelength excites most aromatic compounds. These include the target PAHs but also many derivative aromatics, such as alkylaromatics, phenols, anilines, and heterocyclic aromatic compounds containing pyrrole (indole, carbazole, etc.), pyridine (quinoline, acridine, etc.), furan (benzofuran, naphthofuran, etc.), and thiophene (benzothiophene, naphthothiophene, etc.) structures (Weisman, 1998).

1.8 Conclusion

The current technology, HDS, which is now used to reduce the sulfur content in oil, has many disadvantages: it is enormously costly to install and operates, it needs extremely energy intensive so leads to large greenhouse gas emissions. Thus, necessity dictates to enhance this technology by use of biodesulfurization ability of bacteria and to date, some microorganisms have been identified which can remove sulfur from oil but the commercial development still needs to be accelerated and biodesulfurization needs to be more efficient. To date, the most important challenges in the biodesulfurization area is to isolate a strain with higher desulfurization activity or design a recombinant strain with a stable activity to improve the efficiency of biodesulfurization. Therefore, more work is required to achieve higher desulfurization activity by the bacteria.

1.9 Research objectives, methodology and accomplishments

The main objectives of my research project are to develop a biosystem for sulfur removal from oil. Secondly, I wished to develop an assay with which I could readily quantify the adhesion between bacteria and particles in order to optimize the process. Thirdly, to elucidate why decorated[2] bacteria have enhanced desulfurization ability, I wished to understand how the nanoparticles modify the bacterial physiology. Fourth, I have exploited a uniquely powerful non-invasive optical nanometrology technique (OWLS) to fabricate magnetic nanofilm and monitor cell attachment on the nanofilm.

The accomplishments of this following are:

- Isolation of new strains of bacteria
- Fabrication of magnetic nanoparticles
- Develop a bioprocess to desulfurize organic sulfur compounds using bacteria decorated by magnetic nanoparticles and propose a novel mechanism for biodesulfurization enhancement.
- Self-assembly of Fe_3O_4 magnetic nanoparticles on $Si(Ti)O_2$ to form magnetic nanofilms.
- Measure the kinetics of bacterial adhesion to the particles.

---

[2] Decorated bacteria not completely covered with the nanoparticles.

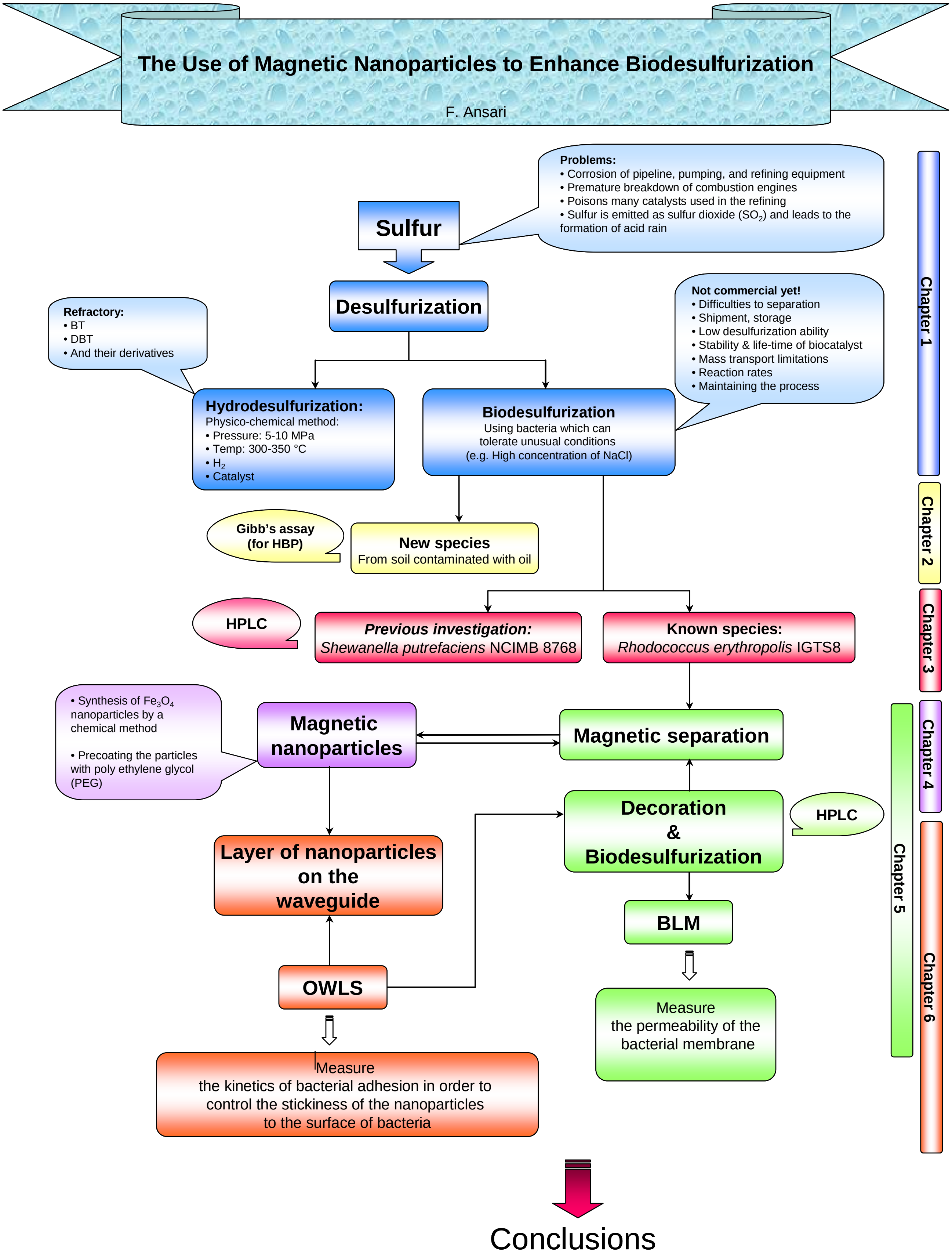

Figure 1.5 : Flow diagram to show structure of work in this thesis.

Chapter 2 : Attempts to biologically enhance biodesulfurization

2.1 Search for new strains

In order to develop biologically enhanced desulfurization technology, a range of bacteria have been previously isolated which have been shown to be able to remove sulfur from organic compounds that commonly exist in petroleum (Mohebali and Ball, 2008). However, this activity is unlikely to be sufficient for commercial applications where the requirement is for microorganisms with high activity and selectivity for different sulfur compounds (Yang and Marison, 2005). To achieve this requirement, there needs to be about a 500–fold increase in the rate of biodesulfurization of currently used bacteria (Kilbane, 2006). Therefore due to a range of problems (one of which is the low desulfurization capability of the bacteria employed, which makes the process uneconomical) this technology area needs to be enhanced by new developments.

Bacteria, which exist in the oil fields, have a great potential to degrade sulfur compounds in fuel (Lee and Levy, 1991). Research over the last few years has shown that oil fields contain microbial communities that influence the petroleum quantity and yield of petroleum produced and its quality. Professionals in the petroleum industry today clearly understand the critical role that regulating microbial activity has in enhancing the beneficial effects. Accordingly newly isolated strains of bacteria continue to attract attention for their potential application to desulfurization. Since DBT is a typical recalcitrant organic sulfur compound in petroleum, it has been a model reactant in the treatment of oil (Kilbane, 1990; Monticello, 1995). In 1985 a strain of

Psedomonas that could desulfurize DBT was described by Isbister and Koblynski, but unfortunately before the metabolic pathway could be fully characterized, this strain was lost (Gallagher et al., 1993). After 40 years of research effort, Kilbane (1990) isolated a suitable bacterium named *Rhodococcus erythropolis* IGTS8. Since then many researchers have isolated bacteria capable of degrading DBT via the 4S pathway and a variety of DBT- desulfurizing bacteria have been reported a list of which by Mohebali and Ball, 2008 (table 2.1). This list is however incomplete, omitting for example *Shewanella putrefaciens*.

Table 2.1: List of isolated bacteria that are capable of selectively degrading DBT and its derivatives via the 4S pathway (Mohebali & Ball, 2008).

Bacterium	**Reference**
Agrobacterium sp. strain MC501	Constanti et al. (1994)
Arthrobacter sp. strain ECRD-1	Lee et al. (1995)
Arthrobacter sulfureus	Labana et al. (2005)
Bacillus subtilis strain WU-S2B	Kirimura et al. (2001)
Bacillus brevis strain R-6	Jiang et al. (2002)
Bacillus sphaericus strain R-16	Jiang et al. (2002)
Bacillus subtilis strain Fds-1	Ma et al. (2006c)
Corynebacterium sp. strain SY1	Omori et al. (1992)
Corynebacterium sp. strain P32C1	Maghsoudi et al. (2000)
Corynebacterium sp. strain ZD-1	Wang et al. (2006)
Desulfovibrio desulfuricans	Yamada et al. (1968)
Gordona sp. strain CYKS1	Rhee et al. (1998)
Gordona sp. strain WQ-01	Jia et al. (2006)
Gordonia alkanivorans strain 1B	Alves et al. (2005)
Gordonia sp. strain F.5.25.8	Duarte et al. (2001)
Gordonia sp. strain ZD-7	Li et al. (2006)
Gordonia alkanivorans RIPI90A	Mohebali et al. (2007)
Klebsiella sp.	Dudley & Frost (1994)
Mycobacterium sp. strain G3	Nekodzuka et al. (1997)
Mycobacterium sp. strain X7B	Li et al. (2003)
Mycobacterium sp. strain ZD-19	Chen et al. (2008)
Mycobacterium goodii strain X7B	Li et al. (2007c)
Mycobacterium phlei strain SM120-1	Srinivasaraghavan et al. (2006).
Mycobacterium phlei strain GTIS10	Kayser et al. (2002)

Nocardia globelula	Wang & Krawiec (1994)
Nocardia asteroids	Olson (2000)
Nocardia globerula strain R-9	Jiang et al. (2002); Luo et al. (2003)
Paenibacillus sp. strain A11-2	Konishi et al. (1997)
Pseudomonas abikonensis strain DDA109	Yamada et al. (1968)
Pseudomonas jianii strain DDC279	Yamada et al. (1968)
Pseudomonas jianii strain DDE27	Yamada et al. (1968)
Pseudomonas sp. strain ARK	Honda et al. (1998)
Pseudomonas delafieldii strain R-8	Jiang et al. (2002)
Pseudomonas putida strain CECT5279	Alcon et al. (2005)
Rhodococcus erythropolis strain IGTS8	Kilbane (1992)
Rhodococcus sp. strain UM3	Purdy et al. (1993)
Rhodococcus sp. strain UM9	Purdy et al. (1993)
Rhodococcus erythropolis strain D-1	Izumi et al. (1994)
Rhodococcus sp. strain ECRD-1	Lee et al. (1995)
Rhodococcus erythropolis strain H-2	Ohshiro et al. (1995)
Rhodococcus sp. strain SY1	Omori et al. (1995)
Rhodococcus sp. strain X309	Denis-Larose et al. (1997)
Rhodococcus sp. strain B1	Denis-Larose et al. (1997)
Rhodococcus erythropolis strain I-19	Folsom et al. (1999)
Rhodococcus erythropolis strain KA2-5-1	Kobayashi et al. (2000)
Rhodococcus sp. strain P32C1	Maghsoudi et al. (2000)
Rhodococcus sp. strain T09	Matsui et al. (2001)
Rhodococcus sp. strain IMP-S02	Castorena et al. (2002)
Rhodococcus sp. strain FMF	Akbarzadeh et al. (2003)
Rhodococcus sp. strain DS-3	Ma et al. (2006d)
Rhodococcus sp.	Labana et al. (2005)
Rhodococcus erythropolis strain XP	Yu et al. (2006)
Rhodococcus sp. strain 1awq	Ma et al. (2006a)
Rhodococcus erythropolis strain XP	Yu et al. (2006)
Rhodococcus erythropolis strain DS-3	Ma et al. (2006b)
Rhodococcus erythropolis strain DR-1	Li et al. (2007a)
Rhodococcus erythropolis strain NCC-1	Li et al. (2007b)
Rhodococcus erythropolis strain LSSE8-1	Xiong et al. (2007)
Rhodococcus erythropolis strain FSD-2	Zhang et al. (2007)
Sphingomonas sp. strain AD109	Darzins & Mrachko (1998)
Sphingomonas subarctica strain T7b	Gunam et al. (2006)
Xanthomonas sp.	Constanti et al. (1994)
Several unidentified bacteria	Abbad-Andaloussi et al. (2003)

2.2 Genetic engineering

Even with this number of isolated bacteria, the desulfurization activity of naturally occurring bacterial cultures is not high enough for the requirements of industry and a successful commercial process is still awaited. To achieve this, therefore we need to isolate new species and identify the genes responsible for desulfurization and manipulate the system involved by genetic engineering techniques and it is highly likely that future biodesulfurization research will focus on development of this promising research area along these lines. One of the popular strategies in metabolic engineering of the bacteria is to change host strains in order to take advantage of another strain's properties to get a higher metabolic rate. For example, several research studies have focused on over expression of the enzymes involved in microbial desulfurization. The DNA encoding the Dsz enzymes can be transferred into a host cell (Squires et al., 1999) or the gene amplified with designed primers (Matsubara et al., 2001). Matsui et al. (2001) used a recombinant strain capable of desulfurizing both DBT and BT as the sole source of sulfur. To improve the uptake of sulfur compounds in oil fractions, Watanabe et al. (2003) transferred the *dsz* genes from *Rhodococcus erythropolis* KA2-5-1 into the *Rhodococcus erythropolis* MC1109. The desulfurization activity of the new strain was about twice that of the previous strain. In order to enhance the expression of the genes involved, the dsz genes from *Rhodococcus erythropolis* DS-3 were integrated into the *Bacillus subtilis* and yielded recombinant strains with higher desulfurization efficiency (Ma et al., 2006). Li et al. (2007) enhanced the desulfurization ability of *Rhodococcus erythropolis* DR-1 by transferring the gene overlap in the operon.

As mentioned above, changing the genes of the host cell for those involved in desulfurization is a popular strategy in metabolic engineering to take advantages of desirable properties another strain such as its physical properties, growth properties or higher intrinsic metabolic rate. Since these are not yet understood, a better understanding of the factors that contribute to the biodesulfurization pathway is needed so as to achieve high level expression of the gene (Kilbane, 2006) and future research to isolate new strains and identify the biocatalyst would be helpful to develop this promising research area.

2.3 Experimental part of the research

2.3.1 Soil samples

Soils contaminated by crude oil were collected from four different sites around oil fields (Iran) and were placed in polyethylene bags, closed tightly and stored at 4 ± 1 °C.

2.3.2 Preparation of basic salt medium (BSM)

In order to avoid precipitation and turbidity of the medium, the preparation of BSM was performed in 2 parts separately and then these two parts were mixed together to get one litre of BSM.

Part a: The chemicals listed in table 2.2 were dissolved in 850 mL of deionised water in a rotary shaker.

Part b: The chemicals listed in table 2.3 were dissolved in 150 mL of water in a shaker.

After mixing these two parts, the pH was adjusted to 7.0.

Table 2.2: Composition of BSM (part a).

Component	Amount
KH_2PO_4	2.44 *g*
Na_2HPO_4	5.57 *g*
NH_4Cl	2.00 *g*
Glycerol	1.84 *g*
Water	850 mL
pH	7.0 ± 0.2

Table 2.3: Composition of BSM (part b).

Component	Amount
$MgCl_2.6H_2O$	0.20 *g*
$CaCl_2.2H_2O$	0.001 *g*
$FeCl_3.6H_2O$	0.001 *g*
$MnCl_2.4H_2O$	0.004 *g*
Water	150 mL
pH	7.0 ± 0.2

2.3.3 Isolation of bacterial strains from soil contaminated with oil

The bacteria in this investigation were collected from oil contaminated soils and thus they have been growing with the help of compounds found in oil fields. Since crude oil had been present at those sites for a long time, bacteria have been adapting to survive in this polluted area and probably have developed the necessary enzymes to metabolize sulfur compounds. To isolate mixed bacterial cultures from natural fields, in order to increase the precision of the experiment I opted to use two different methods to ensure that the bacteria were identified correctly as the only bacteria in the samples.

2.3.3.1 Enrichment of cultures able to grow on DBT

Enrichment is a technique to isolate microorganisms from their natural environment by inoculating natural sources of bacteria into a selective media and then growing under physiological conditions optimum for the desired organisms (Christopher et al., 1995). Initial enrichment cultures were prepared by adding 10 *g* soil samples to 150 mL BSM in a 250 mL flask supplemented with 0.5 mM of DBT and incubating in a shaker at 100 rpm at 30 °C for 7 days. The flasks were then allowed to stand for 5 min. A 10% aliquot of the supernatant was transferred to 100 mL of BSM in a 250 mL flask containing DBT. Enrichment was continued for one month. These cultures are mixed bacterial cultures, some of which may utilize DBT.

2.3.3.2 Dilution method

Sub samples of 1g of soil were suspended in sterile deionised water (containing 9 mL of NaCl 10% and Tween 0.05%), agitated in a shaker at 100 rpm for 60 min at 30 °C and since the bacteria in natural samples are too numerous to count directly, these must be diluted to obtain an accurate count. Samples were serially diluted up to a factor of 10^{-3}. Figure 2.1 shows a three-fold dilution series of a soil sample. In the first tube on the left, 1 gram of soil was added to 9 mL of water to make a 1:10 (1×10^{-1}) dilution of soil. One mL from the 1:10 tube was then added to 9 mL of water in the second tube from the left to make a 1:100 (1×1^{-2}) dilution of soil. This process was repeated for the last tube to make a 1:1000 (1×10^{-3}) dilution of soil. After preparing the dilutions, aliquots of 0.1 mL from each dilution were spread over the surface of agar plates (petri dish-triple vented).

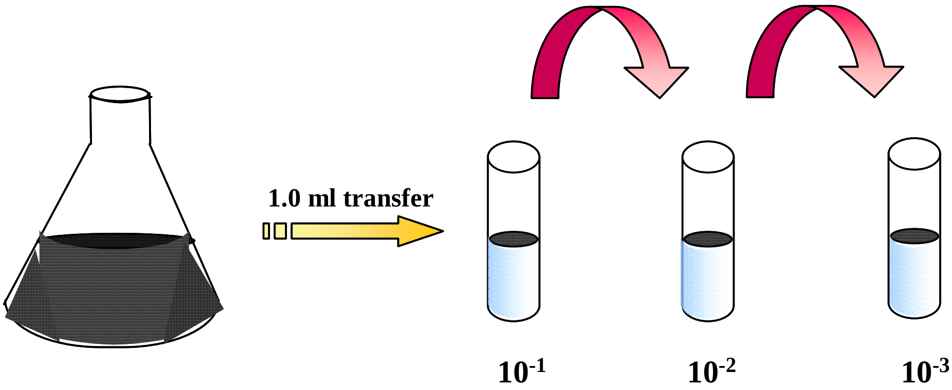

Figure 2.1: A three-fold dilution series of the soil sample. Soil dilutions range from 1:10 (1×10^{-1}) on the left to 1:1000 (1×10^{-3}) on the right.

Microorganism isolation was carried out using a selective medium (BSM).This medium contained 1 Litre BSM, 15 *g* agar (1.5% agar) and DBT as a sulfur source which was added aseptically to sterile BSM at a final concentration of 0.5 mM. After preparation of dilutions (10^{-1}– 10^{-3}), selective agar media were inoculated and incubated at 30 °C.

2.3.4 Preparation of pure cultures

For bacterial strain selection, the colonies were transferred to separate selective media. In this way each strain was spread on to a separate plate. To do this a loop of culture was first streaked on to the BSM agar plates and these plates were incubated for 48–72 hours at 30 °C. After identifying different colony forms, individual colonies were transferred on to individual plates all having the same medium. The procedure streaking out on to plates was repeated to isolate different purified colonies.

2.3.5 Selection of isolates able to convert DBT to HBP

To identify the bacterial colonies using DBT as sole source of sulfur the Gibb's assay technique was used. This technique is able to identify the bacterial colonies that desulfurize DBT by the specific oxidative pathway (4S) to HBP (Omori et al., 1992). Flasks containing BSM with 0.5 mM of DBT as sole sulfur source were inoculated by isolated strains, three flasks per strain. Then they were shaken at 100 rpm for two weeks at 30 °C. To investigate the growth of bacteria, the absorbance change (turbidity) of the mineral medium was measured by spectrophotometry at a wavelength of 600 nm. This absorbance change was used as the evaluation criteria for microorganism adaptation in the media used. In order to carry out the Gibb's assay, aliquots (5 mL) from each flask were taken daily and production of 2-HBP as the results of biodesulfurization was determined by spectrophotometery at a wavelength of 610 nm. *Rhodococcus* was used as the control organism and its activity was compared against the activity of the isolated strains. Uncontaminated BSM was used as a blank.

2.3.6 Gibbs assay

The 2-hydroxybiphenyl (2HBP) produced as a consequence of the BDS of DBT was determined using Gibbs reagent (2, 6-dichloroquinone-4-chloroimide). The media must be adjusted to pH 8.0 before the Gibb's reagent is added. Gibb's reagent, the principle reagent of this assay, can react with the aromatic hydroxyl groups at pH of 8.0 to form a blue-coloured complex which can then be monitored spectrophotometerically at 610 nm after 30 min incubation at room temperature. Thus, the assay can be summarized as follows:

Aliquot (5 mL) of supernatant culture broth was put into the tubes and centrifuged (1200 rpm, 10 min) to remove cells. The supernatant (2 mL) was then transferred to an Eppendorf tube. Gibb's reagent (0.1 *g*) (2,6-dichloro-quinone-4-chloroimide) was dissolved in 10 mL absolute ethanol in a test tube, and quickly protected from light by wrapping the tube in foil. Each Eppendorf tube contained 2.0 mL supernatant adjusted to pH 8.0, and each of these 20 µL Gibb's reagent was added. The assays were incubated at 30 °C for 30 min to complete the colour development. The optical density at 610 nm was measured on a Jenway-6505 UV/vis. Spectrophotometer and absorbance changes were converted to HBP concentration with the aid of a 2-HBP-generated standard curve.

$$\textbf{HBP + Gibb's reagent} \rightarrow \textbf{Blue colour} \qquad (1)$$

2.3.6.1 Gibb’s assay calibration

Gibb’s assays were undertaken to detect 2-hydroxybiphenyl (2-HBP), which is produced from DBT degradation. The absorbance of the supernatant determined at 610 nm was converted to concentration (*mg*/L) with the aid of 2-HBP generated standard curve. The standard curve was prepared from the development of the blue colour produced by the reaction between Gibb’s reagent and aromatic hydroxyl group (2-HBP) in the range of 0 - 0.4 mM which gave the absorbance curve presented in Figure 2.2.

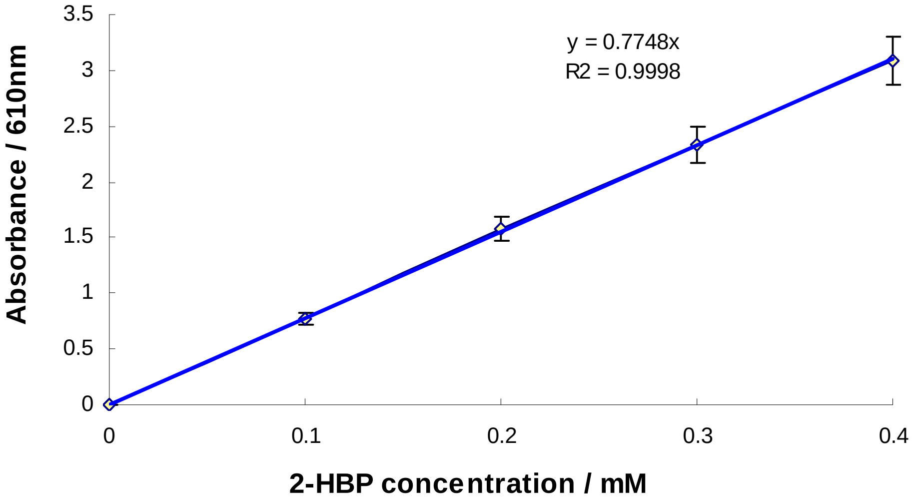

Figure 2.2: Standard curve of 2HBP obtained by Gibb's assay. Each point is a mean of 3 replicates and the error bar is one standard deviation.

2.3.7 General characterization of isolated strains

Traditionally the first steps in the identification of unknown bacteria, are based on phenotypic properties of the isolates such as cell shape and colony morphology. Various staining methods are then applied to obtain information about the bacterial cell wall and to monitor cell structures. After this, genotypic characterization (determination of the DNA and RNA characteristics of the bacteria) is becoming more widely practiced, to characterize and identify bacteria. The general characterization of bacteria refers to determination the shape, Gram reaction, motility etc by use of microbiological techniques and light microscopy was carried out in the follows manner.

2.3.7.1 Colony morphology

Colonies of the isolated strains that produce HBP were grown on BSM agar plates. Observation using a stereomicroscope (magnification 50X) was used to identify the different colony shapes, sizes, colours and textures (dry or wet).

2.3.7.2 Cell shape and arrangement

Individual cells were observed in the light microscope (magnification 100x with oil immersion) to identify the overall shape of the cells e.g. coccus, bacillus (rod shape), coccobacillus, curved or “V” shaped rod.

2.3.7.3 Motility: the hanging drop test

One drop from a freshly prepared culture was added to a microscope cover slip. A plasticine ring was placed on a microscope slide and then the slide inverted over the cover slip so that the drop is in the centre of the plasticine ring and the coverslip sealed in position by the plasticine. The microscope slide with the coverslip is reinverted so that the bacterial cells are freely moving in the drop and motility can be observed by using phase contrast microscope (magnification 40X) as a darting motion.

2.3.7.4 Catalase test

Approximately 0.2 mL of hydrogen peroxide solution was placed in a test tube. A colony of the bacteria to be tested was placed inside the tube and rubbed against the wall of the tube. The tube was then capped and tilted to allow the hydrogen peroxide solution to cover the colony. If the colony forms bubbles, the organism is said to be catalase-positive and if not, the organism is catalase-negative.

2.3.7.5 Staining procedure

Bacterial smears were prepared, air dried and heat fixed on a microscope slide using standard procedures. The smears were stained for Gram reaction (Carter and Wise, 2003): Gram staining allows bacteria to be divided into two major groups, gram-positive and gram-negative. The two groups have different cell wall structures, as well as other different characteristics. Cell wall contains either a thick peptidoglycan layer or a thin peptidoglycan layer with an additional lipopolysaccharide layer. The gram stain method can be summarized as follows:

The prepared smear was stained with a drop of 0.5% methyl violet for 60 seconds and rinsed with water. Then the bacteria were stained with a drop of 2%KI/1%I (Lugol's iodine) for one minute. The slide was rinsed with water and immediately decolorized with ethanol for a short time until the violet colour no longer ran out. The slide was rinsed with water and the sample was counterstained with 0.1% saffranin for a minute. Then the slide was rinsed briefly with water and allowed to dry. The slide was observed under the microscope (Olympus BH2 Microscope) by using UplanFI 100*/1.30 oil lens

2.3.8 Identification of isolates

After colony characterisation and Gram staining the isolates, screw capped bottles (20 mL) containing BSM agar as a solid slant were prepared and streaked with isolated strains under sterile conditions and sent to George Kvesitadze, Durmishidze Institute of Biochemistry and Biotechnology, Tbilisi.

2.3.9 Bacterial growth and population density of isolates

Growth of isolates was measured from their optical densities at 600 nm (A_{600}) using a Jenway- 6505 UV/Visible (Paterson Scientific, UK) spectrophotometer. A 10 mL solution of BSM was inoculated with the bacteria Using sterilized conditions (flaming under a laminar flow hood and incubated at 100 rpm at 25 ºC for two days. Bacteria growing on these plates were then harvested. The bacterial isolates were cultured by using 1 ml inoculum added to a 100 mL of basic salt medium (BSM) in a 250-mL flask. Flasks were then incubated on an orbital shaker (Luckham model R300, UK) at 100 rpm at 25 ºC. Samples were taken every three hours and monitored for the optical density of these suspensions by UV spectrophotometery at 600 nm until a stable optical density was reached (All the experiments were run in triplicate).

2.4 Results and discussion

At the end of enrichment, bacteria inherent in the soil were isolated by plating the enrichment cultures on BSM agar plates with DBT. By repeating streak out on plates of the same medium the different colonies were obtained (Fig. 2.3).

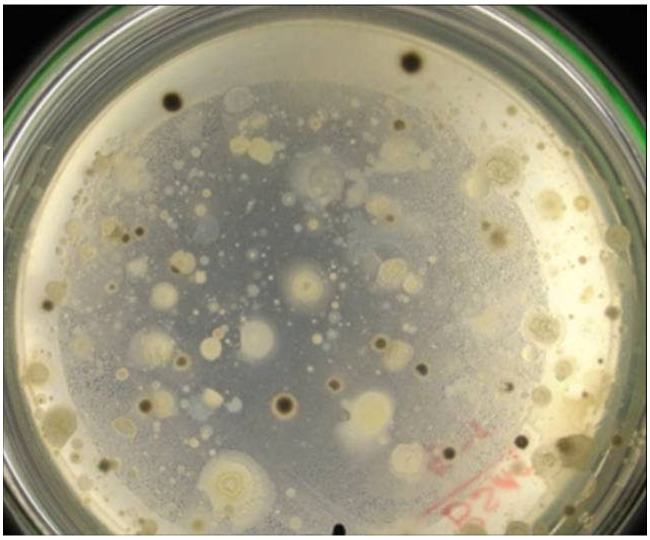

Figure 2.3: Photograph of typical spread plates produced by culturing on BSM agar plates. This figure shows the growth of a range of microorganisms on an agar plate containing 0.5 mM DBT as the sole sulfur source.

Production of 2-HBP, caused by desulfurization of the isolated bacteria was determined by spectrophotometery at 610 nm and typical results are presented in Table 2.4.

Table 2.4: Gibb's assay results. Coloration observed after addition of Gibb’s reagent. Control (contained HBP). Blue coloration identifies HBP production; brown coloration identifies complete degradation of DBT.

Sample No.	**Coloration**	
	Blue	**Brown**
1	–	+
2	–	+
3	–	+
4	+	–
5	–	+
6	–	+
7	–	+
8	–	+
9	–	+
10	–	+
11	–	+
12	–	+
13	–	+
14	+	–
15	–	+
16	+	–
17	–	+
18	+	–
19	–	+
20	–	+
21	–	+
22	–	+
23	+	–
24	–	+
R. erythropolis	+	–
Control (HBP)	+	–

The selected colonies were transferred to a separate BSM agar supplied with DBT at a final concentration of 0.5 mM. This method was used for two reasons: (1) to confirm that only one bacterial species was transferred to a medium, thus creating a pure culture, and (2) to assess the specific characteristics of isolated colonies and eliminate the similar colonies which lead to select 5 strains among the isolates. The streak-plate method was used to transfer the micro-organisms. Selected plates are shown in Fig. 2.4. All agar plates were 90 mm Petri dishes and were on BSM agar contain 0.5 mM DBT.

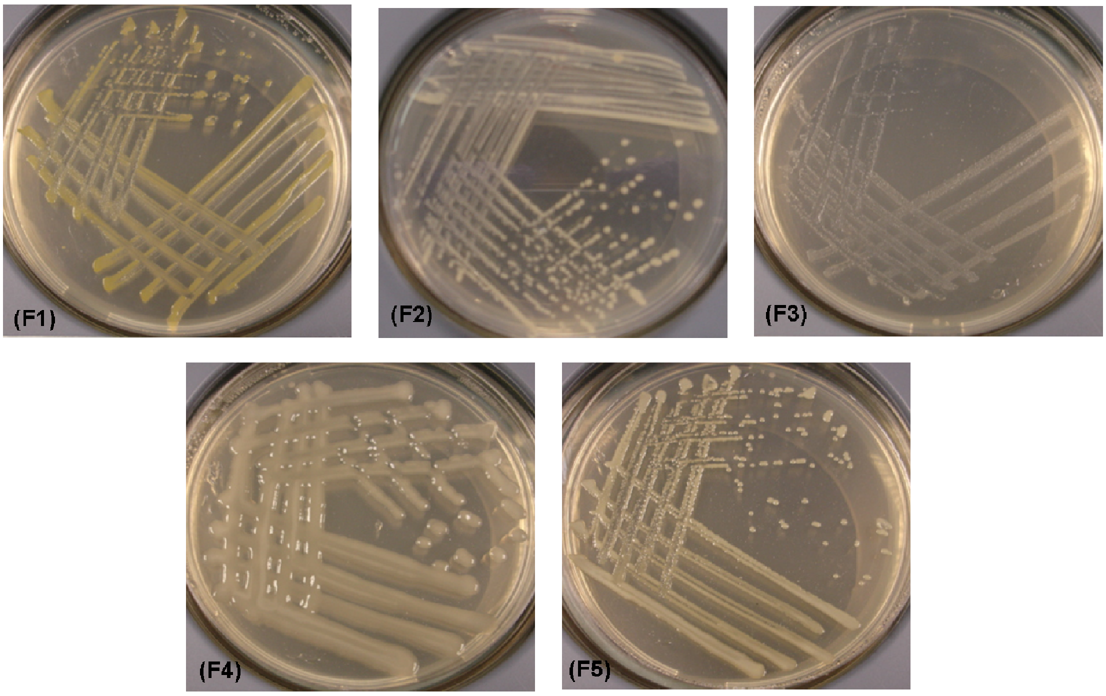

Figure 2.4: The streak plates of micro-organisms used to isolate pure cultures.

The Gram stain results of selected isolates are shown in Figure 2.5. The blue/violet coloration indicates that F3 and F5 are Gram positive while Gram negative cells (F1, F2 and F4) show the pink colour of the counter stain.

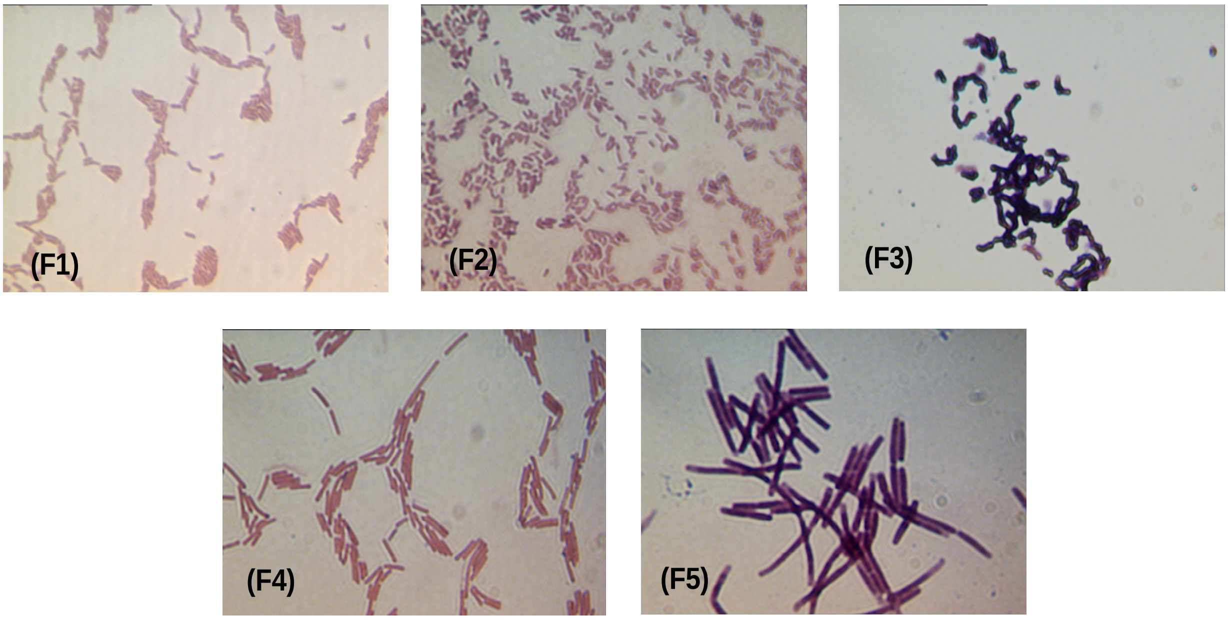

Figure 2.5: Gram stains of isolated bacteria.

The growth of isolated bacteria was measured using a dilution series and typical results are shown in Figure 2.6. As can be seen the growth rate of isolates in BSM liquid cultures is slow at first, and then after 10-15 h becomes rapid. Of the isolates studied here, F3 had the shortest lag period, approximately six hrs and that of isolate F5 was twenty hrs longer. The exponential phase was From 10 h to 20 h.

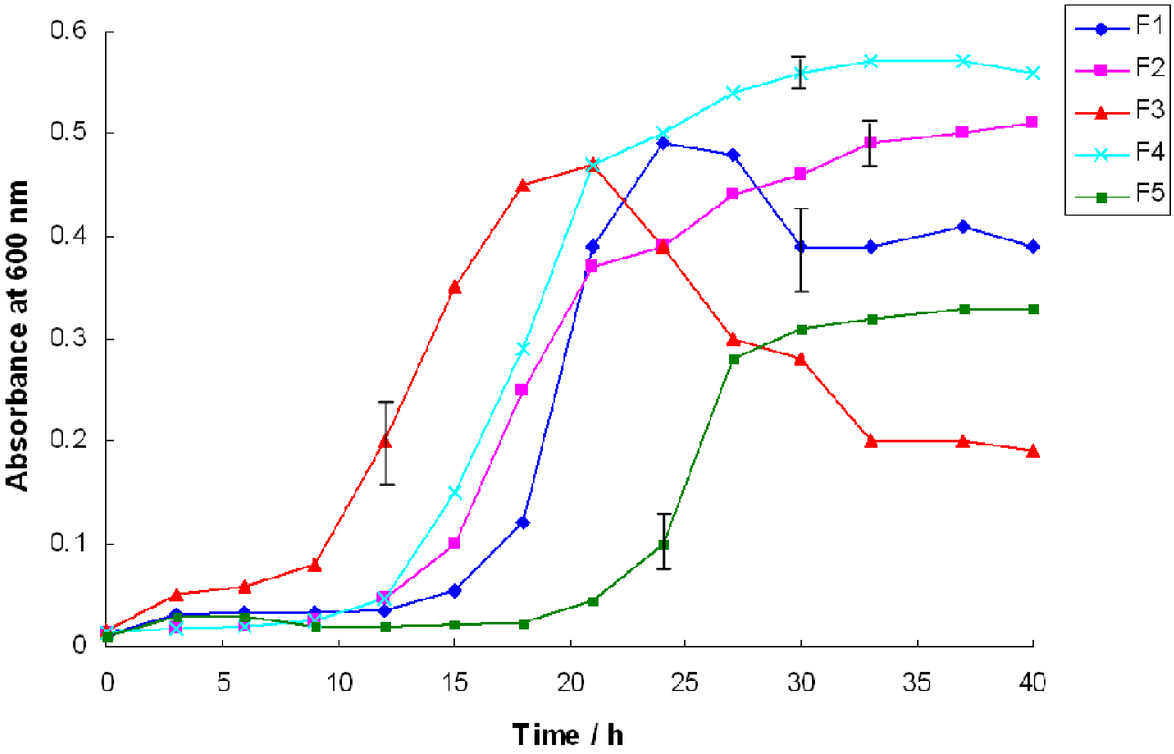

Figure 2.6: Growth of isolates in BSM at 30 ºC over a 40 hr incubation period. Each point is the mean of three experiments. To avoid overcrowding the graph, one representative error bar giving the standard deviation is shown for each curve.

To identify the characteristics of the unknown bacteria – phenotypic properties of the isolates – techniques were applied to obtain general information about the isolated bacterial. The characterization results for five isolates are summarised in Table 2.5.

Table 2.5: General characteristics of HBP producing isolates. All the cultures were freshly cultured on BSM containing DBT as the sulfur source at 30 ºC.

Isolates:	**F1**	**F2**	**F3**	**F4**	**F5**
Colour	yellow	creamy	pink	creamy	creamy
Shape of cells	rod	rod	rod	rod	rod
Cell size (µm)	0.5 ×1.0-3.0	0.5-1.0 ×1.2-4.5	1-1.6 × 0.3-0.65	1.0 × 3.5-5.0	5.0 × 5.0
Colony form	round	round	round	round	round
Margin	notched edges	even	even	even	even
Size of the colony (mm)	1-4	1-2	1-2	1-2	1-2
Appearance	Slightly convex	Smooth & convex	Smooth &glittering	Smooth & convex	smooth
Motility	-ve	+ ve	- ve	+ ve	- ve
Spore formation	-ve	- ve	- ve	- ve	- ve
Catalase	-ve	+ ve	+ ve	+ ve	- ve
Gram reaction	-ve	- ve	+ ve	- ve	+ ve

For the genotypic characterization (determination of the DNA and RNA characteristics of our bacteria), the five isolates were sent to Institute of Biochemistry and Biotechnology, Tbilisi. The results showed strain F2 and F4 were isolates of *Psedomonas*, strain F1 was a *Flavobacterium* and F3 belonged to the genus of *Rhodococcus*. But the identification of F5 was not successful however with high probability it was a known strain.

2.5 Summary

Soil samples were collected from different natural sites around oil contaminated fields in Iran. Enrichment, isolation and purification were applied under aerobic mesophilic conditions in minimal medium containing DBT as the sole source of sulfur. 24 colonies isolated were obtained from these samples. The purity of the bacteria was confirmed by subculturing the colonies a few times. To identify the bacterial colonies using DBT as sole source of sulfur by the specific oxidative pathway (4S) the Gibb's assay was used. The results showed that only five out 24 isolated colonies gave a blue coloration indicating that DBT had been oxidised to HBP and 19 gave a brown coloration indicating that in these isolates which completely degrade DBT they are not be able to produce HBP (Table 2.2). The five colonies shown to produce HBP were named as F1, F2, F3, F4 and F5. In all five isolates, DBT was degraded and they show the ability to produce HBP which demonstrates similar pathways of *R. erythropolis* to desulfurize DBT. The ability of the selected isolated microbes to convert organic sulfur compound to sulfate without degrading the calorific value of the fuel but the isolates were not reported as new strains. Therefore I continued by focusing on processes for the deliberate development of biodesulfurization by the known bacteria.

2.6 Conclusion

In view of the disappointing results (failure to have discovered a novel strain), I decided to turn to finding ways of enhancing the best presently known biodesulfurization agent.

Chapter 3 : Biodesulfurization by R. erythropolis and S. putrefaciens

3.1 Desulfurizing bacteria

Several kinds of microorganisms have been suggested to metabolize sulfur compounds. In the development of a BDS process the most important (in number and diversity) is bacteria that have the ability to consume DBTs as their energy source. However, the first attempt for BDS failed because these species could not specifically remove sulfur. Some of the microorganisms could use DBT as carbon and sulfur sources (Kirshenbaum, 1961; Malik, 1980) and metabolized them into products which significantly inhibited microbial growth and DBT oxidation (Kodama et al., 1973, Monticello, 1985). Several different genera have been reported that attack carbon atoms in the DBT phenyl ring, known as the Kodama pathway, and the majority of investigations have focused on Psedomonas cultures (Hartdegen et al., 1984). Monticello in 1985, showed the Kodama pathway in *Psedomonas alcaligenes and P. putida*. In this oxidation pathway one of the phenyl rings is attacked by bacteria and results in the breakage of a phenyl ring. This pathway could not specifically remove sulfur from the molecule; therefore it is not considered a sulfur removal approach. After this attempts were made to isolate a variety of strains that could remove sulfur from DBT without ring cleavage and resulted in Kilbane, in 1990, proposing the 4S pathway that implied consecutive oxidation of DBT by *Rhodococcus erythropolis*. Researchers tried to isolate bacteria that could remove sulfur non-destructively. *Brevibacterium*, (Van Afferdin et al., 1990) and *Arthrobacter* sp. K3b (Dahlberg et al., 1993) was also reported to act similarly to *Rhodococcus*. Although the reported desulfurization pathway was partly similar to the 4S pathway, but still the aromatic compounds were still degraded during the process.

Several microorganisms have been suggested for the BDS process but the majority of the studies have been conducted on the selective removal of organosulfur compounds with *R. erythropolis* and other microorganisms as the biological catalyst. To date, several genera have been reported to selectively remove sulfur from several model compounds however; most of them belong to the *Rhodococcus* genus. A number of DBT-desulfurizing *Rhodococcus* species have been reported, including *R. rhodochrous* IGTS8 (Kayser *et al*., 1993), *R. erythropolis* I-19 (Folsom et al., 1999), *Rhodococcus* strain P32C1 (Maghsoudi et al., 2000), *R. erythropolis* rKA2-5-1 (Kobayashi et al., 2000), *R. erythropolis* strain T09 (Matsui et al.,2000), *Rhodococcus* strain WU-K2R (Kirimura et al., 2002) and *Rhodococcus* strain ECRD-1 (Grossman et al., 1999) which was initially classified as *Arthrobacter* (Lee et al., 1995) and sometimes classified as *R. erythropolis* X310 (Denis-Larose et al., 1997). The American Type Culture Collection (ATCC) assesses that they have compared these closely related strains and *R. erythropolis* IGTS8 has the highest desulfurization capabilities.

Several bacterial species can utilize the organic sulfur compounds in crude oil yet preserve fuel value and have therefore been explored for the purpose of desulfurization. The most employed microorganisms belong to genus *Rhodococcus*, such as *Rhodococcus erythropolis* IGTS8. *Rhodococcus* strain IGTS8 is able to utilize a wide range of organic sulfur compounds as the sole source of sulfur, i.e. thiophenes, sulfides, disulfides, mercaptans, sulfoxides and sulfones (Kayser et al., 1993). Therefore this bacterial strain has been used in this work in the first instance.

3.1.1 The importance of **Rhodococcus erythropolis**

The value of Rhodococci is clearly revealed in its diverse range of metabolic capabilities and these features are presented in various environments. Rhodococci, because of their environmental persistence, tolerance to starvation, frequent lack of catabolite repression are ideal candidates for bioremediation of contaminated sites. These bacteria possess the capability for degrading a large number of organic compounds including various chemical pollutants such as aromatic hydrocarbons, simple hydrocarbons, nitroaromatics, chlorinated polycyclic aromatics such as polychlorinated biphenyls (PCBs), and other refractory toxicants (Bell et al., 1998; Larkin et al., 2005). Another class of hazardous chemicals that are persistent in the environment are polychlorinated biphenyls, which are widely used in industry, are known to be degradable by Rhodococci and may also help in the bioremediation process (Bell et al., 1998). *Rhodococcus* species could be considered the ideal candidates to enhance the bioremediation of contaminated sites because of the following characteristics which they possess: tolerance to starvation; environmental persistence and their frequent lack of catabolite repression (Vellore, 2001). Some species of *Rhodococcus* can grow using gaseous hydrocarbons including butane, acetylene and propane (Bell et al., 1998). *R. erythropolis* strain IGTS8 has the ability to remove organic sulfur compounds from fossil fuels such as coal and petroleum. This strain specifically breaks the carbon-sulfur bonds in DBT without degrading the aromatic ring.

This biocatalytic desulfurization of IGTS8 does not affect the fuel value of the compound so is being developed by the biotechnology industry (Gray et al. 1996).

3.2 Experimental

3.2.1 Bacterial strains

Rhodococcus erythropolis IGTS8 (ATCC 53968) was obtained from the American Type Culture Collections. *Shewanella putrefaciens* (NCIMB 8768) was obtained from the National Collections of Industrial and Marine Bacteria Ltd (Aberdeen, UK).

3.2.2 Media

The compositions of nutrient agar and nutrient broth are presented in Table 3.1 and 3.2 The basic salt medium was prepared in two solutions as shown in Table 2.2 and 2.3 (Patel et al., 1997). All media were sterilised by autoclaving at 121 °C for 15 min.

Table 3.1: Composition of nutrient agar.

Component	Amount
Peptone	5.0 *g*
Meat extract	3.0 *g*
Agar-agar	12.0 *g*
Water	1.0 L
pH	7.0 ± 0.2

Table 3.2: Composition of nutrient broth.

Component	**Amount**
Lab- Lemco powder	1.0 *g*
Yeast extract	2.0 *g*
Peptone	5.0 *g*
Sodium chloride	5.0 *g*
Water	1.0 L
pH	7.4 ± 0.2

3.2.3 Bacterial revival

Freeze-dried cultures were rehydrated and revived according to the instructions of The National Collections of Industrial and Marine Bacteria Ltd. (Aberdeen, UK). An opened vial was rehydrated with 0.5 mL of medium (nutrient medium). The contents were mixed without frothing. The suspension was divided into two aliquots and each aliquot was sub-cultured into 5 mL of medium in a Universal bottle. The Universal bottles were incubated on an orbital shaker (L.H. Engineering Co. Ltd., UK) at 100 rpm and 25 °C for 24 hours. The cultures were then transferred to 250 mL flasks containing 100 mL of medium and incubated at 100 rpm and 25 °C.

3.2.4 Bacterial growth

Growth of *S. putrefaciens* and *R. erythropolis* under their optimal conditions were measured from their optical densities at 600 nm (A_{600}) using a Jenway- 6505 UV/Visible (Paterson Scientific, UK) spectrophotometer.

A 10 mL of solution prepared liquid media (Nutrient broth) was transferred to a universal using sterilized conditions (flaming under a laminar flow hood) and inoculated with the bacteria and incubated at 100 rpm at 25 ºC for 12 hours to reach the exponential growth phase. Both bacterial strains were cultured by using 1 ml inoculum added to a 100 mL of nutrient broth in a 250-mL flask. Flasks were then incubated in an orbital shaker (Luckham model R300, UK) at 100 rpm at 25 ºC. Samples were taken every three hours and monitored for bacterial growth by a spectrophotometer at 600 nm until a stable optical density was reached (All the experiments were run in triplicate).

3.2.5 Population density of bacteria

The inoculum (1 mL) prepared as in Section 3.2.5 was added to 100 mL nutrient broth and incubated at 100 rpm. The procedure was carried out for subsequent incubation periods of 1, 3, 5, 7, 9, 12, 15, 18, 22, 25 and 30 hours. After each incubation period, the harvested cells were resuspended in Ringer's solution, the optical density (600 nm) measured, spread plates prepared using the 1×10^{-5}, 1×10^{-6}, 1×10^{-7}, 1×10^{-8} and 1×10^{-9} suspensions of the ten-fold dilution series, 0.1 mL of each dilution of cell suspension pipetted onto separate BSM agar plates, and then spread across the surfaces of the plates. Three replicates were made of each dilution. All plates were incubated at 25 ºC for 2-3 days, or until colonies were countable, i.e. large enough to be visible, but not so large as to make distinction between colonies difficult. Then, the colonies of each plate were counted. Using the dilution factor and volume of suspension added to each plate, the number of colony forming units (CFU) was then calculated. Once the population density of the original suspension had been calculated, so that the dilution factor and turbidity displays the population density value.

3.2.6 Dry weight detection

The cells (10 mL) prepared as in Section 3.2.5 were washed twice with sterile distilled water by centrifugation at 12000 *g* for 10 min. Cells were resuspended in a small volume (1 mL) of sterile distilled water and transferred to pre-weighed cups. The centrifuge tubes were washed with a further volume of water (1 mL) and the water plus cells was added to the cups. The cups were placed in the oven and set at 110 °C overnight. After this the cups were cooled in a desicator, and then reweighed and the average dry weight of the cells (g/L) calculated.

3.2.7 Bacterial harvest

The cultures were grown until the mid-exponential growth phase in a liquid medium and then centrifuged (Hettick-EBA 20-Germany Centrifuge) at 1400 *g* for 10 min. The supernatant was discarded and the cell pellets were washed twice with Ringer's solution. The Ringer's solution was prepared by dissolving 1 tablet (Fisher) in 500 mL of water. The cells were then resuspended in the same solution to $A_{600} = 1.0$ and used on the day of harvesting.

3.2.8 Bacterial maintenance and storage

The bacteria were maintained by sub-culturing into a liquid medium or plating on a solid medium (nutrient agar) weekly. For long-term storage, 0.85 ml of culture was transferred to 0.15 ml of sterile glycerol (sterilized by autoclave at 121 °C for 15 min) in a screw cap tube. All tubes were mixed by vortex to ensure that the glycerol was evenly dispersed. The tubes were kept in a labelled airtight gasket and frozen at 80 °C. The bacteria can be recovered by scraping the frozen surface of the cultures with a sterile inoculating needle, and then immediately streaking the cells that adhere to the needle onto the surface of a nutrient agar plate or transferring the defrosted cells to fresh liquid medium.

3.2.9 Biodesulfurization of DBT by S. putrefaciens

In a previous investigation carried out at Cranfield University, it has been found that using the bacterium *S. putrefaciens* in clay desulfurization, sulfur odour was reduced. Experiments have also been carried out to examine the use of this bacterium for coal desulfurization (Prayuenyong, 2001). The present study is therefore also aimed at studying the desulfurization ability of the bacterium *S. putrefaciens* strain NCIMB 8768 and comparing its biodesulfurization activity profile with those achieved using the widely studied strain *R. erythropolis* (strain IGTS8).

3.2.10 Bacterial enhancement

The original culture of *S. putrefaciens* did not grow using DBT as a sole source of sulfur. Therefore, to enhance bacterial growth on DBT, experiments were carried out by enrichment of bacteria. A sulfur source (DBT) was added aseptically to a 250 mL flask containing 100 mL BSM. One mL of inoculum which contains bacteria grown in nutrient medium was added into the flask at 30 ºC and 100 rpm. After 3 days a further 2 mL of inoculum was added to the same flask and it was left for 3 more days so as to get a good growth of the culture.

After enhancement of the bacteria the capabilities of *R. erythropolis* IGTS8 and *S. putrefaciens* NCIMB 8768 for desulfurization with DBT as the sulfur model compound were investigated.

3.2.11 DBT desulfurization capability

In this study of desulfurization capability of *S. putrefaciens* (NCIMB) and *R. erythropolis* IGTS8, DBT was the sole sulfur source in BSM.

Cells were grown until the mid-exponential growth phase and harvested by centrifugation at 6000 rpm for 15 min. The cells were then resuspended in the same solution to $A_{600} = 1.0$ and used on the day of harvesting. One mL of inoculum was added to 250 mL flasks containing 100 mL of BSM with 0.3 mM of DBT-ethanol solution and incubated at 30 °C (100 rpm).

3.2.12 Effect of DBT concentration

To study DBT degradation by the two bacteria, *S. putrefaciens* (NCIMB) and ***R.*** *erythropolis* IGTS8, the bacteria grown in BSM with DBT were harvested as described in the experimental section, and resuspended back in BSM to $A_{600} = 1.0$. One mL of inoculum was added to 250 mL flasks containing 100 mL of BSM with DBT at a final concentration of 0.3, 0.6 and 0.9 mM and incubated at 30 °C (100 rpm). Control flasks without bacterial cells were also incubated. Samples (5 mL) were taken daily and monitored for bacterial growth at A_{600} and analysed DBT and HBP concentration using high-pressure liquid chromatography (HPLC) (details in 3.3.1).

3.3 Analytical methods

3.3.1 Measurement of hydrocarbons by HPLC

Due to the high resolution of the stationary phase, HPLC is an effective technique for identification of compounds in a mixture. The concentrations of DBT and HBP were analyzed by high-performance liquid chromatography (HPLC) using a HPLC Model LC-10AD VP (Shimadzu) equipped with a Nova Pak phenyl column (3.9×150 mm) with a Restek guard column, (Thames Restek, UK Ltd). An isocratic elution with 60% acetonitrile and 40% water at 1.5 mL/ min was used and detection was realized with a 117 UV detector fixed at 233 nm wavelength. The mobile phase, a mixture of HPLC grade water and acetonitrile was sonicated for 10 min and further deaerated with helium before use.

A high-pressure liquid chromatography (HPLC) method was developed to analyse the concentrations of DBT, and HBP. Samples from experiments described in Sections 3.2.12 and 3.2.13 (1.0 mL) were transferred to ependorf tubes. The bacterial cells were removed by centrifugation at 13000 rpm for 15 min by microcentrifuge (SANYO-MSE micro centowr-UK). The supernatant from each tube was kept in a vial (Fisher, UK) stored at -4 °C until analysed.

3.3.1.1 HPLC calibration

HPLC was carried out by isocratic elution with 60% acetonitrile and 40% water at a flow rate of 1.5 mL/min. Retention times of DBT and its derivatives detected using UV detector at 233 nm are shown in Table 3.3.

Table 3.3: Retention times of DBT and 2-HBP under gradient elution.

Compound	T_R (min)
DBT	9.21
2-HBP	5.57

A chromatogram of DBT and 2-HBP added to the sterile medium growth is shown in Figure 3.1.

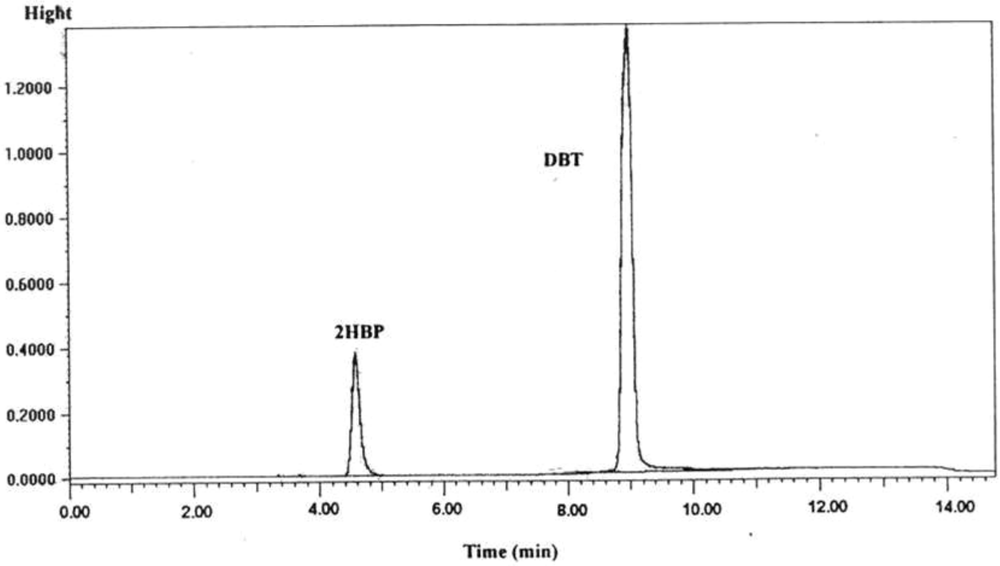

Figure 3.1: HPLC chromatogram of DBT and 2-HBP in sterile medium growth without bacterial inoculum. Concentration of each of compound was 0.1 mM.

To plot the calibration curves of DBT, for HPLC chromatograms, 1 mM of DBT was prepared as stock solution and used for preparing different dilutions. However, this concentration was too high and so for optimum results it was reduced to 0.1 mM. Table 3.4 shows the dilutions used to prepare the standard curves.

Table 3.4: Preparation dilutions of DBT for plotting calibration curve of HPLC analysis.

DBT (0.1 mM) in ethanol (mL)		Acetonitrile (mL)
1	0	2
2	0.4	1.6
3	0.8	1.2
4	1.2	0.8
5	1.6	0.4
6	2	0

The same preparation was carried out for 2-HBP and the calibration curves are presented in Figures 3.2 and 3.3 respectively.

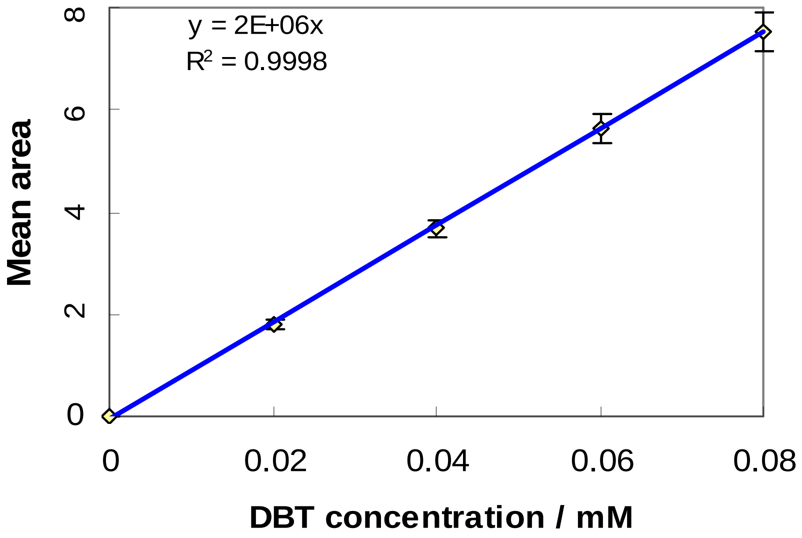

Figure 3.2: Calibration curve of DBT by HPLC analysis. The mean area (calibration units) of the HPLC chromatogram was converted to DBT concentration. Each point is a mean of 3 replicates and the error bar is one standard deviation.

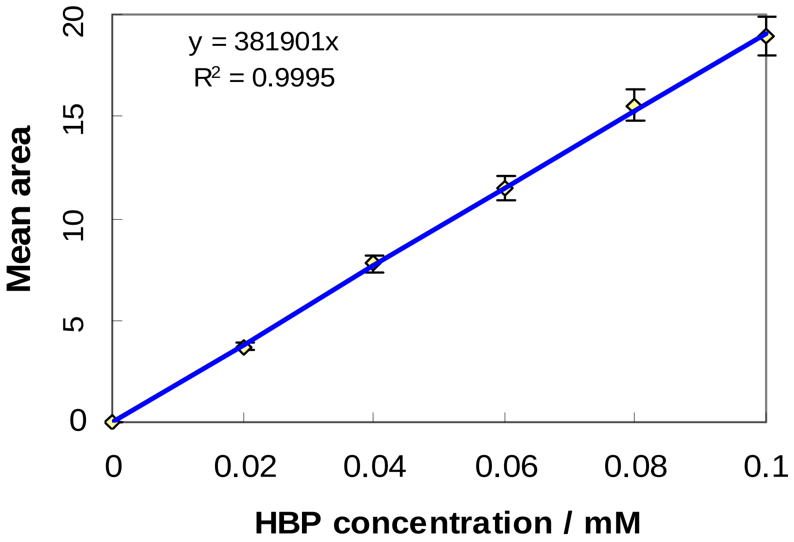

Figure 3.3: Calibration curve of 2-HBP by HPLC analysis. The mean area (calibration units) of the HPLC chromatogram was converted to 2-HBP concentration. Each point is a mean of 3 replicates and error bar is one standard deviation.

3.4 Results

In this study two aerobic bacterial strains were investigated: *Rhodococcus erythropolis* IGTS8 (ATCC 53968) and *Shewanella putrefaciens* (NCIMB 8768). *R. erythropolis* IGTS8 have been patented by the Institute of Gas Technology and licensed for commercial development to Energy Biosystem Corporation (McFarland, 1998). Colonies formed by *R. erythropolis* have a distinct orange, salmon pink or cream pigmentation (which is caused by the presence of carotenoids) and they are smooth and large with a diameter of 2-4 µm. *Shewanella putrefaciens* (NCIMB 8768) formerly called *Pseudomonas rubescens,* has been isolated by Pivnick (1955) and in both solid and liquid media is often recognizable by its bright pink colour. *S. putrefaciens* is the only non-fermentative Gram-negative rod that produces hydrogen sulfide (Tsai and You, 2006) but not been proved to possess the capacity to degrade the thiophenic compounds present in oil. Some of the characteristics of these microorganisms are summarised in Table 3.5.

Table 3.5: Characteristics of the bacteria

Description	***R. erythropolis* IGTS8 (Kilbabe, 1990)**	***S. putrefaciens* NCIMB 8768 (Pivnick, 1955)**
Gram stain	+	-
Motility	-	+
Catalase	+	+
Oxidase	-	+
Shape	Rod (2-3 µm)	Rod(1.5-2 µm)
Colony	Round (diameter: 2-4 mm)	Round (diameter: 1-1.5 mm)
Isolation source	Soil	Oil emulsion

The Gram stain performed in this study is described in section 2.3.5.5. As shown in Figure 3.4, *R. erythropolis* IGTS8 has a thick wall of peptido peptidoglycan overlaying the cytoplasmic membrane which presents a purple colour-a gram positive reaction. *S. putrefaciens* with a multilayered structure composed of a thin layer of peptidoglycan surrounded by an outer layer of protein and lipopolysaccharide presents a pink colour-a gram negative reaction: the cell wall of *S. putrefaciens* is thus rich in lipids compared to the cell wall of *R. erythropolis.*

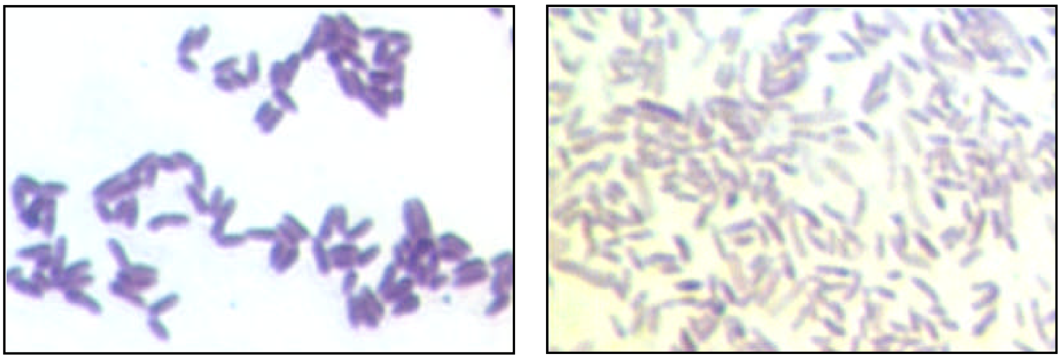

Figure 3.4: Gram stain culture of *R. erythropolis* (left) and *S. putrefaciens* (right) (4000X).

Growth curves of *S. putrefaciens* and *R. erythropolis* in nutrient medium at their optimal temperature are shown in Figure 3.5. Growth patterns of these two bacteria under their respective optimal condition were typical for bacterial growth. An initial lag phase before growth accelerated was observed. After the lag phase they enter to the exponential phase. Cells in exponential growth are usually in their healthiest state, and thus in the mid exponential phase it is often desirable to use then for further studies. The mid exponential phase for *R. erythropolis* and *S. putrefaciens* was after around 12 hours incubation time. As figure 3.5 shows, the growth rate of *R. erythropolis* is slightly faster than *S. putrefaciens* and the deceleration phase of both organisms was seen after approximately 24 hours.

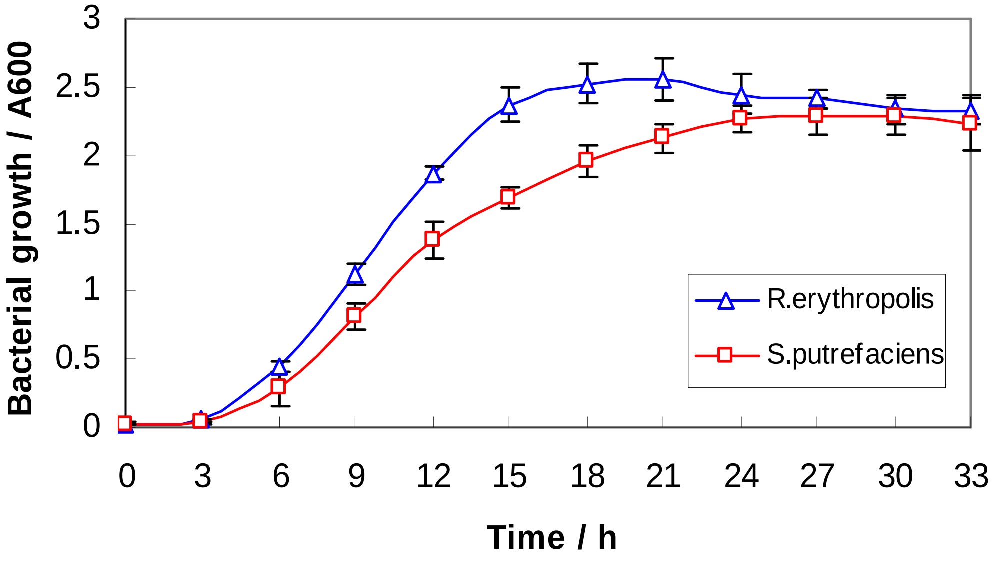

Figure 3.5: Growth of *R. erythropolis* IGTS8 and *S. putrefaciens* in nutrient medium monitored via optical observation at 600nm. Cell grown in nutrient medium and incubated at 30 °C, 100 rpm. Samples taken every 3 hours and were monitored for bacteria growth. Each point is a mean of triplicate, and error bar is a standard deviation.

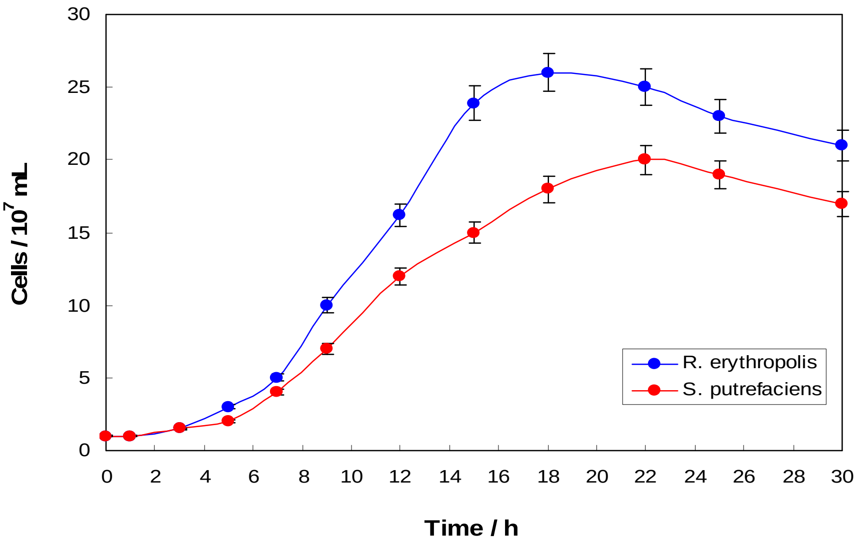

Figure 3.6: Number of cells calculated by colony forming unit for *R. erythropolis* and *S. putrefaciens* cultured in nutrient broth at 25 °C.

Dibenzothiophene (DBT) as a sole sulfur source in BSM in three concentrations (0.3 mM, 0.6 mM and 0.9 mM) was supplied to study the growth of *R. erythropolis* and *S. putrefaciens* separately. Growth patterns of these two strains in different concentration of DBT were not the same (Fig. 3.7). For *R. erythropolis* an initial lag phase before growth accelerated was observed and after the lag phase it grew slightly faster than *S. putrefaciens*. Growth of *R. erythropolis* declined in the higher concentration of DBT. *S. putrefaciens* also grew in BSM+DBT but there was a significant decrease in growth and as is shown, its growth was slower than *R. erythropolis*. The results indicated that these two bacteria are sensitive to high concentration of DBT. There was no DBT degradation in the control flasks (incubated without bacteria cells).

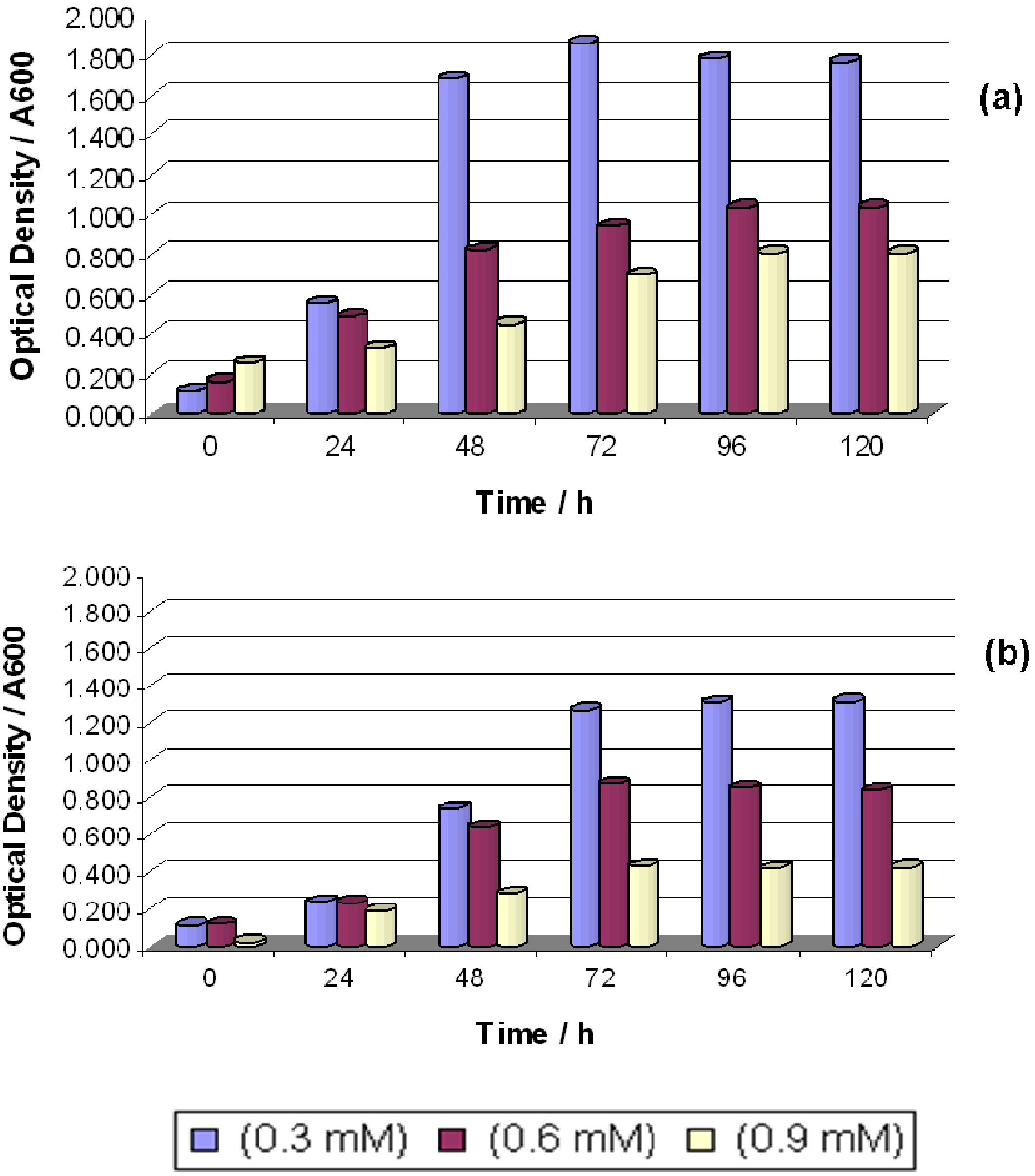

Figure 3.7: Growth of *R. erythropolis* IGTS8 (a) and *S. putrefaciens* (b) in BSM with three concentration of DBT, as the sole source of sulfur. Each value is a mean of three replicate.

Production of 2-HBP from DBT degradation at the concentration of 0.3 mM by growing *R. erythropolis* and *S. putrefaciens* was monitored by HPLC analysis and are presented in Figures 3.8 and 3.9 respectively. The DBT concentration was halved after 3 days, incubation. 2-HBP analysis confirmed that similarly to *R. erythropolis, S. putrefaciens* desulfurized DBT through the selective cleavage of the C-S bonds, resulting in the accumulation of 2-HBP. The detection of 2-HBP, when *Shewanella* utilized DBT as the sole sulfur source indicates that the DBT-desulfurizing pathway is the 4S pathway as reported by Kilbane et al. (1992). This type of reaction is desirable for practical desulfurization since the sulfur atom is removed without C-C bond cleavage, that is, without the loss of calorific energy. The amounts of 2-HBP produced and DBT degraded of *R. erythropolis* were not equivalent (Fig. 3.10) ((Kayser et al., 1993).

It has been reported that 2-HBP is toxic to bacterial cells, hence biodesulfurization is inhibited by accumulation of 2-HBP (Zhang et al., 2005). A complicating factor in this experiment that the end product 2-HBP is somewhat inhibitory to cell growth and possibly to desulfurization activity.

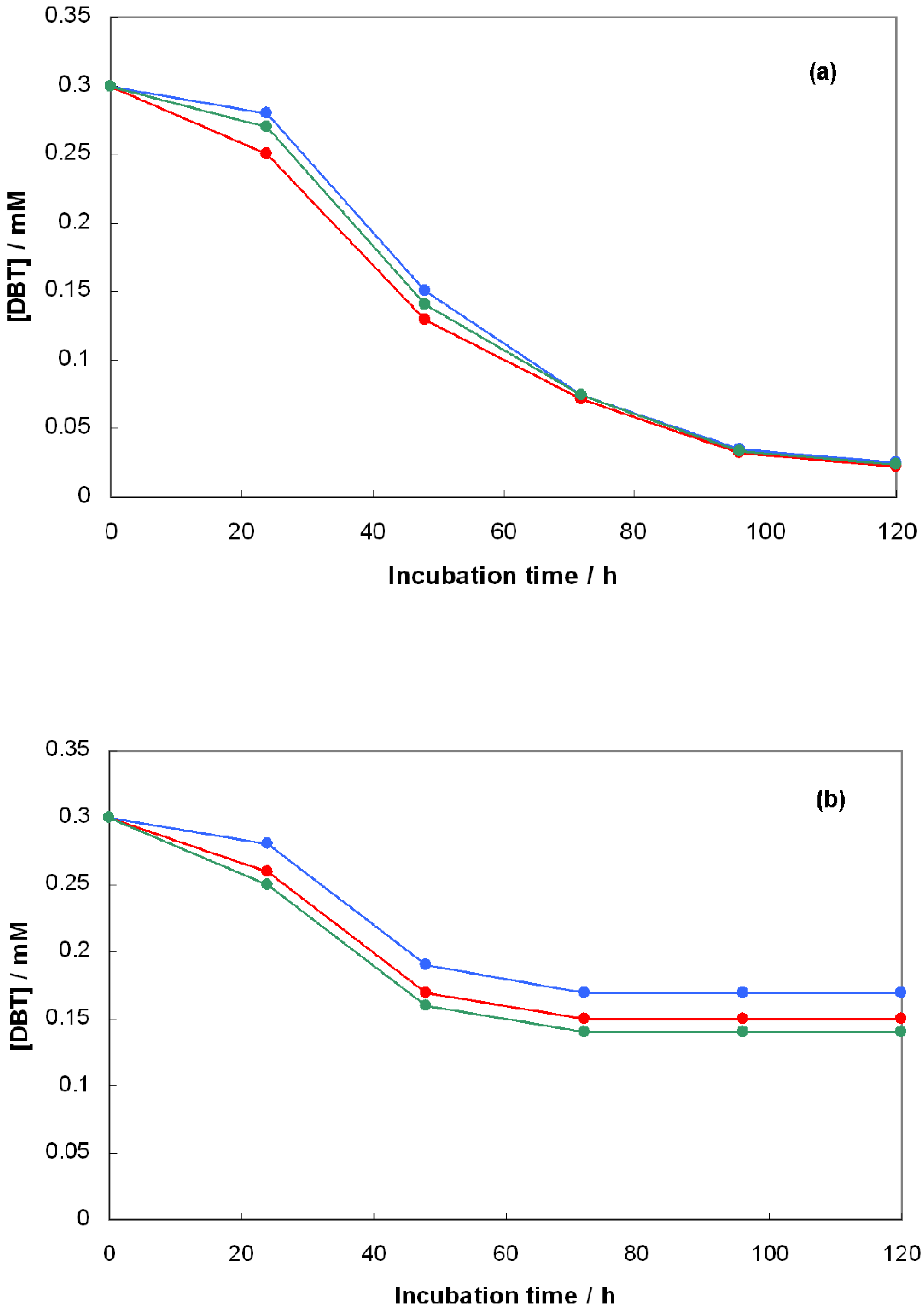

Figure 3.8: DBT degradation by *R. erythropolis* IGTS8 (a) and *S. putrefaciens* NCIMB (b) at the final concentration of 0.3 mM as the sole sulfur source.

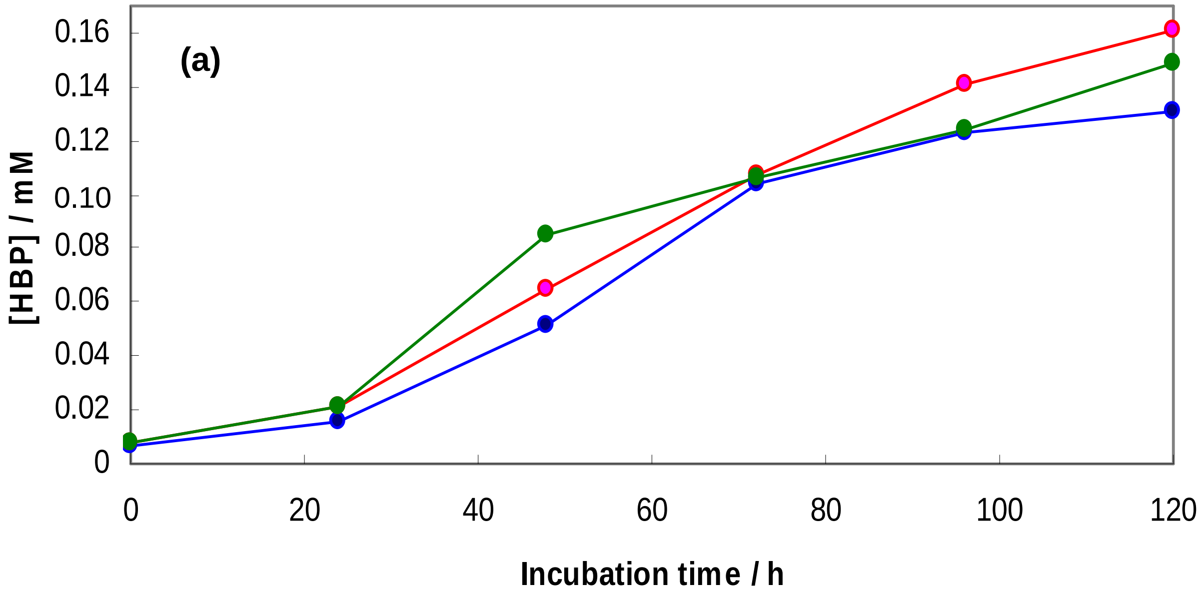

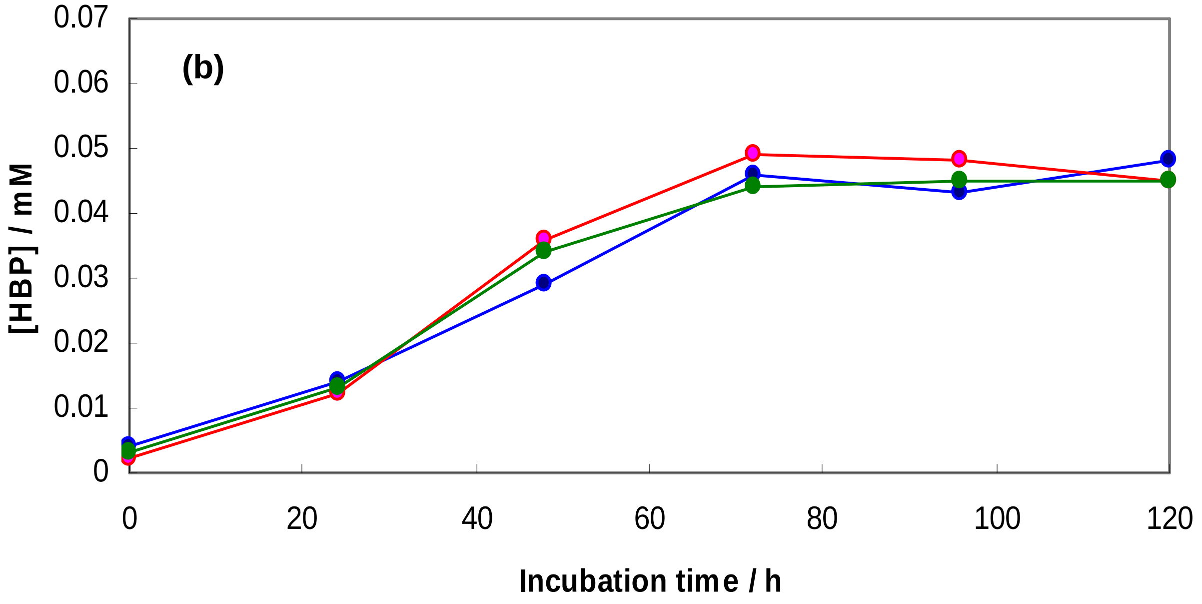

Figure 3.9: HBP production by *R. erythropolis* IGTS8 (a) and *S. putrefaciens* NCIMB (b) in DBT at the final concentration of 0.3 mM as the sole sulfur source.

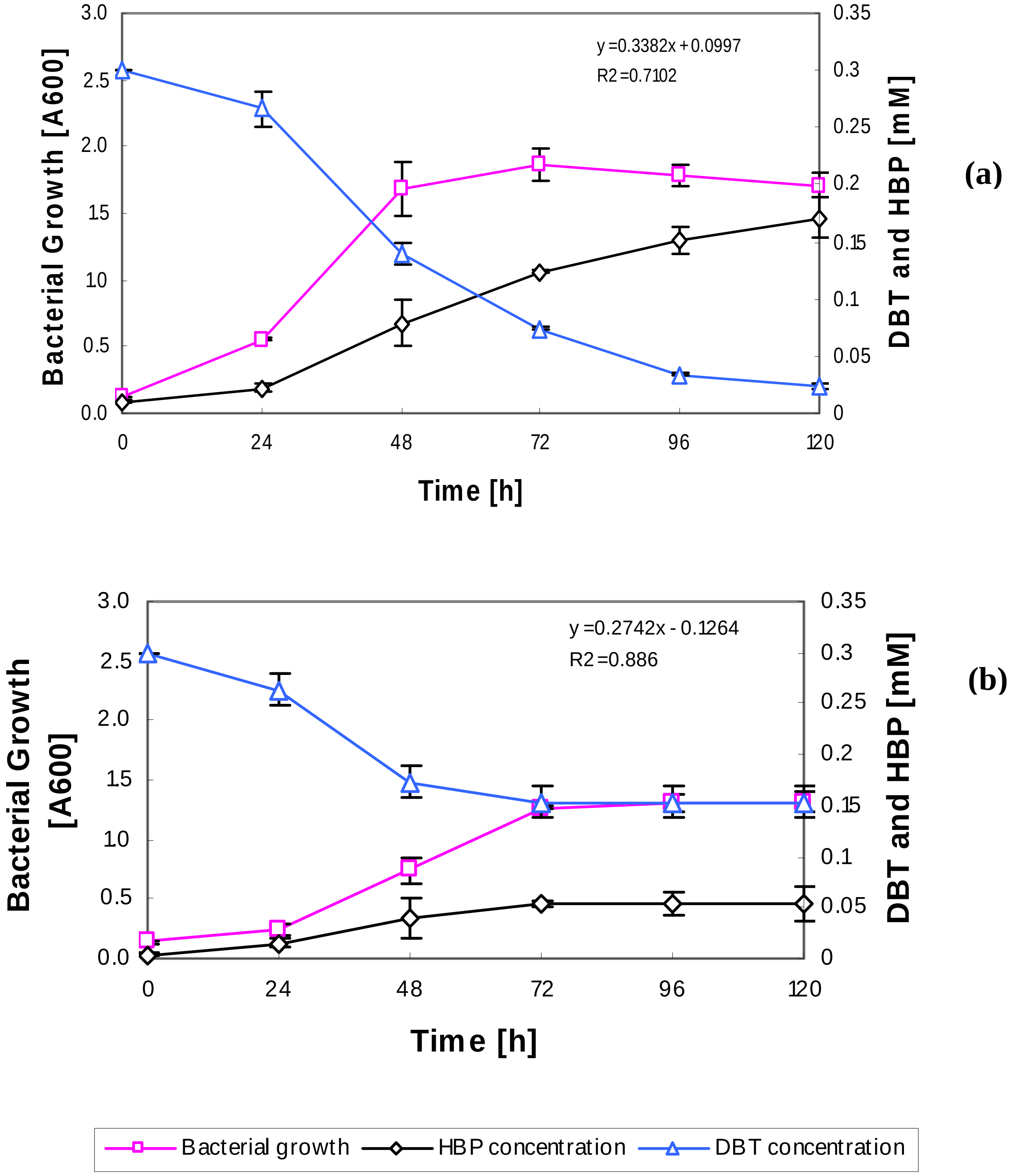

Figure 3.10: Comparison of the desulfurization capability of *R. erythropolis* (a) IGTS8 and *S. putrefaciens* NCIMB (b) in DBT at the final concentration of 0.3 mM as the sole sulfur source.

Figure 3.11 compares the production of 2-HBP by growth of *R. erythropolis* and *S. putrefaciens* in different concentration of DBT. Bacterial growth at higher concentration of DBT is inhibited and a significant decrease of HBP production was observed at 0.6, or 0.9 mM of DBT, presumably because the bacteria could not tolerate high concentration of the sulfur source.

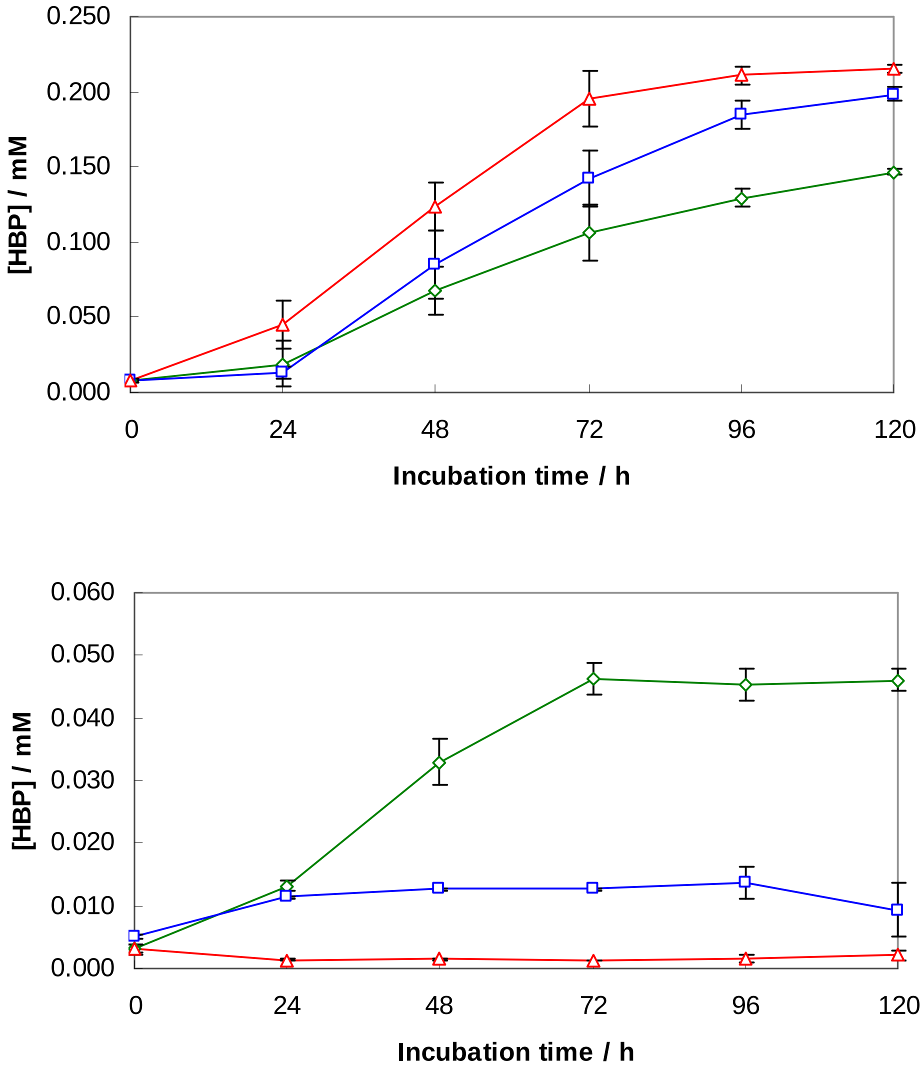

Figure 3.11: Production of HBPby *R. erythropolis* (upper) and *S. putrefaciens* (lower) in different concentration of DBT: —◇— 0.3 mM, —□— 0.6 mM, —△— 0.9 mM

3.5 Summary

S. putrefaciens has shown high activity and stability to remove sulfur from organic compounds that commonly exist in crude oil. However, this activity is unlikely to be sufficient for the design of commercial applications and microorganisms with high activity and selectivity for thiophenes are required. So development of bacteria for sulfur removal and design of new biodesulfurization processes by improvement of the permeabilization of the bacteria are required. This is the topic of the rest of the thesis.

In order to avoid confusion due to the wide variety of conditions found in the literature, I compared S. putrefaciens with what is considered to be the best known BDS strain, *R. erythropolis* IGTS8, under my identical conditions, and found S. putrefaciens to be inferior.

Chapter 4 : Magnetic nanomaterials

In order to render desulfurizing bacteria magnetic, I have explored decorating their outer surfaces with magnetic nanoparticles. Biocompatible magnetic nanoparticles have a wide range of applications in bioscience and they are also able to solve many separation problems in industry. Therefore in the next chapter I describe the synthesis of these nanoparticle coated bacteria.

4.1 Magnetism

From the atomic view of matter, the source of magnetic phenomena in materials is electron motion. Each electron has both angular momentum orbital (from motion around the nucleus) and spin angular (around its own momentum axis) which combine to give the resultant magnetic moment of an atom. Most materials have magnetic properties which are small. Overall, the magnetic behaviour of materials is classified into five types depending on the magnetic response to an external applied magnetic field: ferromagnetism, ferrimagnetism, antiferromagnetism, paramagnetism and diamagnetism. All materials exhibit at least one of these types of magnetism.

Ferromagnetic materials can be permanently magnetized upon application of an external magnetic field for which the susceptibility is positive ($\chi > 0$). Iron, cobalt and nickel are typical ferromagnetic elements. Ferrimagnetism is another type of magnetic ordering in which the unequal magnetic moments of atoms on different sublattices produce spontaneous magnetization in the material below the Currie temperature. Magnetite,

Fe_3O_4, is a common example of a ferrimagnetic mineral in which sublattices consist of different ions (Fe^{2+} and Fe^{3+}). Ferrimagnetism is similar to ferromagnetism and exhibits the same hallmarks of ferromagnetic behaviour. In antiferromagnetic materials the spin moments of neighbouring atoms or ions are in exactly opposite directions and the sublattice moments are exactly equal but opposite, so they cancel one another and result in zero net magnetization of the material (Li et al., 1997; Cullity, 1972). Manganese oxide (MnO) is an example of an antiferromagnetic material. In paramagnetic materials some of the atoms or ions have a net magnetic moment due to unpaired electrons in partially filled orbits, so the individual magnetic moments don't interact magnetically. In the presence of a field, they possess a net positive magnetization but when the field is removed the net magnetization is zero. The coupling of atomic magnetic moment is disrupted by heating and above a certain temperature (called Neel temperature) it disappears entirely. So the susceptibility in this case is inversely proportional to the absolute temperature. Above the Neel temperature a material may possess a small positive magnetic susceptibility ($\chi \approx 0$). Conduction electrons which form an energy band in metallic crystals also exhibit paramagnetism. Since, in this case, the excitation of minus spins to the plus spin band is opposed by an increase of kinetic energy of electrons irrespective of temperature; the susceptibility is independent of temperature. Examples of paramagnets are aluminium, platinum and manganese. Diamagnetism is usually very weak and is a fundamental property of all matter. The origin of this magnetism is the orbital rotation of electrons about the nuclei induced electromagnetically by the application of an external field. When all electron orbits are filled, noncooperative orbital behaviour between electrons when exposed to an external magnetic field results in diamagnetism. Diamagnetic material does not support spontaneous magnetization and displays a negative magnetic susceptibility ($\chi < 0$) (Li, 2000). Examples of diamagnets are copper, silver, gold, bismuth and beryllium.

4.2 Magnetite

Magnetite (Fe_3O_4) is a natural magnet and was the first magnetic material known (Cornell et al., 1996). Today magnetite is commonly found in igneous, metamorphic, and sedimentary rocks. Magnetite is also found in living organisms, such as bacteria (*Aquaspirillum magnetotacticum*), in the brain of bees, termites, birds (e.g. pigeons) and humans (Liong 2005).The presence of this magnetic mineral provides the organisms with natural navigation capability. A picture of magnetite in its natural form is shown in Figure 4.1.

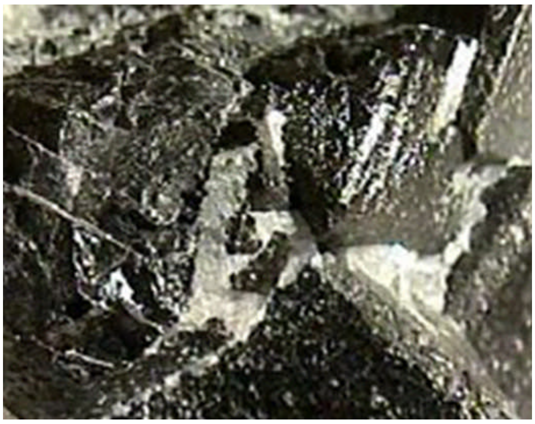

Figure 4.1: Natural magnetite

4.3 Superparamagnetism

The magnetic properties of ferromagnetic particles depend on their size. The large magnetic materials have a multidomain structure and display magnetic properties regardless of the existent of an applied magnetic field. These magnetic domains interact with each other and spin in a single particle coupled together. When the magnetic materials are composed of very small crystallites, i.e. below a critical diameter, depending on the particle material, they contain only one magnetic domain. These particles are at a position of uniform magnetization at any field without interaction with neighbouring domains in one particle or a wall dispersed suspension. If an external magnetic field is applied, the particles will align producing a net moment and display magnetic properties, but when the applied magnetic field is removed, permanent magnetization does not remain. The reason for this phenomenon, superparamagnetism, is that the single domains return to their disordered status. This behaviour in a manner is similar to pararamagnetic materials, but the difference is that each molecule has a large net moment i.e. instead of influencing each atom independently by external magnetic field; the magnetic moment of the entire crystallite tends to align with the magnetic field (Fried et al., 2001; Harris et al., 2003).

Morrish and Yu (1956) determined that Fe_3O_4 particles are single domains when the diameter is 50 nm or less; this threshold is approximately 8 nm for Fe_2O_3 particles (Schmidt 2001). In fact, the critical diameter is the single domain size of the materials. Therefore, these nanosized particles display magnetic properties under an applied magnetic field, but permanent magnetization does not remain when the applied magnetic field has been removed (Harris et al., 2003).

4.4 What is nanotechnology?

Nanotechnology is defined as the design and fabrication of devices and materials with nanometer dimensions (Ramsden, 2005a). Nanotechnology literally means any technology process on a nanoscale that has applications in chemical, physical, and biological systems at scales ranging from individual atoms or molecules to submicrometer dimensions, as well as the combination of the resulting nanostructures into macroscopic systems. According to the NNI (National Nanotechnology Institute) definition, any structure less than 100 nm is a true nanostructure (Grabar et al., 1997) and unique phenomena are expected at that scale.

There are some general factors that interact with most of the nanoparticulate systems; depending on their own physical and chemical properties; these include pH, surface charge (forces of attraction/repulsion), vibration, centrifugation, stirring etc that can easily and effectively impact on a nanoparticulate system. A notable and important aspect of such systems is that of atomic granularity. The system is granular at atomic dimensions; one cannot expect smooth surfaces or interfaces between different particles. The atom–atom interaction determines the nanoparticles shape, size, geometry, and orientation. All the above-mentioned features greatly contribute to the “self-assembly” property of certain nanoparticulate systems, mostly observed in proteins and nature’s biomachines (Goodsell 2004; Zharov et al., 2005).

Nanotechnology is a new way of thinking for a set of technologies, techniques and processes of science or engineering (Ramsden, 2005a). Similar to electronics and biotechnology which have created their own technological revolutions, it is expected that nanotechnology will have a similar impact, in some areas sooner rather than later.

Nanotechnology is already affecting our lives, and its effects will shortly become even more remarkable. We are all now familiar with the results of miniaturisation and there are daily evidences of how small have become our computers, cameras and telephones. Nanotechnology already has some input here in the silicon chips which are the “brains” of these tools; and the application of nanotechnology is also in evidence in ink jet printers, medical applications and so many other applications. Nanotechnology is trying to alter the properties of substances to furnish a new world of products. These product opportunities will be cheaper, less wasteful of precious resources, non-polluting and all are money spinners. And certainly nanotechnology is the revolution of information processing, whether it is the fast decipherment of our genetic 'fingerprint', to the rapid analysis of drug libraries.

4.5 Nanotechnology and industry

Nanotechnology has potentially a vast influence on industry and it is a radically new approach to manufacturing (Taylor, 2002). Faster computers, drug delivery, advanced pharmacology, biocompatible materials, tissue repair, surface coatings, catalysts, sensors, telecommunications and magnetic materials are just some areas where nanotechnology will have a major impact.

Nanotechnology is likely to have an effective impact on our economy and society in the early twenty-first century, comparable to that of semiconductor technology, information technology, or cellular and molecular biology and healthcare, energy, biotechnology, information technology, and national security. It is broadly felt that nanotechnology will be the next industrial revolution (Baumberg et al., 2007). Science continues to move forward in making the fabrication of nanodevices and systems possible for a variety of applications in chemistry, interfacial science, material science, molecular biology and medicine (Ramsden, 2005a).

4.6 Nanotechnology and bioscience

For several reasons, biological systems are relevant to nanotechnology. First, lots of examples of nanotechnological devices could be found in the living world (Drexler, 1981). However, a second key point is that nanotechnology has been driven and inspired by the example of biological systems and the need (for example, in medicine) to influence biological systems at the scale of a single cell (Phillips et al., 2006). In addition, preliminary steps have been taken to harness the nanotechnology of biological systems and use it to perform useful functions.

The size of one to several nanometers is of central importance to life, justifying the term “nature’s yardstick” for this dimension. The size of cellular organelles and other interesting objects with regard to nanotechnology is summarized in the following graph (Fig. 4.2). It is then easy to understand that interacting, controlling, and altering cellular and subcellular organelles can be achieved best with structures at the same size level as the biomolecular components of interest.

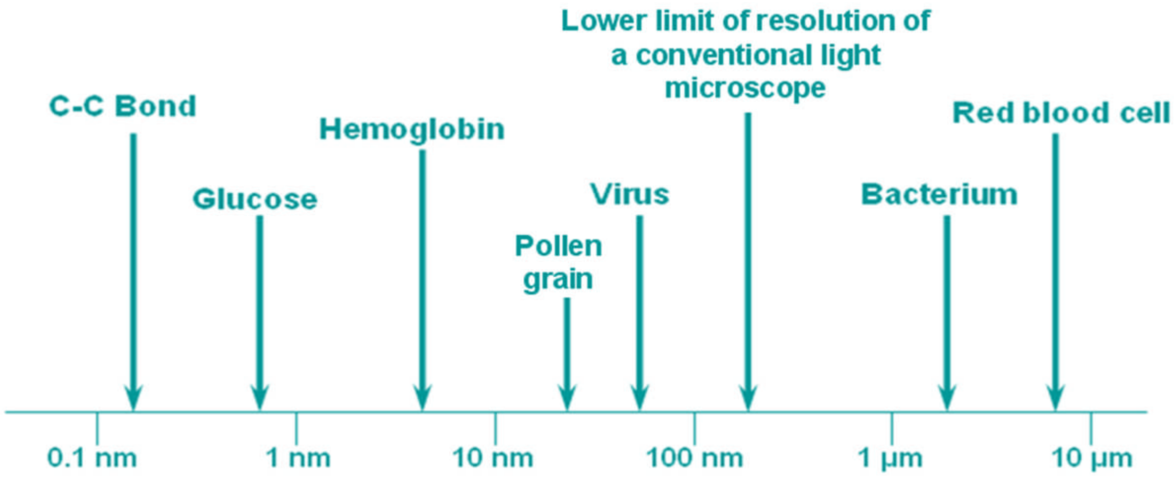

Figure 4.2: Examples of various nanostructures compared with nanostructures and microstructures in biology (Papazoglou & Parthasarathy 2007).

4.7 Applications of magnetic & superparamagnetic nanoparticles

Magnetic nanoparticles are of special interest for their unique magnetic properties due to their reduced size and have potential use in many technological applications (Hyeon 2003). Magnetite is used in a wide range of applications, including data storage (Hyeon, 2003), magnetic fluids (Chikazumi et al., 1987), biotechnology (Gupta, 2004), catalysis (Lu et al., 2004), Magnetic resonance imaging (MRI) (Mornet et al., 2006) and environmental remediation (Elliot et al., 2001; Takafuji et al., 2004) which in all of these applications magnetite is typically used in the form of particles. There are three common magnetite iron oxides, FeO, Fe_2O_3 and Fe_3O_4. From these compounds, magnetic Fe_3O_4 is one of the common iron oxides which has many important technological applications.

The importance of magnetic nanoparticles is the applications of MNPs in separation of biomolecules for characterization or purification and they are a well established alternative to centrifugal separation of biological solutions (Pankhurst et al., 2003), so they can be easily manipulated by permanent magnets or electromagnets, independent of normal microfluidic or biological processes. Therefore the most advantage of the magnetic separation in biotechnology is ease of manipulation of biomolecules that are coated by magnetic particles. Another advantage is a large surface area of particles, which results in a high population of target biomaterials due to a large binding site and high detection signal.

MNPs can resolve many separation problems in industry and are being investigated for a number of different chemical separations applications. The catalysts are easily separated by utilizing the magnetic interaction between the magnetic nanoparticle and an external applied magnetic field that can be easily conjugated with biomolecules (Olsvik et al., 1994; Meza, 1997). The nanoscale particles afford very high surface areas without the use of porous absorbents and can be recovered for reuse. There have been wide studies of magnetic separation techniques of cells, proteins, viruses, bacteria and other biomolecules which achieved enormous success (Prestvik et al., 1997; Olsvik et al., 1994; Neuberger et al., 2005).

Moreover batch magnetic isolation may be faster than other separation methods e.g. standard liquid chromatography procedures. The isolation of biological active compounds, subcellular organelles, and cells composed have been used for many years, therefore the addition of ferrofluids to these systems is useful to speed up the phase separation and the magnetic field of such as additives will induce a faster phase separation (Safarik et al., 2002). On the other hand iron oxide nanoparticles can be easily encased in a biocompatible coating and then functionalized with a biological target agent (Arshady, 2001). Upon placing the MNPs in solution, any target cells can be captured by the functionalized surfaces. By use of a magnet at the side of the solution, a magnetic moment is induced in each of the freely floating particles and sets up a field gradient across the solution. The magnetized particles will move along the field lines and aggregate towards the permanent magnet, separating their bound target from the solution (Fig. 4.3).

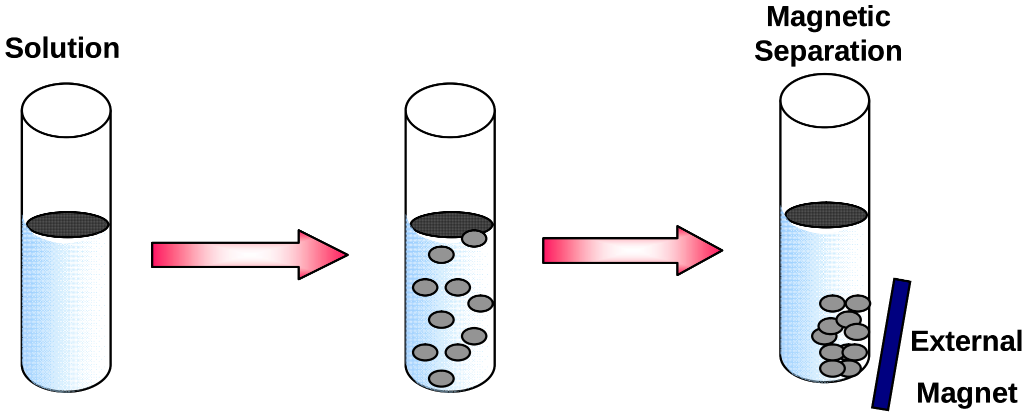

Figure 4.3: Magnetic separation of substances using nanoparticles.

MNPs have several advantages compared to magnetic microparticles, such as high magnetization per unit weight and faster velocities in solution (Moller et al., 2003). Moreover using MNPs in biological applications require compatibility with surface modifireres (Punkhurst 2003). Here I demonstrate the synthesis of nanoparticles that could be utilized in any of these aforementioned applications.

4.8 Fabrication of Fe_3O_4 magnetic nanoparticles

Since the beginning of 19th century, science has had an increasing interest in materials at the nanoscale. Within the field of nanomaterials, the subset of magnetic nanomaterials is of great interest for researchers in a wide range of disciplines and a large amount of research has been dedicated to the synthesis of MNPs. During the last few years particularly many publications have described highly stable, efficient synthetic routes to shape-controlled, and monodisperse MNPs. There are many techniques for the synthesis of MNPs and they have been synthesized with a number of different compositions and phases, including iron oxides, pure metals, spinal type ferromagnets, as well as alloys (Lu et al., 2007).

Although there are many kind of interesting magnetic nanoparticles such as ferrites, cobalt and iron, my study focused on iron oxide magnetic nanoparticles, because they are non toxic, highly magnetic and less susceptible to change due to oxidation. There are three main methods for synthesis magnetic nanoparticles in solution: decomposition of metal organic salts (Park et al., 2004; Sun et al., 2003), microemulsion (Vestal et al., 2002; Christy et al., 2004; Li et al., 2003) and chemical coprecipitation (Gee et al., 2003; Rajendran et al., 2001; Yeong et al., 2003; Yeh et al., 2004). The coprecipitation method is the least expensive, for example iron salts when mixed with a precipitating agent such as sodium hydroxide can form nanoparticles and this is the simplest approach to synthesize them. Decomposition methods need an organic medium at temperatures (200 ºC to 340 ºC) much higher than the coprecipitation method (Sun et al., 2003). Microemulsion reactions are usually the same as for coprecipitation but they require a much larger reaction volumes than the chemical coprecipitation method for equivalent levels of productivity.

For these reason chemical methods of synthesis was examined in the lab and the co-precipitation technique was selected for optimization for the present study. This method is much simpler, cost effective for bulk quantity production and shows great promise for proreducing the high quality nanoparticles needed for future applications. The most significant advantage is that chemical methods have considerable control of particle size distribution, composition and even the particle shape (Gupta 2004).

Moreover, surface modification of the particles during synthesis is easily achieved, providing additional functionality to the nanoparticles (Willard et al., 2004). Whereas, the application of other methods, such as the non-aqueous system, even with excellent particle size distribution, shape, dispersion status and simpler synthesis procedure, have been limited by poorly engineered surfaces. Hence chemical routes often provide the best method for preparation of magnetic nanoparticles, due to their molecular homogeneity and cost effective bulk quantity production and so in this research work, chemical synthesis has been chosen.

4.8.1 Chemical synthesis

In order to use magnetic nanoparticles in magnetobioscence the chemical method could control the morphology, composition and particle size. Moreover the agglomeration could be reduced by different particle coating which is necessary for reliable for reproducibility. Therefore, the chemical method is controllable for different conditions without compromise. However, in practice the difficult task is design the process to achieve the proper characteristics and this needs careful control with subsequent well though out.

One of the chemical techniques for the synthesis of magnetic nanoparticles is the precipitation of products from solution. Coprecipitation was first reported by Welo and Baudisch in 1925 with a study of phase transformations in iron oxide with temperature. Early research on coprecipitation focused on the magnetic behaviour of single domain structures (Slaten, 1960; Kaiser and Miskolczy, 1970; Coey, 1971), but current studies of the synthesis of magnetic nanoparticles concentrate on the improvement of nanoparticle quality and potential applications. This method, because of its simplicity and versatility, is one of the preferred techniques for synthesis of nanoparticles. Synthesis of other types of ferrites, such as $CoFe_2O_4$ and $MnFe_2O_4$ merely requires changing the metal salt.

In this technique, the metal salts are dissolved in water, and a precipitating agent is added to form an insoluble solid. Co-precipitation is a simple and convenient way to synthesize iron oxide nanoparticles and is carried out under an inert atmosphere at room temperature or at elevated temperature. The overall reaction is described by the following equations (1):

$$Fe^{2+} + 2Fe^{3+} + 8OH^{-} \longrightarrow Fe_3O_4 + 4H_2O \qquad (1)$$

$$Fe_3O_4 + 0.25O_2 + 4.5H_2O \longrightarrow 3Fe(OH)_3 \qquad (2)$$

As Fe_3O_4 contains ferrous cations it may oxidise in an oxygen rich environment. This reaction is shown in equation (2). The major advantage of this technique is that large quantities of particles can be synthesized. The size, shape, and composition of the magnetic nanoparticles very much depend on the type of salt used in the reaction, the Fe^{2+}/Fe^{3+}ratio, the temperature of the reaction, the pH value and ionic strength of the media. The iron salts commonly used in chemical coprecipitation are $FeCl_3$ and $FeCl_2$. However, several groups selected iron sulfate and iron nitrate in place of $FeCl_3$ and $FeCl_2$. For the precipitating agent, the majority of works have used NaOH or NH_4OH. The range of reaction temperature reported are from room temperature to 100 ºC with reported the nanoparticle diameters from 2 – 51 nm. The temperature is the major factor in controlling the particle size: increasing the temperature of the reaction, leads to larger particle size (Liong, 2005).

4.8.2 Surface modifications

The synthesised nanoparticles have large surface areas and form agglomerates as a result of attractive van der Waals forces, and of the tendency of the system to minimize the total surface area or interfacial energy. Agglomeration can occur during any of the following stages: synthesis, drying, handling or post-processing (Willard et al., 2004). In many applications where dispersed particles are required, undesirable agglomeration must be prevented and strong repulsive force are needed to counteract the surface-related attraction (Yang et al., 2008; Shan et al., 2004) because it render to reduce the energy associated with the high surface area to volume ratio of the nanoparticles (Lu et al., 2007). On the other hand, for some of my experiments I need a stabilized particle solution in order to make nanofilms. In these the strong repulsive forces between particles lead to agglomeration of particles and increase the thicknesses of the layers.

Therefore I needed to develop protection strategies to chemically stabilize the naked particles so as to get valid data for making nanofilms and investigate the attachment requirements. This stabilization can be achieved by use of surfactant (a synonym for ‘surface-active agent’). Coating the surface of particles with ionic compounds increases electrostatic repulsion when the particles are close together, but coating particles with large molecules, such as polymers with long chains of hydrocarbons offers more efficient stabilization. Recent studies have revealed that coating with hydrocarbons will greatly enhance the stability of the particles (Lu et al., 2007). Several polymers have previously been reported for the surface modification of NPs, because they are ampiphilic and compatible in organic and aqueous media (Wu et al., 2003; Dubertret et al., 2002; Gao et al., 2004; Pellegrino et al., 2004). It must be considered that the selection of a proper surfactant is an important issue for the stabilization of the particles.

4.8.2.1 Surface modification by polymers

A surfactant is a substance which affects the surface or interfacial tension of the medium in which it is dissolved. Surfactants are any substances that lower the surface or interfacial stress of the medium in which they are dissolved. Thus, surfactants by spreading over a surface or interface may decrease or increase surface tension.

Recently, major advances in preparing monodisperse magnetite nanoparticles, of different sizes, have been made by the use of organic additives as surfactants. During nanoparticles synthesis surfactants are used in order to reduce interactions between the particles through an increase in repulsive forces.

There are a number of different polymer matrices, which could be utilized for bio-applications. However dextran and poly ethylene glycol (PEG) are more attractive for bioapplication researches because of their proven resistance to protein adsorption and their functional derivatization (Arshady, 2001; Shi, 2006). These are the reasons for the popularity of dextran or PEG coated magnetic nanoparticles for bio-applications. PEG is broadly used to coat nanoparticles bio-applications for the following reasons:

1) It has a low interfacial free energy in water so PEG improve the uptake of nanoparticles and result of solubilisation of the particles in the cell membrane (Gupta and Curtis 2004).

2) Surfaces covered with PEG can improve biocompatibility and reduce non-specific binding, i.e. nonantigenic and nonimmunogenic (Andrade et al., 1996; Golander et al., 1992). Because PEG has high surface mobility and uncharged hydrophilic residues lead to high steric exclusion (Zhang et al., 2002).

3) Nanoparticles coated with PEG can dissolve in both polar and nonpolar solvents and can interact with cell membranes resulting in enhanced cellular response (Golander et al., 1992).

Amphiphilic polymers like PEG contain both hydrophobic and hydrophilic segments in which the hydrophobic domain interacts with the alkyl chain of the ligands on the surface of the nanoparticle, whereas the hydrophilic group faces outwards and renders the nanoparticle water soluble. The amphiphilic polymer coating is generally thin and can be made from biocompatible polymers; in contrast, the crosslinked dextran coating layer increases the particle radius significantly (Yang et al., 2008). Therefore magnetic nanopaticles coated by PEG may be more compact because the polymer coating is thin and well defined and they should be more favourable in binding kinetics.

Hence the -COOH groups on PEG may lead to undesirable problem, crosslinking, giving rise to massive aggregation of the nanoparticles and destruction of the stable suspension. PEG has two or more –COOH groups on the long chain of the molecule which may lead to binding with two or more particles surrounding it. A possible way out of this problem is to increase the separation between the particles by use of a high concentration surfactant solution during the coating process. Thus, the chance of one surfactant molecule reduce to meet two or more particles before the –NH_2 groups were replaced with –COOH groups on the molecule.

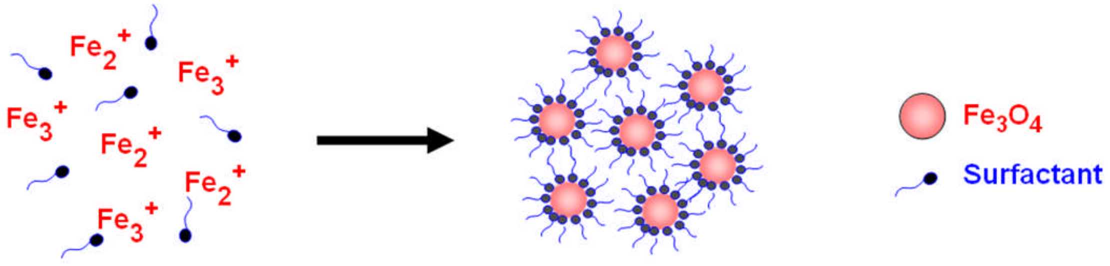

Figure 4.4: The schematic growth of Fe_3O_4/PEG superparamagnetic nanoparticles.

For bioapplications, the size, surface chemistry and charge of the magnetic nanoparticles is important and strongly effective (Chouly et al., 1996). So, in order to produce particles without agglomeration, we used surfactants to control the dispersion during synthesis.

4.9 Experimental procedure for chemical synthesis

In this study, two chemical methods for producing magnetic ferrofluid have been selected based on the criteria that the techniques are accessible. The materials used are commercially available and the least expensive to produce in large quantities (of the order of grams). They have successfully been utilized to synthesize magnetic nano-particles. In the first method, the magnetic fluid was prepared at room temperature and in the second approach a stable dispersion of magnetite fluid was obtained at higher temperature with non-polar diameters of 50 nm. Details of the second method will provide further understanding of the work that has been carried out. The main characteristics of these methods are to obtain an ultrafine magnetic oxide by a chemical reaction from an aqueous solution containing ferrous (Fe^{2+}) and ferric (Fe^{3+}) ions, and to achieve strong adsorption of cells on the magnetic particles in a water solution. These methods do not require a long preparation time as in the grinding method and they are suitable for mass production of magnetic fluids. A disadvantage suffered by all the techniques is heterogeneity in the size distribution of the resulting magnetic particles.

4.9.1 Synthesis of Fe_3O_4 nanoparticles at room temperature

Magnetic nanoparticles were synthesized using the procedure described by Yeh et al., (2004) to obtain Fe_3O_4 nanoparticles: briefly, 25 mL of 0.2 M ferrous chloride ($FeCl_2$) was mixed with 100 mL of 0.1 M ferric chloride ($FeCl_3$) solution in a flask at room temperature and then 3 mL of 2 M HCl solution was added to make the solution slightly acidic. Then 1 *g* of glycine was added, and 11 mL 5 M NaOH solution was slowly dripped into the mixture to increase its pH to over 10, to provide an alkaline environment for Fe_3O_4 to precipitate; next, an additional 3 g of glycine was added, and the mixture agitated with an FB15024 vortexer (Topmix, UK) for 10–15 min and then sonicated for 30 min; subsequently 5 mL acetone was added and agitated. The resulting precipitate (Fe_3O_4) was isolated with a permanent magnet and the supernatant discarded by decantation. The precipitate was washed twice with ultrapure water followed by centrifugation at 2500 *g* for 5 min to remove excess ions in the suspension and obtain water-dispersible nanoparticles. Finally, the washed precipitate was dispersed in ultrapure water for further investigation.

4.9.2 Synthesis of 50 nm Fe_3O_4 nanoparticles at 75 °C

Ferric salt, $Fe(NO_3)_3$, was dissolved in 12.5 mL of ultrapure water in a 100 mL 3-neck flask to make a 0.9 mM solution and purged with nitrogen for at least 30 min. Ferrous salt, $FeSO_4$, was then added to give the same concentration, and the nitrogen purge was continued. NaOH was dissolved in 125 mL of ultrapure water in a 500 mL 3-neck flask at a concentration of 0.5 M, purged with nitrogen and then heated to 75 °C. The iron solution was added dropwise into the basic solution. Black precipitates formed immediately (Fig. 4.5). The reaction solution was mixed vigorously for a further 30 min, after which the contents were emptied and centrifuged for 15 min at 3000 *g*. The nanoparticles were separated using an external permanent magnet. The supernatant was discarded by decantation (Fig. 4.6) and the particles were rinsed a few times with deoxygenated water followed by centrifugation at 3000 *g* for 10 min to remove excess ions in the suspension. Finally the particles were rinsed with approximately 100 mL of 0.01 M HCl. The particles were collected and dried overnight in an oven at 80 °C. Their concentration is henceforth expressed in terms of dry weight per volume of suspension medium. The pH of a suspension in ultrapure water was 7.0.

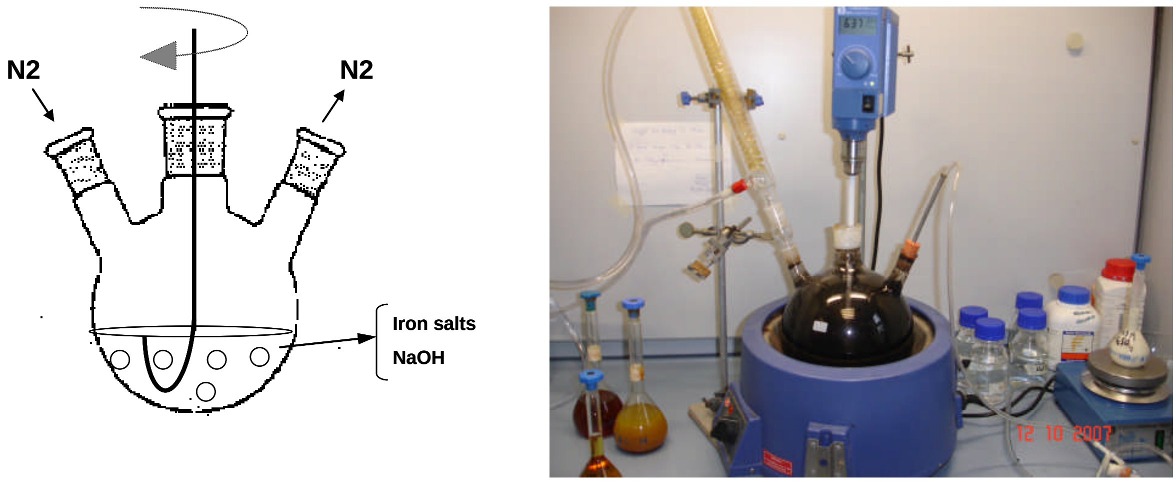

Figure 4.5: Dispersing of ferrite nanoparticles and embedding them in a three neck flask under nitrogen. The displacement of air by N_2 gas during preparation prevented oxidation of ferrous ion in the aqueous solution and also controlled the particle size.

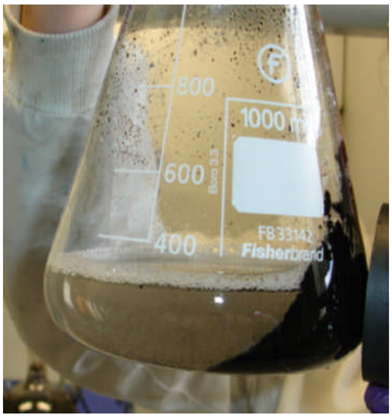

Figure 4.6: Photograph of fabricated nanoparticles. Nanoparticles were gradually concentrated and collected on one side of the vessel by an external permanent magnet.

4.9.3 Surface modification by coating the particles with PEG

Magnetic nanoparticles coated with PEG were prepared and characterized as reported in section 4.9.2. In the first step, 20% solution of PEG was mixed with an equal volume of the iron salts and added dropwise into the caustic soda and then purged with nitrogen for at least 30 min. The prepared iron solution was added dropwise into 125 mL NaOH (0.5 M) which had been preheated to 75 °C. Black precipitates formed immediately upon addition of the iron salt solution (Fig. 4.5). The reaction solution was mixed vigorously for 30 min while the black precipitates formed. The flask was removed and the washing procedure was repeated to get nanoparticles coated with PEG.

4.10 Results and discussion

4.10.1 Transmission & scanning electron microscopy

Ttransmission electron microscopy (TEM) and scanning electron microscopy (SEM) were used to characterize the particles. TEM has the ability to view nanostructures because the wavelength of an electron beam can be adjusted to a few hundredths of an angstrom. In order to prepare TEM samples, the final nanoparticle slurry was sonicated for approximately 5 min to better disperse the nanoparticles. A drop was placed with a carbon-coated copper TEM grid (200–300 mesh) and then left to dry in air. The particle diameters were determined directly from the TEM images to be in the range of 45–55 nm (Fig. 4.7). Further characterization of the synthesised Fe_3O_4 nanoparticles was obtained using a FEI XL30 field emission SEM (Fig. 4.10). Since SEM uses the reflection properties of surfaces for imaging it should be possible to visualize the binding of nanoparticles on various surfaces. In order to prepare SEM samples, the particle suspension was washed several times in deionized water to remove any salt residue, diluted using deionized water, and finally, using a pipette, a drop of it was placed on an Al-stub and left to dry overnight, before mounting the stub on the SEM sample holder. The operating voltage was in the range of 10–20 kV to minimize charging of the sample. The SEM image were not subjected to quantitative analysis, but merely served to gain a visual impression.

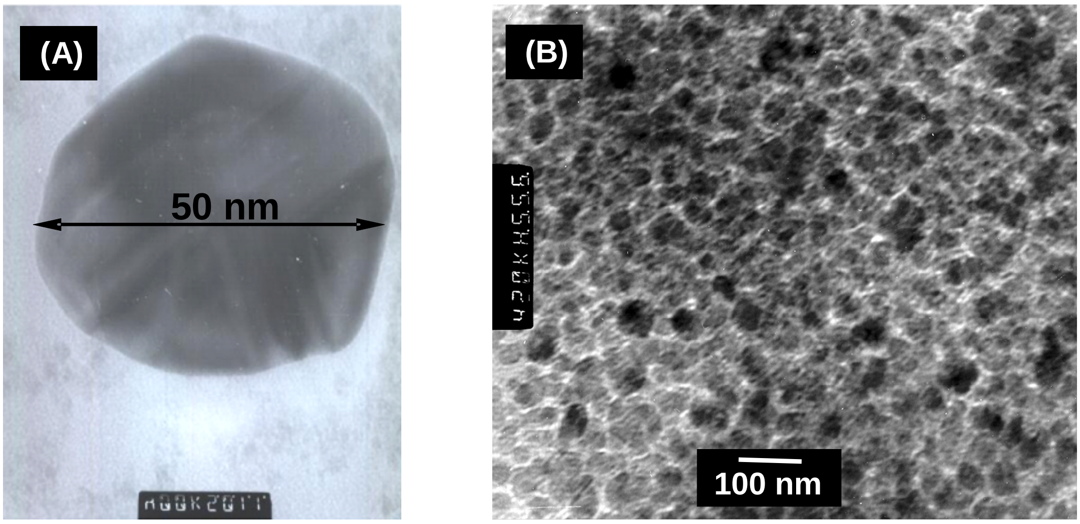

Figure 4.7: TEM images of the 50 nm. Capillary forces during drying of the suspension on the grid result in the aggregation visible on the micrographs.

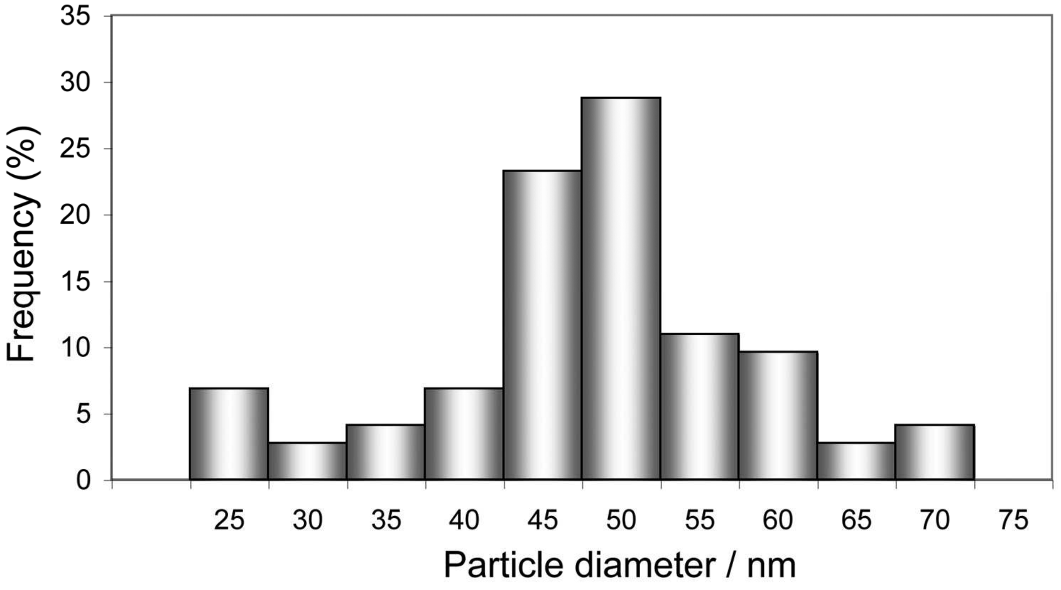

Figure 4.8: Bar chart of the particle sizes from a typical preparation determined from TEM images (a total of 100 particles were measured). Mean size is 47.22 ± 0.96 nm (s.d.)

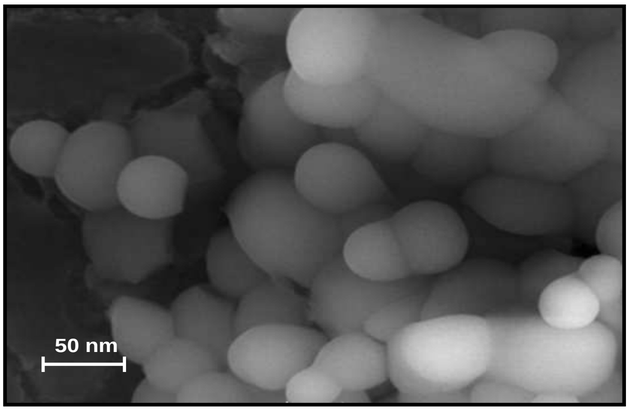

Figure 4.9: SEM images of the 50 nm synthesized Fe_3O_4 nanoparticles.

4.10.2 X-ray diffraction (XRD)

In order to understand the chemical composition of synthesized nanoparticles, XRD analysis was performed. The output from XRD analysis yields a plot, which shows intensity versus diffraction angle and it can determine the crystallographic planes that are being diffracted. Since the wavelength and diffraction angle is known, using Bragg's law the repeat distance, d, can be calculated, which can be utilized to create a map of the crystal structure. Alternatively, a collection of standards can be utilized to compare the diffractogram of the sample with database and allowing one to identify crystal planes (Fig. 4.11).

Figure 4.10: Black powder of synthesised Fe_3O_4 nanoparticles.

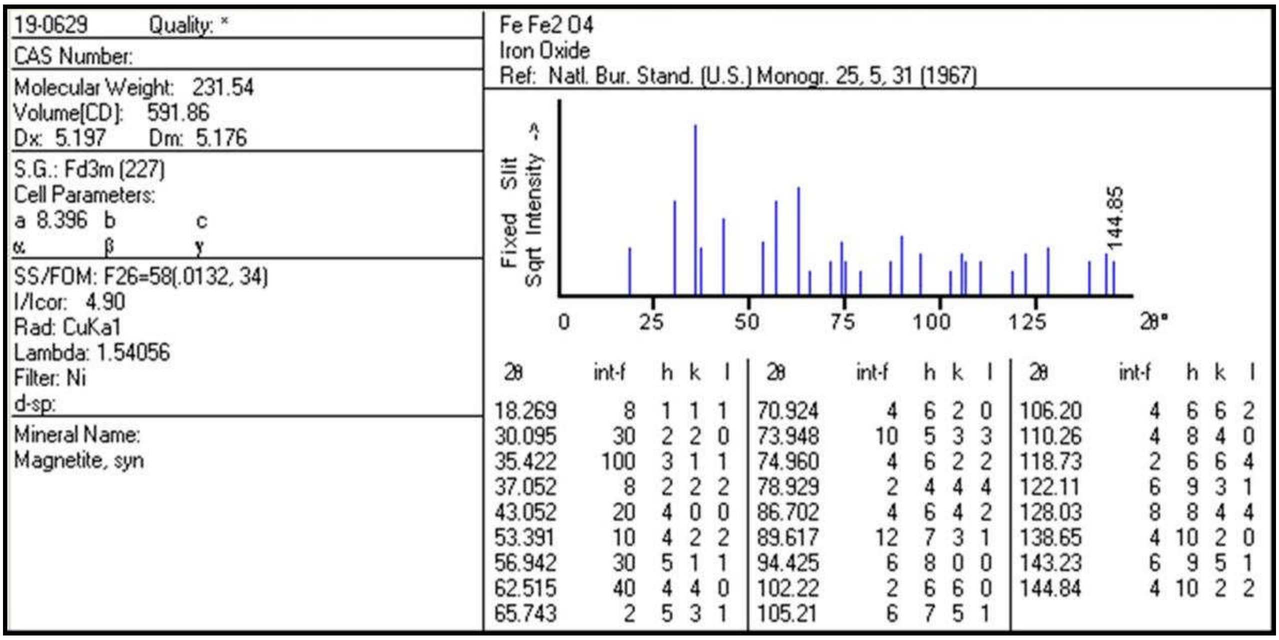

19-0629 Quality: *
CAS Number:
Molecular Weight: 231.54
Volume[CD]: 591.86
Dx: 5.197 Dm: 5.176
S.G.: Fd3m (227)
Cell Parameters:
a 8.396 b c
α β γ
SS/FOM: F26=58(.0132, 34)
I/Icor: 4.90
Rad: CuKa1
Lambda: 1.54056
Filter: Ni
d-sp:
Mineral Name:
Magnetite, syn

Fe Fe2 O4
Iron Oxide
Ref: Natl. Bur. Stand. (U.S.) Monogr. 25, 5, 31 (1967)

2θ	int-f	h	k	l	2θ	int-f	h	k	l	2θ	int-f	h	k	l
18.269	8	1	1	1	70.924	4	6	2	0	106.20	4	6	6	2
30.095	30	2	2	0	73.948	10	5	3	3	110.26	4	8	4	0
35.422	100	3	1	1	74.960	4	6	2	2	118.73	2	6	6	4
37.052	8	2	2	2	78.929	2	4	4	4	122.11	6	9	3	1
43.052	20	4	0	0	86.702	4	6	4	2	128.03	8	8	4	4
53.391	10	4	2	2	89.617	12	7	3	1	138.65	4	10	2	0
56.942	30	5	1	1	94.425	6	8	0	0	143.23	6	9	5	1
62.515	40	4	4	0	102.22	2	6	6	0	144.84	4	10	2	2
65.743	2	5	3	1	105.21	6	7	5	1					

Figure 4.11: XRD pattern of iron oxide (Fe_3O_4).

In my studies powder X-ray diffraction (XRD) studies were performed between 10 ° and 85 ° using a Copper Kα x-ray source (Siemens). The XRD pattern of dark brown powder collected from the vessel indicates the presence of predominantly Fe_3O_4 crystals. The discernible peaks which can be clearly identified in the scan in Figure 4.12 can be matched to, the (220), (311), (400), (422), (511) and (440) planes of a cubic Fe_3O_4 unit cell, and it reflected by the well matching of the diffraction peaks with the magnetic pattern and it corresponds to that of magnetite structure.

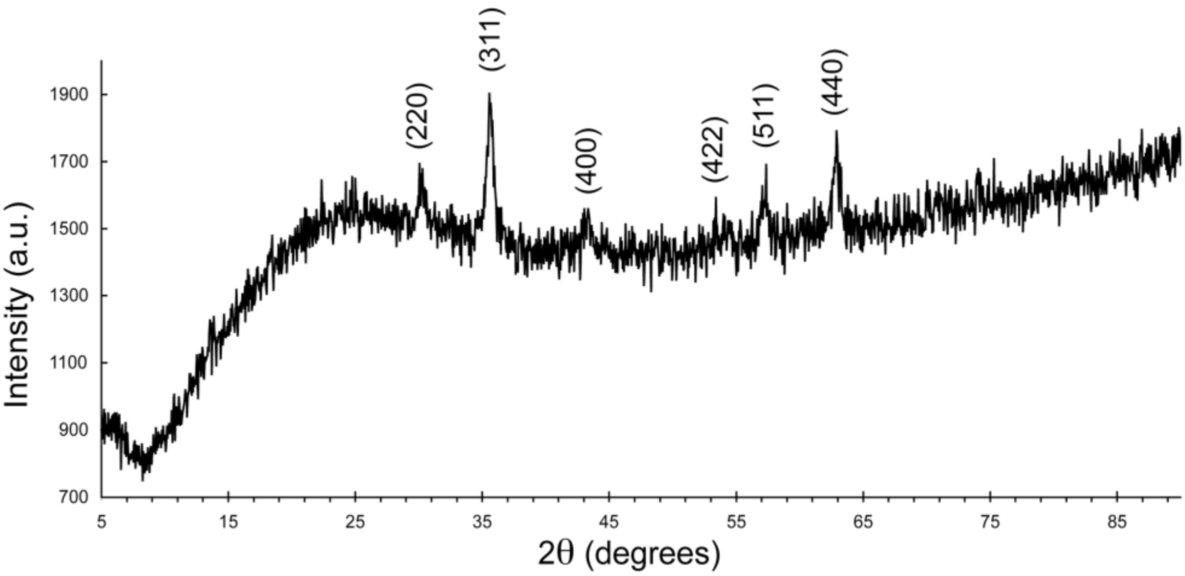

Figure 4.12: X-ray diffraction pattern of the nanoparticles. The numbers in parenthesis are reference standard pattern of Fe_3O_4 and give the Miller indices of pure Fe_3O_4 (NBS, 1976) assigned to the observed peaks.

The mean crystallite size is determined by Scherrer's equation:

$$\text{Crystallite size (Å)} \sim 0.9\ \lambda / (\text{FWHM} \cos \theta) \qquad (3)$$

Where λ is the radiation wavelength (which in this case is 1.54 Å), and FWHM is the full width half maximum of the peak. This calculation determined the mean size of the synthesized particles to be 80 nm.

4.10.3 Magnetization study

Magnetic hysteresis loops of the samples were measured using a magnetic measurements (Peterson Instruments, UK) variable field translation balance (MMVFTB). High field conditions were used to assure that saturation magnetization was achieved and measured. Saturation magnetization (9.9 emu/g) was obtained from the hysteresis loop resulting from applying a magnetic field from -8 to +8 kOe at room temperature. Figure 4.13 shows the magnetization (M) versus applied field (H) magnetization of the Fe_3O_4 nanoparticles. The hysteresis loop of synthesized magnetite indicates superparamagnetic behavior at room temperature, as evidenced by zero coercivity and remanence on the magnetization loop.

The paramagnetic component was removed by assessing the gradient of the magnetization curve (B vs H) once saturation had been reached. It should be emphasized that the residual magnetization is almost negligible for these particles, which is very likely important for achieving good dispersibility of the nanoparticles in a fluid.

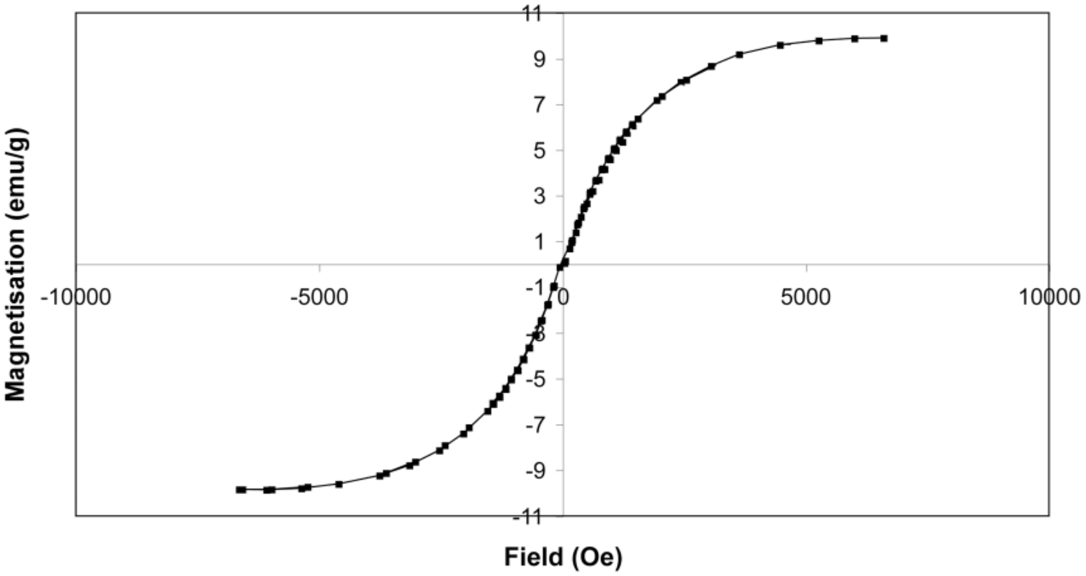

Figure 4.13: Magnetic hysteresis loop of the 50 nm Fe_3O_4 nanoparticles measured at room temperature. The paramagnetic component of the magnetization has been removed according to a standard procedure. Saturation magnetization; emu, electromagnetic unit; Oe, Oersted.

The temperature dependent magnetization of the sample was measured in an applied field of 8000 Oe measured with the VFTB. Figure 4.14 shows the plot of temperature versus normalized magnetization in an applied magnetic field. It can be seen that the heating and cooling curves are different. This shows that the sample is not stable to heat. This is probably showing alteration of magnetite to maghaemite.

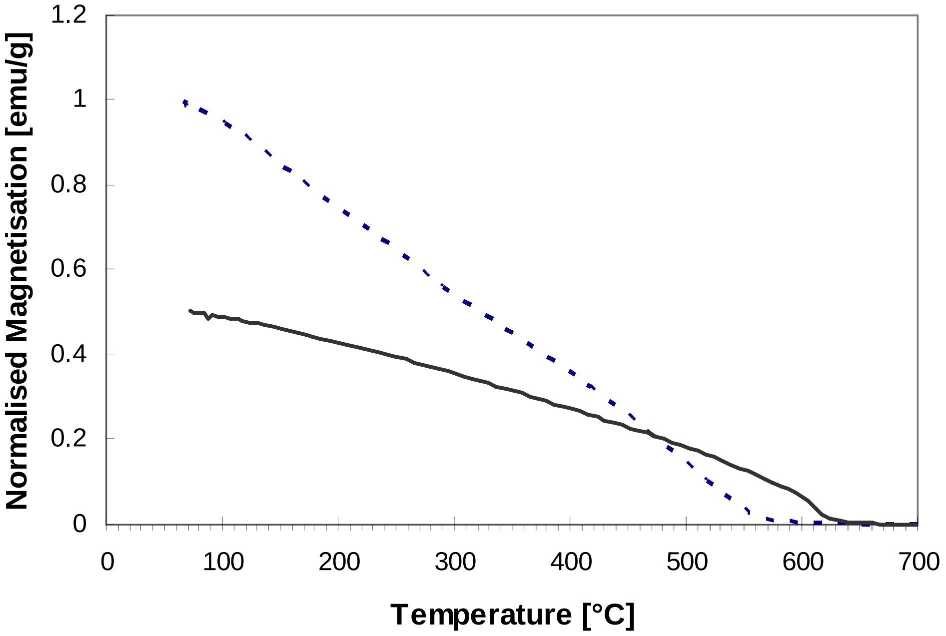

Figure 4.14: Temperature dependence of the magnetization under heating ---- and cooling — conditions for the sample.

The iron oxide magnetic nanoparticles show superparamagnetic behavior at high temperature (---), however with cooling of the sample, the magnetization increased and show ferromagnetic behavior.

4.11 Evaluation of the radius of the PEG coated particles

In order to measure the radius of the PEG coated nanoparticles, the refractive index increment is an essential parameter to evaluate quantitatively the surface coated by polymer (Haynes and Norde, 1994).

The percentage of PEG was obtained by measuring the refractive index (*n*) of the nanoparticles suspended in water at 25 ºC, 633 nm was measured without and with PEG using a J357 automatic refractometer (Rudolph Research Analyticals, Hackettstown, USA). dn/dc was determined from the best fit slope on refractive index against bulk concentration (*c*) plots with the slop of the fit equating to the dn/dc (Ball and Ramsden, 1998). Then from the variation of refractive index with concentration results straight lines were fitted to the using linear regression as shown in Figure 4.15.

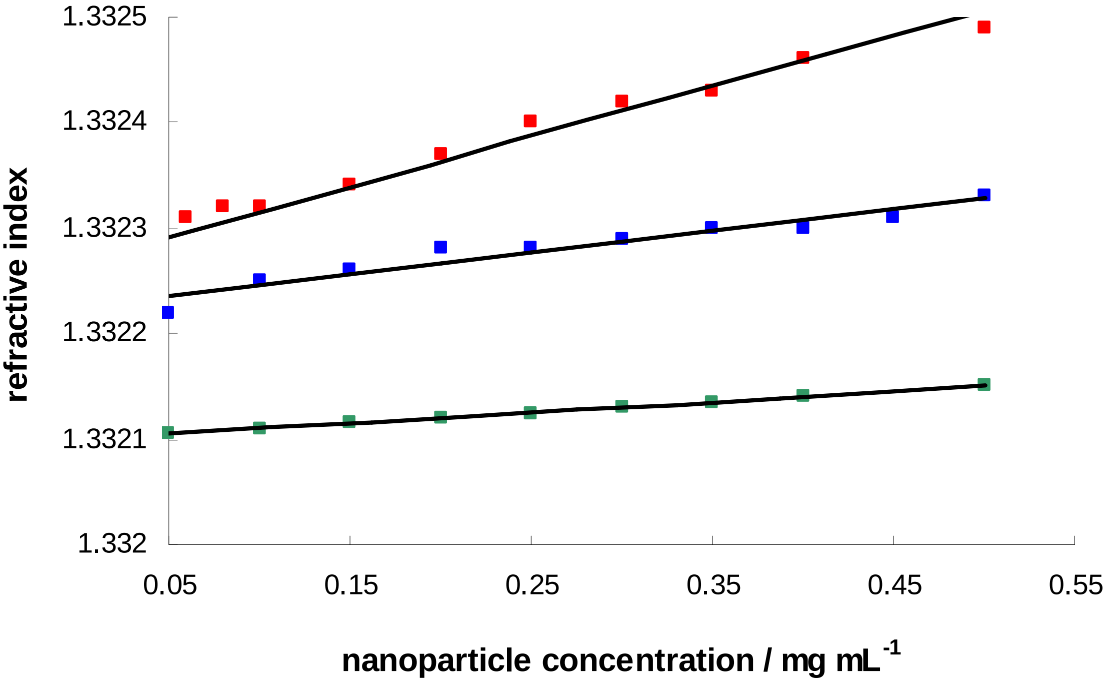

Figure 4.15: Refractive indices of pure PEG (green points), Fe_3O_4 nanoparticles without PEG (red points) and Fe_3O_4 nanoparticles with PEG (blue points) at 25 ºC in water. All measurements were repeated ten times and the average is plotted. The refractive index increments dn/dc are the scopes of the linear repressions which are 0.0001, 0.0004, 0.0002 for PEG, Fe_3O_4 and coated Fe_3O_4 respectively.

From the above calculations the average value of mass concentrations for the nanoparticles and with and without PEG are determined to be 33% and 67% respectively. Then by use of the calculated mass percentage of nanoparticles to PEG, the radius of a particle coated by PEG is determined as follow:

When we add coated nanoparticles to water we increase the refractive index *n* by

$$\delta n_t = \delta n_m + \delta n_p \tag{4}$$

where subscripts *t, m, p* represent coated (hybrid) particle, uncoated particle and pure polymer respectively. Using the refractive index increments we can write:

$$\left.\frac{dn}{dc}\right|_t (\delta c_m + \delta c_p) = \left.\frac{dn}{dc}\right|_m \delta c_m + \left.\frac{dn}{dc}\right|_p \delta c_p \tag{5}$$

Where the *c* are the concentrations, and end up with the following equation

$$\left.\frac{dn}{dc}\right|_t = \left.\frac{dn}{dc}\right|_m \varphi + \left.\frac{dn}{dc}\right|_p (1-\varphi) \tag{6}$$

where φ is the mass fraction of the magnetite in the hybrid nanoparticles.

From our refractive index increments data (Fig. 1) we determine $\varphi = 0.33$. Taking the densities of PEG and magnetite as ρ_p=1.1 and ρ_m=5.17 g/cm^3 respectively (Lidle, 2005), we have the mass of one nanoparticle $m_m = v_m \rho_m = 4/3\ \pi r^3_m \rho_m = 3.34 \times 10^{-10}$ µg. The mass of one Fe_3O_4 nanoparticle with PEG $m_t = m_m / \varphi = 1.01 \times 10^{-9}$ µg. Hence the volume of the PEG surrounding the magnetite is: $v_p = m_p / \rho_p = (m_t - m_m) / \rho_p = 6.16 \times 105\ \mathrm{nm}^3$, and the total volume of a hybrid particle is $v_t = v_m + v_p = 6.8 \times 10^5\ \mathrm{nm}^3$. Hence the radius of a hybrid particle, given by

$$r_t = \left(\frac{v_t}{(4/3)\pi} \right)^{1/3}$$

Equals 55nm, implying that the thickness of the coating is about 30 nm.

I have developed a chemical method to synthesize nanoparticles using ferrous and ferric ions in the presence of nitrogen gas. The synthesis of magnetic nanoparticles in an oxygen-free environment not only protects iron oxide particles from oxidation but also bubbling nitrogen (N_2) gas through the solution during the process could control the reaction kinetics in order to reduce the particle size as compared with methods that do not remove oxygen (Kim et al., 2001).

In the first step, I prepared nanoparticles by a solution-phase metal salt reduction (Yeh et al., 2004) at room temperature and this led to synthesis of nanoparticles which were suitable for coating bacteria for biodesulfurization application. The bacterial coating procedure was effectively applied immediately after preparation of the nanoparticles solution (explained in section 1.13.2.9). Since magnetic nanoparticles have a large ratio of surface area to volume and tend to agglomerate, they were not very appropriate for the next studies. Therefore an appropriate surface chemistry is needed to coat the nanoparticles.

Coating of nanoparticles with different functional surfactants has potential for various applications (Gupta, 2004). The colloidal suspension of magnetite particles, however, can be stabilized by coating the particle surfaces with high molecular weight polymers such as PEG, polyvinylalcohol (PVA), dextran, etc. Such coatings have been postulated as necessary for effective stabilization for ferrofluids (Zaitsev et al., 2007). Colloidal solution of magnetic particles coated with PEG showed very high stability at neutral pH and no sedimentation was observed even after two months of storage at room temperature, whereas uncoated magnetic particles did not form a stable colloidal suspension and sedimented within a week. Therefore in the next step I decided to coat the iron oxide nanoparticles with PEG, in order to increase the colloidal stability, improve bio-interfacial properties and as a result increase attachment.

4.12 Summary

Since the Fe_3O_4 nanoparticles needed for this project were not commercially available; therefore this part of work was developed to synthesis and characterization of magnetic nanoparticles using chemical coprecipitation. This method is easy, the least expensive and most convenient way to synthesize iron oxides from aqueous Fe^{2+}/Fe^{3+} salt solutions by the addition of a base at room temperature or at elevated temperature, and is therefore suitable for large scale industrial applications. In this technique, the size, shape, and composition of the particles greatly depend on the iron salts counterion (e.g. chloride, sulfate, nitrate), Fe^{2+}/Fe^{3+} ratio, temperature of the reaction, pH and ionic strength of the medium.

Chapter 5 : Enhancing biodesulfurization by nanomagnetic particles

In any industrial process using freely dispersed microorganisms as catalysts, they need to be separated from the products after catalysis has taken place and the reaction has reached its conclusion. This is the first step of the downstream processes required to purify the product. Although the free dispersal of microorganisms in a fluid reaction volume optimizes mass transport, it is sometimes difficult to carry out the necessary separation afterwards, and usually the separation procedure compromises viability, i.e. the organisms die.

Therefore it seems that designing new biodesulfurization processes with exchange between biology and nanotechnology and illustrating the role of nanoparticles in this field for enhancing the efficiency of the biocatalysts during this process are crucial factors in maintaining the process. Magnetic nanosized particles are attractive because at this scale atoms and molecules interact and assemble into structures that possess unique chemical, physical, electronic and magnetic properties resulting from their quantum size (Singh et al., 2006). At these scales molecular interactions, processes, and phenomena can be controlled and directed with desirable properties, and due to the high ratio of surface area to volume (Tang et al., 1999), superparamagnetic nanoparticles have significantly different magnetic performance, among magnetic materials. Therefore, these particles have the potential for applications in various fields of industry and science. Furthermore the possibility of synthesizing nanoparticles and the utilization of commercially available mass-produced nanoparticles with properties on demand is taken into account. Simplicity of production would be a main criterion in this case.

5.1 Bacterial membrane and Gram-positive vs. Gram-negative

The bacterial membrane controls many responses of the cells, including environmental stresses. Bacteria can be classified as either Gram-positive or Gram-negative, based on their cell wall structure and their response to the Gram stain. The bacteria that can retain the special dyes during Gram's staining procedure are called Gram-positive bacteria (Beveridge, 1988). The cell wall in Gram-positive bacteria is a thick layer (20-80 nm) consisting of peptidoglycan (PG). The PG consists of secondary polymers like polysaccharids, teichoic acids, teichuronic acids and lipoteichoic acids. In Gram-negative bacteria the PG is significantly thinner (≈7 nm) and it is devoid of secondary polymers, but a special additional layer, the outer membrane (OM) encapsulates the PG. The OM is essentially composed of lipopolysacharides (LPS), which are rich in carboxyl groups (Cabeen Jacobs-Warner, 2005, Beveridge, 1988).

The cell wall surrounds a lipid/protein bilayer called the cytoplasmic membrane (CM). The CM regulates the translation of metabolites and solutes in to and out of the cell and is selectively permeable (Holland, 2004). The CM is associated with several enzymes involved in various metabolic functions of the cell in order to maintain the membrane potential and ion gradients (Stenberg et al., 2005; Ruiz et al., 2006) (Fig. 5.1).

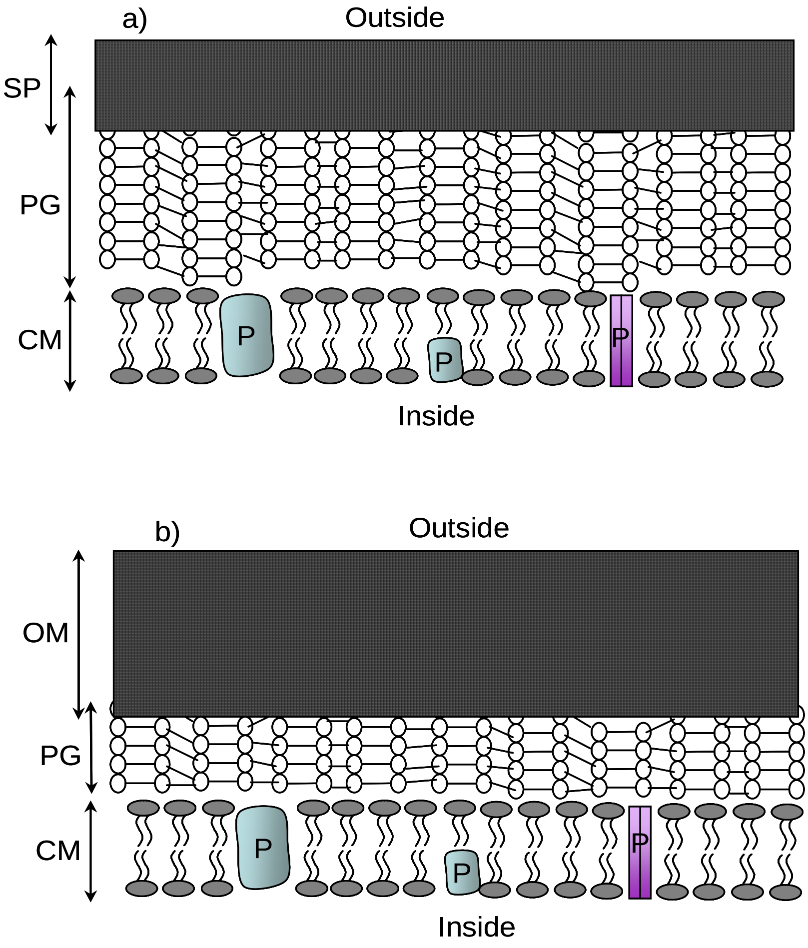

Figure 5.1: Cell wall in a) Gram-positive bacteria and b) Gram-negative bacteria. Cytoplasmic membrane (CM), peptidoglycan (PG), outer membrane (OM), secondary polymers (SP), protein (P).

5.2 Immobilization

Microorganisms used in any industrial process need to be separated from the product, either by filtration or centrifugation (Luo and Sirkar, 2000). Thus the removal of the organisms can be the first instance of the downstream processes required to purify the product. A good solution is to immobilize the cells to enable easy recovery of the cells and reuse of immobilized cells. Immobilization is defined as the ability to physically confine or localise in a defined region or space cells or enzymes or molecules whilst retaining the catalytic activities, for repeated and continuous use.

Although the free dispersal of microorganisms in a fluid reaction volume optimizes mass transport, it is sometimes difficult to carry out the necessary separation afterwards, and usually the separation procedure compromises viability, i.e. the organisms die. Therefore, efforts have been made to immobilize bacteria, typically in the form of biofilms coating reaction vessels with high surface to volume ratios.[3] The starting materials must then simply be made to flow over the biofilm, and no separation is subsequently required (Naito et al., 2001). Furthermore, biofilms offer protection to the cells against adverse environmental conditions, and to some extent at least they are self-renewing and may therefore be used for many production cycles, or even for continuous rather than batch processes. On the other hand, mass transport is much slower than with freely dispersed microorganisms.

Since the microbial enzymes can be immobilized, it seems the immobilization of bacterial cells is more preferable: When enzymes are isolated from their natural environmental source, they are generally unstable and are easily denatured under operating conditions. Therefore by direct immobilization of microbial cells containing

---

[3] Three major techniques are used for immobilizing bacteria: entrapment, adsorption and coupling (Corcoran, 1985). To achieve entrapment, the microbial cells are mixed with a gel-forming polymer, yielding pores smaller than the size of the cells. This ensures retention of the cells, but permits movement of nutrients, starting reagents and products. Adsorption means allowing the bacteria to form weak chemical bonds to the substrate; electrostatic interactions between a charged support and charged cells have been made use of (Yang and Albayrak, 2006). However, the forces involved in cell attachment are then so weak that cells are readily lost from the adsorbent (Shan et al., 2004). To overcome this problem, cells can be covalently bonded (coupled) to an activated support (Hulst and Trumper, 1989).

the desired activities, this problem may be obviated. Furthermore, when bacterial cells are immobilized, the higher yield of activity are obtained rather than free enzymes (Corcoran, 1985) and also the costs are decreased significantly, because it is no longer needs enzyme extraction and purification.

5.3 Decoration of bacteria

Microorganisms used in any industrial process need to be separated from the product, either by filtration or centrifugation. Thus the removal of the organisms would be the first step of the downstream processes required to purify the product. Also it enables the cells to be easily recovered and reused. Researchers have used immobilized cells in order to manage this problem. Immobilization is defined here as the ability to physically confine or localise in a defined region of space cells whilst retaining their activities. Using immobilized cells is not a new idea since in the 18th century immobilized cells were used for production of acetic acid. (Marshall and Rogers, 1941). Similarly in the 19th century sewage treatment utilised a natural film of organisms adsorbed to beds of sand and gravel to convert organic materials in sewage to water, CO_2 and other gases (Marshall, 1948). Ever since, immobilized microbial cells have been used in bioconversions, biotransformation, and biosynthesis processes due to their stability, easier separation from products for possible reuse, and satisfactory efficiency in catalysis compared to free cells (Pakula 1996, Ohshiro 1999, Naito 2001, Luo 2003, Gill 2000). Nevertheless, there are major drawbacks to apply this technique: diffusional limitations, mass transfer involved in diffusion of a substrate to a reaction site, also this technique is generally limited by biomass loading, strength of adhesion, biocatalytic activity, and operational stability. This is because immobilization involves attachment of cells to the surface of an adsorbent like Celite, and the forces involved in cell attachment are so weak which they are not strongly adsorbed and are readily lost from the surface of the adsorbent.

In this investigation, a new technique was developed in which microbial cells were decorated with MNPs by adsorption. The cells could be separated by applying an external magnetic field. The NPs were strongly adsorbed on the surfaces of bacteria. Application of a magnetic field enabled us to concentrate the coated cells and to get clear media, and minimal mass transfer problems were experienced with the decorated cells. Thus, this technique has advantages over conventional immobilization. Furthermore, it can overcome drawbacks such as limitations in biomass loading and in the loss of cells from the carrier associated with conventional immobilization.

5.4 Methods to detect permeability of the bacterial membrane

The membrane surrounding the bacterial cell serves several functions such as control of solute permeability and recognition events. In order to investigate the process occurring at the cell membrane, artificial lipid membranes are useful models and many different model systems have been developed to elucidate the properties of lipid bilayers and various methods have been used to create artificial lipid membranes such as liposomes, supported bilayer lipid membranes (sBLM), polymer-supported bilayer lipid membranes (psBLM), tethered bilayer lipid membranes (tBLM) and black lipid membranes (BLM).

Liposomes can be modified in a desired manner (Lasic, 1998); however, the accessibility to one side of the membrane limits the usefulness of liposomes for our investigation. Solid supported membranes in sBLM can be accessed by a variety of sensitive surface analysis techniques, but the lack of a well defined ionic reservoir on the bilayer is a major drawback when studying transmembrane transport due to ion carriers and channels (Guidelli et al., 2001). On the other hand, the polymer-supported BLMs have low impedance, which is insufficient to match the electrical properties of a biological membrane; therefore it may also prevent the incorporation of the channel peptides and proteins (Tien et al., 2003, Kiessling et al., 2003). Tethered bilayer lipid membranes can be formed with high insulation electrical properties similar to the biological natural membrane (Raguse et al., 1998), however, the decreased bilayer fluidity possesses a problem particularly for the incorporation of large peptides and channel proteins. Thus, an alternative approach should be found so that all the channels could be incorporated. Unlike liposomes, black lipid membranes are formed by spreading a lipid solution in a small hole of a wall separating two aqueous compartments. BLMs are very suitable for electrochemical measurements, since there is easy electrochemical access to both sides of the membrane. The ability to control the constituents of each side of the membrane and both the membrane and incorporated functionalities are likely to be close to their native state. Even though the physical stability of these BLMs is low (Tien et al., 2003) and because of the size limitation, it is impossible to form large area BLMs (Purrucker et al., 2001), nonetheless they have been extremely valuable in the history of membrane research.

5.4.1 Black lipid membrane technique

In order to better understand the basic mechanism of biological systems, it is often necessary to reduce the number of parameters. The black lipid membrane (BLM) a model system were devised almost 45 years ago Mueller et al. (1962) and since then applied enormously to understand biological membranes, mass transport in and out of cells, and so forth. This model is reasonably similar to an actual cell membrane, because it permits simultaneous access to the solution and electrical control on both sides of bilayer, allowing for the mimicking of physiological conditions.

BLMs consist of three components: lipid bilayers, a thicker annulus that forms at the interface between the supporting substrate and the bilayer, and microlenses (pockets of decane), which all participate in this evolution. Cell membranes are a fluid system that temporally evolves according to the phase behaviour of the lipids. Since the thickness of the lipid bilayer is only a few nanometers, optical images of BLMs tend to appear black or grey. BLMs depend not only on the lipids and supporting material but also on the process used to create the bilayer; consequently, even simple observables such as the membrane capacitance are not always straightforward to interpret because of changes in the bilayer area and solvent content within the bilayer. Bacterial membrane permeability measurements are fundamental to studies of the effect of nanomaterials. NPs may perturb the membrane structure, leading to the formation of channels in the CM, leading to permeabilization.

5.5 Experimental part of research

5.5.1 Decoration of Rhodococcus with magnetic nanoparticles

The bacteria were grown in BSM until the mid-exponential growth phase and harvested by centrifugation at 1400 *g* for 10 min. The cell pellets were washed twice with Ringer’s solution and resuspended back in BSM to A_{600} = 1.0. The cells were then decorated with MNPs as follows: 10 mL of a suspension containing 100 µg/mL Fe_3O_4 nanoparticles per mL of water were mixed with 100 mL of the cell suspension in BSM with DBT at a final concentration of 0.5 mM. The ratio of NPs to bacterial biomass was 1.78 w/w.

5.5.2 Batch biodesulfurization of DBT by decorated bacteria

Biodesulfurization was carried out using the cells in 100 mL of BSM containing DBT at a final concentration of 0.5 mM, in a 250 mL flask incubated on a rotary shaker at 120 rpm and 30 ºC (0.5 mM of DBT are equivalent to 0.092 *g* DBT/L). For analysing the supernatant using HPLC it should not have any contamination (like free bacteria) which would damage the HPLC column. Therefore, the cells were separated from the reaction mixture by centrifugation at 6600 *g* for 10 min, and the supernatant analysed. So that the same procedure could be used for decorated & nondecorated controls. Nondecorated cells were used as controls.

5.5.3 Nanoparticle-induced membrane permeability assay

(P. Grigoriev)

Lipid bilayer membranes were formed by the method of Mueller et al. (1962) from a cardiolipids: phosphatidylcholine 5:95 mixture mimicking the bacterial membrane. The membrane current was measured by an OPA 129 operational amplifier (Burr-Brown) used as a current-to-voltage converter. In this method a lipid solution is spanned over a hole between two aqueous compartments as shown schematically in figure 5.2.

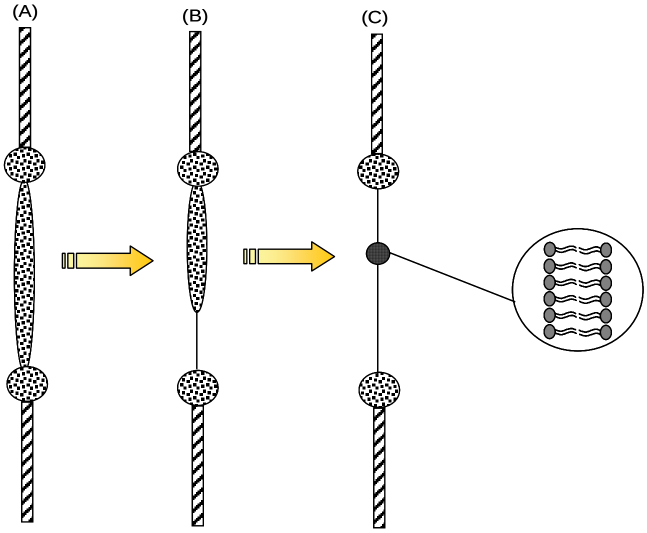

Figure 5.2: Formation of a biomolecular lipid membrane (Benz et al., 1982). First a thick lamella (A) is formed and within seconds or min black dots appear in the membrane (B), and finally grow together until the whole membrane appears black because of destructive optical interference (C).

In this state the membrane consists of an oriented biomolecular film (Mueller et al., 1962) formed by self-organization of the amphiphile molecules as described above. These model systems are most commonly used to study the electrical properties of membranes and the effects of incorporation of carriers in membranes. Even single molecules such as gramicidin or natural porins (Benz et al., 1982) embedded in the plane of the membrane can be detected by these sensitive measurements.

After formation of BLM, NPs are added at one side of the membrane. After about 1 minute required for the diffusion and adsorption of NPs to the BLM interface fluctuations of the membrane current are observed, reflecting that pathways for ions across the lipid bilayer are being formed. It is suggested that transmembrane NP form structures resembling classical model ion channels formed, for example, by the polypeptide antibiotic alamethicin (Angelova et al., 2000). Molecules of alamethicin forming the channel are in such a conformation when one side (which faces the polar interior of the formed oligomer channel structure) is polar and the other is hydrophobic (facing the hydrophobic interior of the lipid bilayer). In a case of the NP, probably the Fe-part can be considered as hydrophobic and the O part as polar. Van der Waals molecular forces stabilise alamethicin channels, but magnetic forces could stabilise the ion-conducting transmembrane structure formed by NP.

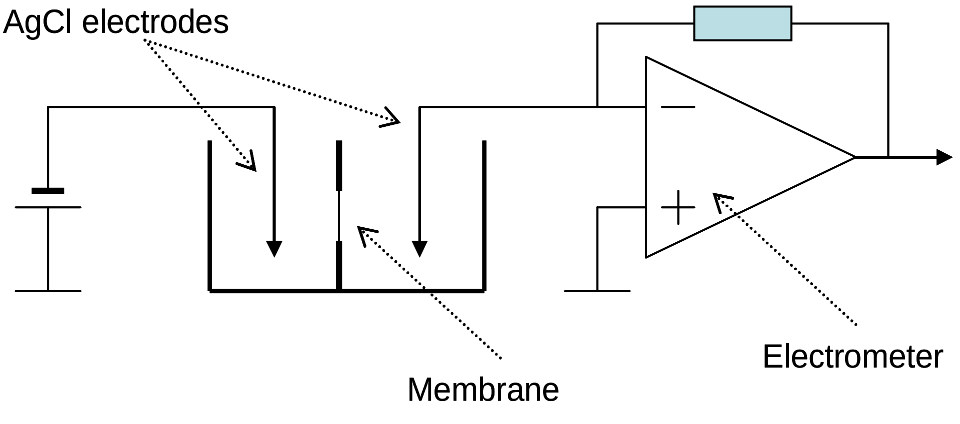

Figure 5.3: Schematic diagram of the BLM current setup. The current is measured with the voltage clamp method.

5.6 Results

5.6.1 Bacteria characterisation by scanning electron microscopy

The cultures were grown until the mid-exponential growth phase in liquid medium and harvested. The cell pellets were washed and resuspended back in water at a. A typical microbe is shown in Figure 5.4.

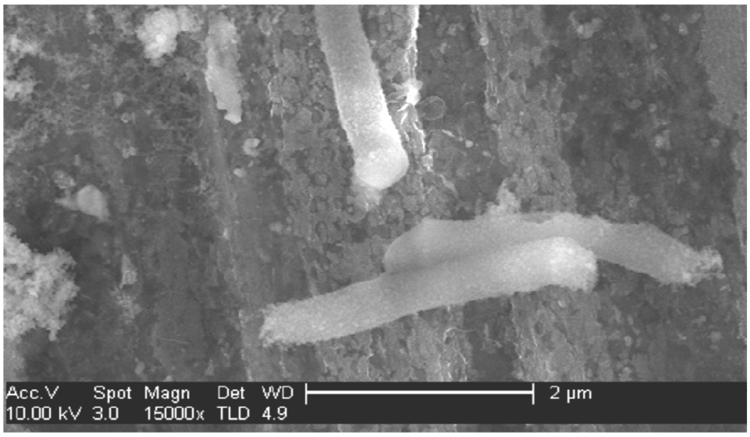

Figure 5.4: SEM image of *Rhodococcus erythropolis* IGTS8 bacteria before coating with nanoparticles. (dimension ≈ 3500 nm x 500 nm).

The cells were then decorated with magnetic nanoparticles as mentioned in experimental section. The ratio of nanoparticle mass to biomass was 1.78 w/w. this ratio makes sufficient particles available per bacterium to yield a suitable level of decoration (Fig. 5.5).

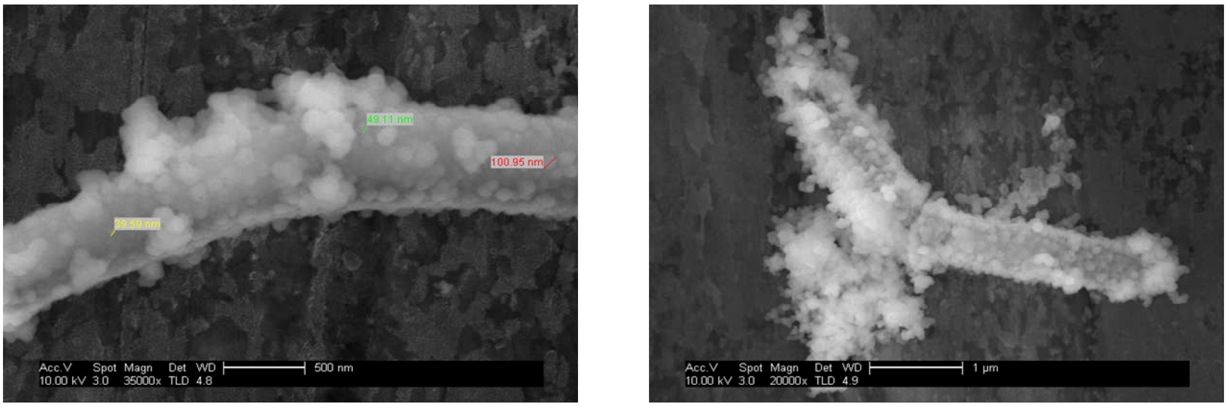

Figure 5.5: SEM images of two different *Rhodococcus erythropolis* IGTS8 bacteria decorated with magnetic nanoparticles. The bacterium shown on the right panel is about to undergo division.

5.6.2 How many particles are able to coat the surface of one bacterium?

Diameter: 50 nm
r=25

Length: L= 3000 nm
Diameter: D = 500 nm
R = 250

The area of one bacterium can be calculated by:

$$A_0 = L \times (2\pi R) + 2(\pi R^2) = 3000 \times (2 \times 3.14 \times 250) + 2 \times 3.14(250)^2 = 5102500 \text{ nm}^2 \qquad (1)$$

And the area of one particle is:

$$A_0 = 4\pi r^2 = 4 \times 3.14 \times (25)^2 = 7850 \text{ nm}^2 \qquad (2)$$

Using these values the number of particles covers the surface of one bacterium calculated as follow:

$$\text{Particles} = \frac{5102500}{7850} = 650$$

5.6.3 Magnetic separation

Figure 5.6 shows a suspension of bacteria coated by NPs in a holder equipped with a removable slide-out magnet: the decorated cells in the liquid culture medium could easily be separated by bringing an external magnet into their vicinity.

Figure 5.6: Photograph of nanoparticle-coated cells (*Rhodococcus erythropolis* IGTS8) in Eppendorf tubes showing, successively: (A) dispersed cells coated with MNPs; (B and C) coated cells were gradually concentrated and collected towards the rear of the tube by an external permanent magnet (within the white housing behind the tubes); (D) liquid medium free of suspended NPs, which are visible as a thin dark stripe at the back of the tube.

5.6.4 Biodesulfurization with coated Rhodococcus by magnetic nanoparticles

Figure 5.7 and 5.8 compare the degradation of DBT with nondecorated and nanoparticle-coated cells. The results show that the production of HBP was significantly higher in the latter. It can be seen that whereas the production rate of the nondecorated cells falls off to almost zero after about 70 hours, the decorated bacteria continue producing more vigorously until at least 100 hours, with a concomitant increase in DBT HBP conversion.

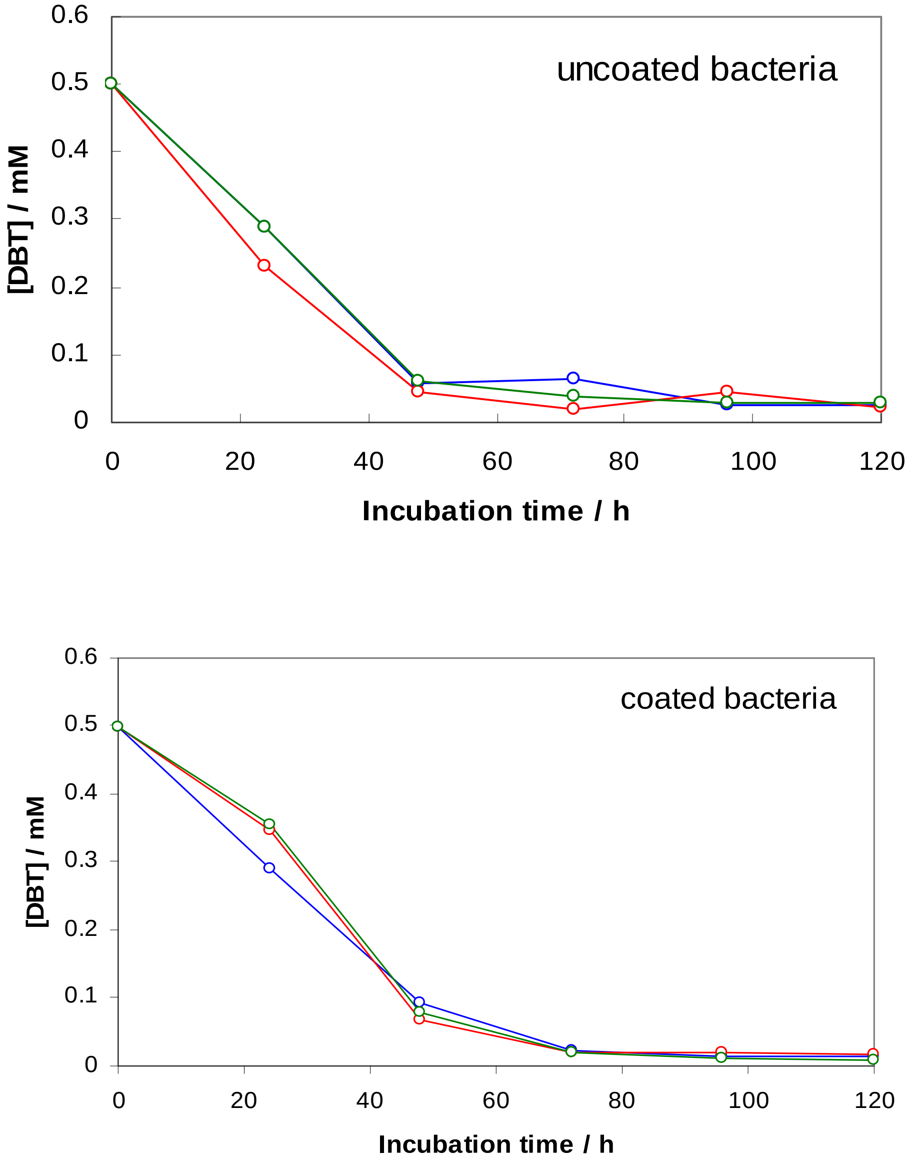

Figure 5.7: Degradation of DBT by *R. erythropolis* IGTS8 without (up) and with (down) decoration by NPs, in BSM with DBT at the initial (*t* = 0) concentration of 0.5 mM as the sole sulfur source.

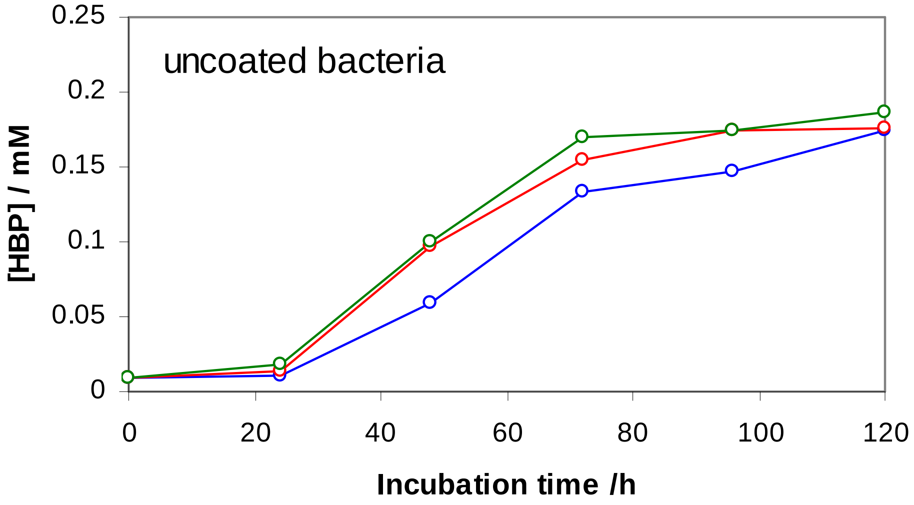

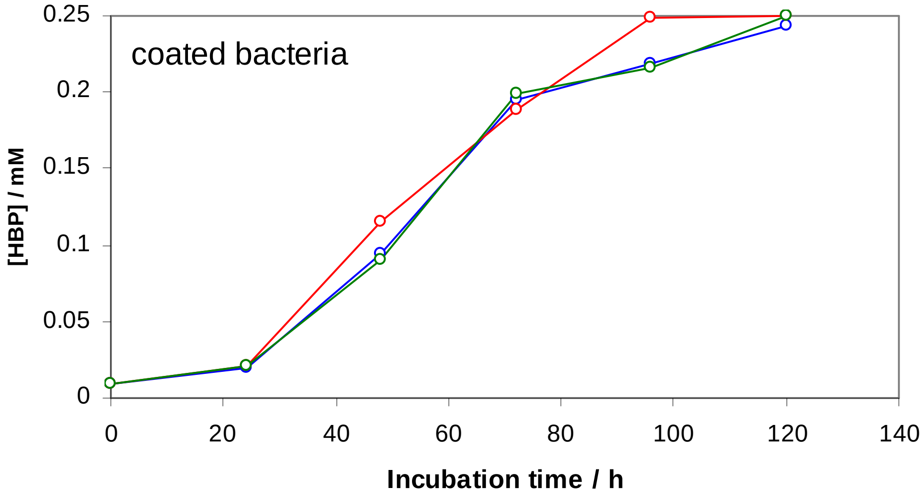

Figure 5.8: HBP production by *R. erythropolis* IGTS8 without (up) and with (down) decoration by NPs, in BSM with DBT at the initial (*t* = 0) concentration of 0.5 mM as the sole sulfur source.

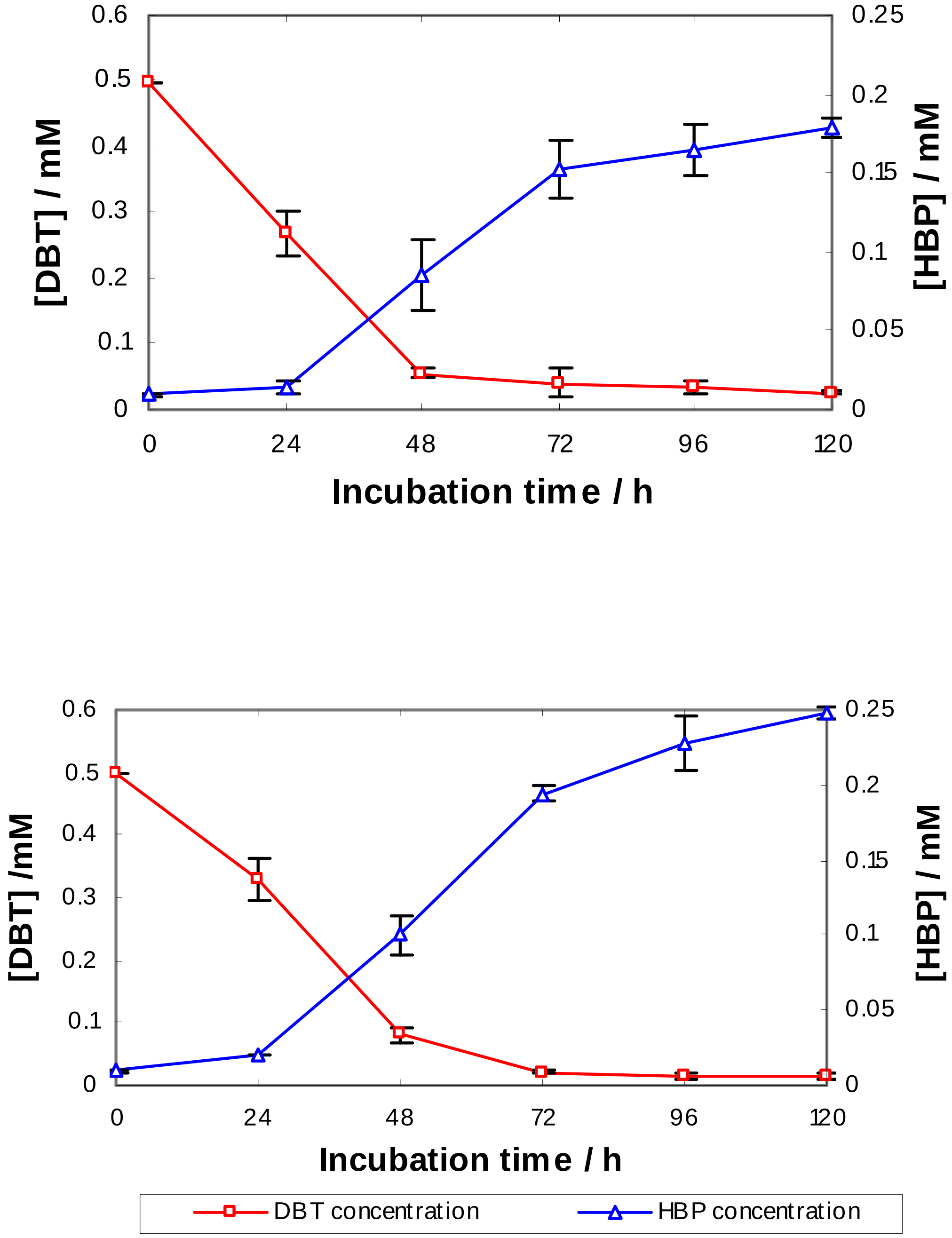

Figure 5.9: Comparison of DBT degradation of *R. erythropolis* IGTS8 without (up) and with (down) decoration by nanoparticles, in BSM with DBT at the initial (t = 0) concentration of 0.5 mM as the sole sulfur source.

5.7 Membrane permeabilization

The observation of significantly increased HBP production in the decorated cells suggests that the MNPs somehow facilitate transport of HBP out of the cells — assuming that it is produced in the cytoplasm. A possible mechanism for the enhancement is then that the NPs bound to the bacteria make their membranes more permeable. In order to investigate this hypothesis, the possible effect of NPs on membrane permeability was assessed in a model membrane system mimicking the bacterial membrane (Grigoriev, 2002). Figure 5.10 shows typical results. They provide evidence for nanoparticle-induced permeabilization, supporting the proposed enhanced ingress of DBT into the decorated bacterial cells.

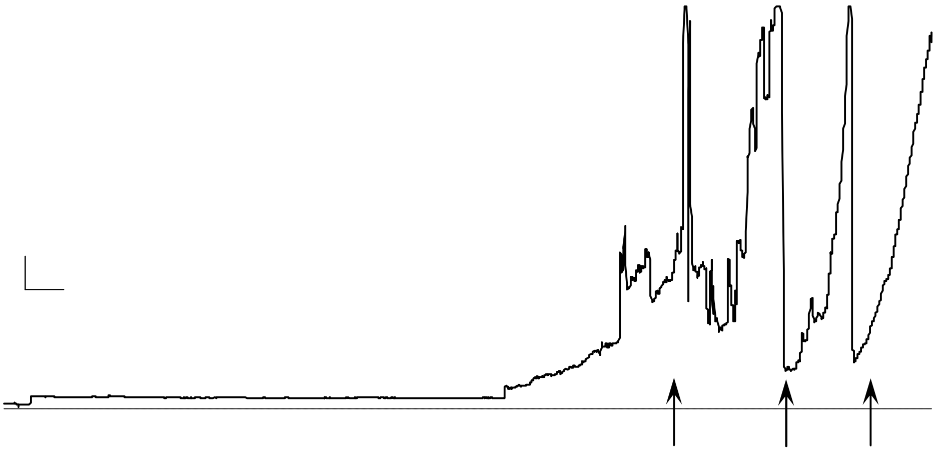

Figure 5.10: Temporal change of membrane current (ordinate), in the presence of NPs. The sensitivity of the current recording device was changed during the recording (at the moments marked by arrows) from 1 nA/V at the start of the trace to 1 μA/V at the end. Conditions: NP concentration 300 μg/mL, 200 mM KCl, pH 6, transmembrane voltage 60 mV. The plane of the lipid bilayer was vertical and it was situated about 10 mm above the floor of the glass chamber. Calibrations: vertical 5 pA (initially), horizontal 10 s.

In the model experiments, the added NPs diffuse to the surface of the membrane and are adsorbed. The adsorbed particles diffuse within the membrane, and self-assemble into a conducting transmembrane system, resulting in an increased transmembrane current. Step by step the membrane conductance is increased: it is a dynamic, reversible process, the pore-forming substance can also leave the membrane and the conductance then decreases. The step-like fluctuations of the membrane current at the start of the trace probably correspond to the formation of discrete ion-conducting 20 pS pores.

5.7.1 Analysis of the biodesulfurization kinetics

The overall biodesulfurization reaction is:

$$\text{DBT} \longrightarrow \text{HBP} \qquad (3)$$

Writing *D* and *H* for the concentrations of DBT and HBP respectively, the corresponding kinetic equation is

$$\frac{dH}{dt} = kDB \qquad (4)$$

where *B* is the concentration of the bacteria and *k* the rate coefficient. The integrated form is

$$\ln\left(1 - \frac{H}{D_0}\right) = kBt \qquad (5)$$

where D_0 is the initial DBT concentration (0.5 mM). Linear regression of the data from Figures according to eqn (2) yields *k* (Table 5.1). It can be seen that decoration increases the biodesulfurization activity by 56%.

Table 5.1: Rate coefficient for biodesulfurization (eqn 4)

	k / $cm^3 s^{-1}$(means ± s.d.)
Nondecorated	$1.01 \times 10^{-10} \pm 5.92 \times 10^{-12}$
Decorated	$1.58 \times 10^{-10} \pm 6.85 \times 10^{-12}$

5.8 Discussion

In order to combine the advantages of immobilization—i.e. ease of separation and microbial longevity—with those of free diffusion—i.e. good mass transport—another approach is possible, namely to decorate the bacterial cells with magnetic nanoparticles. After completion of the reaction, the bacterial cells can be separated from the products using a magnetic field. This is a much milder and more cost-effective process than centrifugation, and allows the bacteria to be reused many times and magnetic separation is compatible with any automated platform that can be equipped with a magnet.

The reason of choosing 50 nm for my experiments was for primary aim of this investigation that was to study the effect of attachment of magnetic particles to the bacteria, in order to enable convenient post-reaction separation, and not to optimize every experimental parameter.

If the particles are large, their Brownian energy overwhelms the relatively weak attachment forces. Preliminary experiments using iron oxide particles with a diameter of 1 µm (Dynabeads, Dynal Biotech) showed that they did not attach to the bacteria (Figure 5.11). Furthermore, the particles should be small enough to be superparamagnetic, i.e. smaller than the critical magnetic domain size (Morrish et al., 1956; Schmidt 2001; Zhang et al., 2006). This critical diameter is around 50 nm for our material.

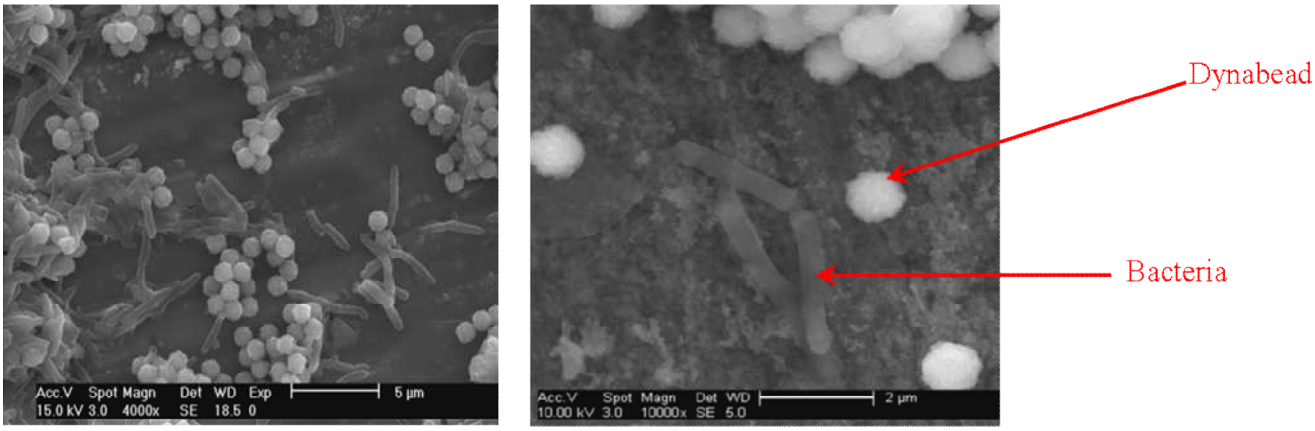

Figure 5.11: Dynabeads with the diameter of 1 µm did not attach to the surface of bacteria.

So the bacteria were decorated with Fe_3O_4 nanoparticles to facilitate cell separation at the end of the desulfurization process; decoration is facilitated by electrostatic attraction between the nanoparticles and the bacteria.

I found that I could thereby achieve a 56% higher rate of desulfurization. I favour the view that the rate limiting step of the process is transport of DBT into the cell, where it undergoes desulfurization. The results shows increase the permeability of a model black lipid membrane, thereby enhancing ingress of the DBT into the cell. The use of *Rhodococcus* decorated by magnetic nanoparticles also facilitates its recovery and reuse; hence it offers a number of advantages for industrial applications compared to nondecorated cells. The generation of stable, inexpensive and nontoxic adjunct materials for use with microbial cells greatly facilitates the separation of the cells from the products during bioreactor process development, and the removal of the cells from the medium at any time via magnetic decantation.

5.9 Conclusion

The main discovery emerging from these experiments is that the decorated bacteria are significantly more active in desulfurization–could thereby achieve a 56% higher rate of desulfurization. Here I discussed possible reasons, starting with the open issue that if the biodesulfurization takes place within the cytoplasm the bacterial surface constitutes the rate limiting barriers to the process (transport of DBT into the cell or HBP out). I proposed that permeabilization of the bacterium is improved through decoration by nanoparticles, and some supporting evidence in a model system was obtained.

Chapter 6 : A novel assay for optimizing nanoparticle-bacterium interactions

From previous experiments I have found that biodesulfurization activity is enhanced if bacteria are decorated with ferrous nanoparticles but appraisal of particle adhesion to bacteria had been largely qualitative, based on visual assessment of decorated bacteria (e.g., Fig. 5.5). In order to develop this quantitatively, I investigated the adhesion of bacteria to the nanoparticles by first depositing a thin layer of Fe_3O_4 magnetic nanoparticles onto a planar $Si(Ti)O_2$ waveguide surface. The rationale is that we can use high resolution molecular microscopy (HRMM) to determine with great precision the adhesion of an object to a planar surface (Fig. 6.1). Therefore the objectives of my work in this chapter are to understand the attachment of bacteria to the magnetic nanofilm; the nanofilm fabrication also required me to gain further understanding of the kinetics of deposition of the particles. An overview of the techniques and the experimental procedures used is given. Finally the effect of pH on the surface potential of the nanoparticles is presented.

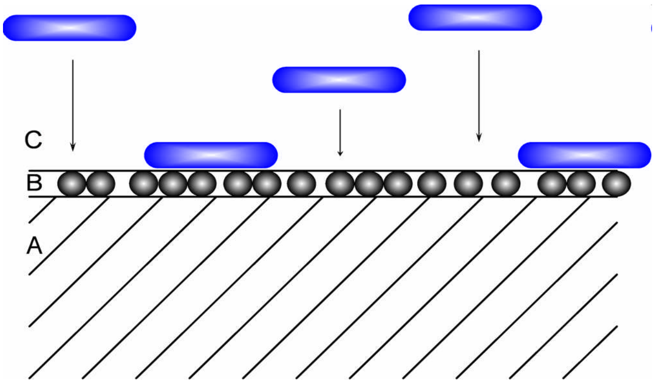

Figure 6.1: Diagram showing idealised adsorbed nanoparticle layer (B), cover medium (C) containing bacterial cells in solution and the substrate (A) onto which the particles adsorb.

Previously reported work has focused mainly on identifying particular bacterial surface molecules whose presence is correlated with adhesion and biological aspects of adhesion (Fletcher 1996). Very little work on kinetics has been reported; Wiencek and Fletcher 1995 have presented a low resolution study and the measurement of adhesion processes had been hitherto mostly achieved by use of optical or scanning electron microscopy (SEM) but these methods requires the cell to be killed and the force of adhesion can be obtained by determining the centrifugal force necessary to dislodge the cells (Guarnaccia and Schnaar, 1982). The study of attachment of biomolecules is one of the most effective methods for extracting further parameters which characterise the biomolecular environment. For example, Ramsden’s studies in 1995 led to a better understanding of cell attachment at solid-liquid interfaces. McColl et al. (2008) have demonstrated the ability to manipulate the surface characteristics providing a mechanism for directly influencing cell behaviour, monitored by optical waveguide lightmode spectroscopy (OWLS), also known as HRMM. Their results show the application of surfaces for controlling cell behaviour.

In the present work, in order to optimize the decoration of bacteria, it was necessary to investigate in detail the actual adhesion process, under hydrodynamic conditions that are amenable to exact analysis. OWLS is extremely powerful for investigation of kinetics of attachment of bacterial cells to the surfaces. It was used as the principle method of monitoring the creation of magnetic nanofilms and investigating the attachment of particles on surfaces. Hence, to simulate the adhesion process (in which, in practice, suspensions of the nanoparticles and the bacteria are simply mixed), I have deposited a monolayer of the particles on a planar optical waveguide, and flowed the bacterial suspension above it under laminar flow conditions.

6.1 Bacterial adhesion to minerals

Bacterial adhesion is probably a very complicated process with many different physicochemical factors involved such as environment, temperature, van der Waals attraction forces, Brownian motion, gravitational forces, hydrophobic interactions and the electrostatic charge of the surface (Dankert et al., 1986; Krekeler et al., 1989). Adhesion of bacteria to minerals has already been widely investigated (Somasundaran, 2006). These studies have highlighted the importance of both the characteristics of the bacteria (cell wall, growth phase and metabolic state) and environmental composition (pH, ionic strength, sorbent concentration and temperature). Many of these variables are known to affect adsorption by a variety of electrically charged particles (Stumm and Morgan 1996), but a few are especially relevant to biological sorbents. It is presumed that bacterial adhesion is strongly dependent on the environmental situation and the ability of the bacteria to adhere to mineral surfaces directly depends chiefly on their electrostatic properties.

6.2 Background

It is known that the orientation and conformation of bacterial coat biomolecules (e.g., proteins, polymers, lipids) are important in determining how bacteria sense the surface of an artificial material and there is an enormous literature to support the contention that the behaviour of bacteria in aqueous environments is mainly related to surfaces (Costerton et al., 1987; Lachlan et al., 2004).

Bacterial interaction with different surfaces may explain differences in their internal metabolism behaviour but it is complex and the vast array and diversity of bacteria makes the field poorly understood (Haynes et al, 1994) and a lot of question still remain unanswered. To gain insight into these interactions a logical approach is to investigate the media on which bacteria attach. Bacterial adhesion to a surface can be illustrated by two-phase process, which was first proposed by Marshall, 1985: *i*. an initial, immediate and reversible phase (deposition) and *ii*. a time-dependent and irreversible phase (adsorption) (Fig. 6.2). Once adsorbed, the bacteria are attached.

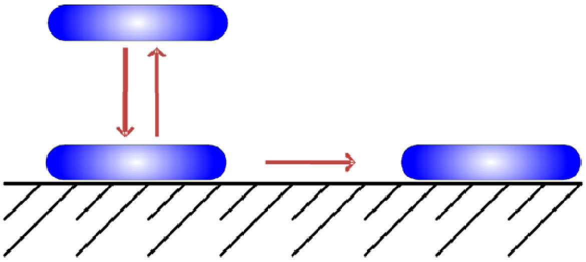

Figure 6.2: Bacterial deposition (left) and adsorption (right).

6.3 Controlling the stickiness of the bacteria to the surfaces

Bacteria when attached to surfaces appear to differ metabolically from their free living counterparts (Melo et al., 1992). And there are also metabolic differences when they approach to the surface, and on post-approach (An and Friedman, 1998). This is because bacterial surface attachment leads to changes in physicochemical conditions at the interface, which influence bacterial metabolism through environmental effects. The effect of ions on the solution/solid interface is considerable and the structure of the cell membrane is expected to depend on the nature of the surfaces with which they are in contact (Cacace et al., 1997).

Numerous studies have been carried out to investigate ways in which solid surfaces influence bacterial activity and influence the ‘stickiness’ of the bacterial surfaces to the solid interface. However because of the diversity of bacteria it has been impossible to formulate a general principle to describe the influence of surfaces on bacterial physiology (Dankert et al., 1986). Hence the relative significance of influential factors are dependent not only the physiological capabilities of the bacteria, but also on ambient conditions such as salt concentrations, pH, nature of the solid surface (e.g. surface charges) and many other factors and consequently bacterial adhesion excites our interest to design surfaces to control adhesion and so contribute to the development of bio-active nanofilms.

6.4 Surface charge

Since many of the important properties of systems concern directly or indirectly the electrostatic charge on the particles, which determines the adsorption of ions and dipolar molecules, hence the interaction energy between the particles can be determined by the potential distribution and in many cases this is responsible for the stability of particles (e.g., nonaggregation).

On the other hand, the ability of the bacteria to adhere to mineral surfaces directly depends on their electrostatic properties. To date, adhesion of bacteria to the minerals have been widely investigated and discussed with reference to the characteristics of the bacteria (cell wall, growth phase and metabolic state) and environmental composition (pH, ionic strength, sorbent concentration and temperature). Many of these variables are known to affect ionic adsorption by a variety of electrically charged particles (Stumm and Morgan 1996), but some are especially relevant to biological sorbents. The bacterial cell membrane always has negatively charged surfaces and these are influenced by bacterial age, growth medium and the structure of the bacterial surface (Dankert, 1986) and the negatively charged particles could not be attached to the bacterial membrane with ease. Therefore as input data for predictive physiochemical models of bacterial adhesion to surfaces, the zeta potentials of their surface are frequently measured (Rodriguez et al., 2003).

6.5 Bacterial adsorption kinetics

One of the most effective methods for further understanding the parameters involved is to study the kinetics of bacterial adhesion/adsorption. Therefore, high sensitivity techniques (involving monolayer coverage) which allow the in situ, real time monitoring of such surface processes are valuable in potentially contributing to a better understanding of the attachment of particles or materials under conditions as close to biological environments as possible (Ramsden 1993; Brash and Wojciechowski 1996,; Ulman and Fitzpatrick 1996).

6.6 Attachment measurement techniques

To measure the interaction of biomolecules with a surface, there are a variety of known techniques that can be used to determine biomolecule adsorption processes: enzyme-linked immunoassay (ELISA), solution depletion, gravimetric, surface acoustic wave, spectroscopic (IR, fluorescence), ellipsometry, radiolabeling, electric, hydrodynamic and other techniques. However, none has the required sensitivity to follow the monolayer adsorption process, or they are not suitable for in situ, real time measurements, which reduces their value for dynamic studies. There are number of techniques used to measure the amount of mass deposited onto a surface in a several nanometers thick layer (Malmsten 2003). Among these techniques, optical and acoustic methods are widely used to obtain continuous measurement of macromolecular adsorption on variously modified surfaces and study the deposition process and the structure of thin films (Ramsden 1994a; Potyrailo et al. 1998; Ramsden 1999). These methods are consistent with the requirements for high surface and high detection sensitivity and can be applied to study in real time the dynamics of molecular processes at solid surfaces such as: optical waveguide lightmode spectroscopy (OWLS), total internal reflection florescence (TIRF), scanning angle reflectometry (SAR), surface plasmon resonance (SPR), resonant mirror (RM), and ellipsometry (ELM). These techniques by providing in situ characterization of the films are extremely useful on a small scale. Non optical methods also exist, such as quartz crystal microbalance (QCM) which is based on measuring the change of the piezoelectric quartz crystal frequency when a small amount of mass is attached. Each of these methods or techniques offers various advantages and of course, disadvantages (Brusatori 2001). For example, TIRF requires a particle with both a natural or attached fluorescent label and the QCM technique requires careful accounting of viscous drag of the contacting liquid. In contrast, OWLS does not have any of these problems (Brusatori 2001), and has been shown to provide precise and accurate kinetic adsorption data for several particle/surface systems (Kurrat et al., 1997; Ramsden and Máté 1998).

Since in my investigation I needed an appropriate technique to provide precise and continuous kinetic measurements of biomacromolecular adsorption, I used OWLS to obtain continuous measurements of particle attachment (Horvath et al., 2005; Ramsden et al., 1995b; Li et al., 1994). Optical waveguide lightmode spectroscopy (OWLS) is an optical biosensor which is suitable for monitoring of continuous adsorption processes on the surfaces and provides the required high-accuracy kinetic data required with excellent time resolution. This has enabled me to probe the processes involved in bacterial adhesion with nanometric precision.

On the other hand, OWLS is a very sensitive method which can measures the effective refractive index above a solid surface within a sensing distance of about hundreds nm (Ramsden 1994b). Changes in electronic polarizability in the evanescent field of an optical waveguide change the phase velocity of guided waves. This change can be interpreted as the change of mass and/or shape of adherent bacteria. Interaction of the cell body with the evanescent field produces a significant change in the waveguide propagation parameters. From the above consideration the aim of this work has been to investigate whether interaction energies determined by average physicochemical properties of bacterial and adsorbing nanomagnetic surfaces play a determining role in adhesion. The OWLS technique enables kinetic information on cell response to different pH of substrata to be obtained. Thus, the optical waveguide is a powerful biological sensor for the detection of cell adherence.

6.7 Optical waveguide lightmode spectroscopy (OWLS)

OWLS is an extremely powerful technique for measuring thin films at liquid/solid interfaces and it is sensitive to the effective refractive index and the thickness of the adsorbed layer, and so it can be used to calculate the mass adsorbed onto a thin film (Kurrat et al., 1994; 1997; Ramsden, 1997). OWLS is based on the confinement of light in a high refractive index layer (Ramsden 1994a), and can be used for studying adsorption and adhesion of macromolecules onto surfaces and biospecific binding processes (Ramsden 1993; Kurrat et al., 1998; Ramsden 1999).

An optical waveguide in the form of a thin slab of high refractive index material surrounded by lower refractive index material (usually a glass substrate) exhibits a discrete spectrum of modes when for example the polarized light from a He-Ne laser is coupled to it, discrete incident angles: transverse electric (TE) and transverse magnetic (TM) mode. The evanescent field extends a few hundred nanometers above the surface of the waveguide and it probe changes in the refractive index upon mass adsorption at the waveguide surface (Fig. 6.3). The evanescent field will interact with cells or indeed anything else sitting on the waveguide. Any change at the waveguide surface results in a change to the measured propagation constants of the guided modes and results in a shift in the incoupling angles (Ramsden 1995a).

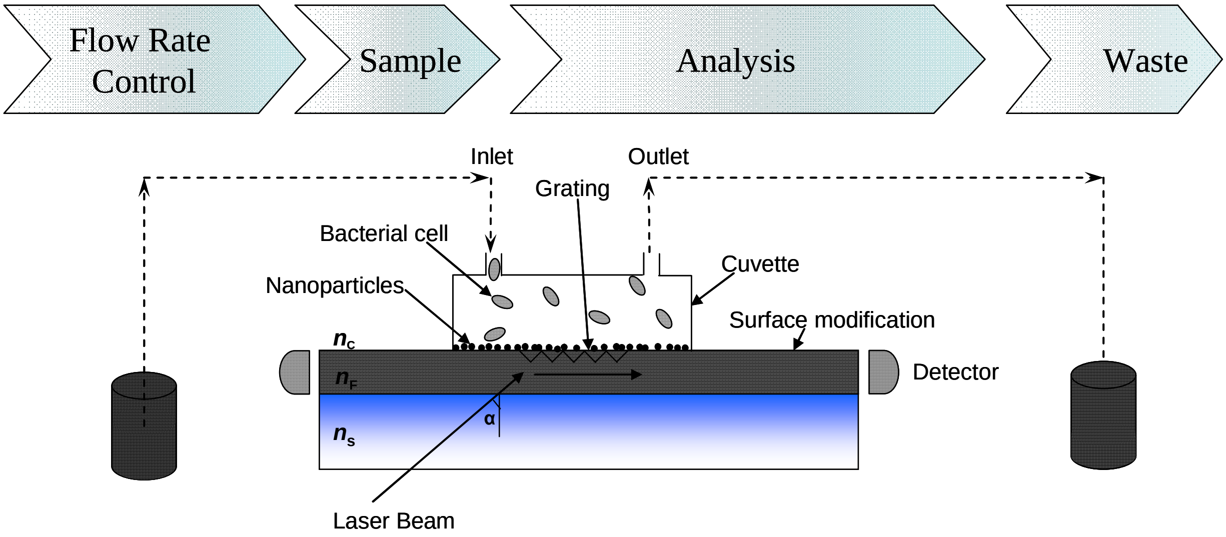

Figure 6.3: Diagram of OWLS principle. OWLS flow-through deposition cuvette placed on the top of the waveguide, which forms its bottom. The polarized laser beam is incident on the bottom with coupling angle α. The whole system is rotating left and right and the light is diffracted, incoupled and made to reflect and propagate along the waveguide at certain angles. The resonance peaks are recorded by detectors on the ends of the waveguide.

Figure 6.3 illustrates a waveguide with a cover medium (C) which can be modified, film F with grating and optical glass support (S). The incoming laser beam makes an angle α termed the coupling angle with the normal of the grating. The laser beam is coupled into the waveguide by frustrated total internal reflections is then diffracted by the grating and out put peaks are detected by the detector at the end of the waveguide while the coupling angle of the laser beam is scanned with high precision. During this procedure sample suspension under test flows through a cuvette, with the incident polarized laser beam entries from underneath and at the same time the whole system rotates left-right (Horvath et al., 2001).

At the interface, light penetrates approximately 100 nm into the sample medium, which corresponds to the penetration depth of the evanescent wave. If species type such as molecules, nanoparticles or cells are adsorbed at the interface (Hug et al., 2002) (within the penetration dept of the evanescent wave), the extent of the phase-shift depends on the total amount of adsorbed molecules. Due to this phase-shift the light intensities of both the transverse electric (TE) and transverse magnetic (TM) modes reach their individual maxima at certain coupling angles.

6.7.1 OWLS principle

This method is a common approach to measuring the propagation constants of the guided lightmodes (Ramsden 1993). As shown in Figure 6.4 in a planar dielectric waveguide light from an external beam (typically a highly monochromatic, wavelength λ, linearly polarized laser) is guided in the waveguide film by total internal reflection

(TIR) at the film/cover- and the film/substrate-boundaries. For more detail about the principle and equations of this technique see appendix A.

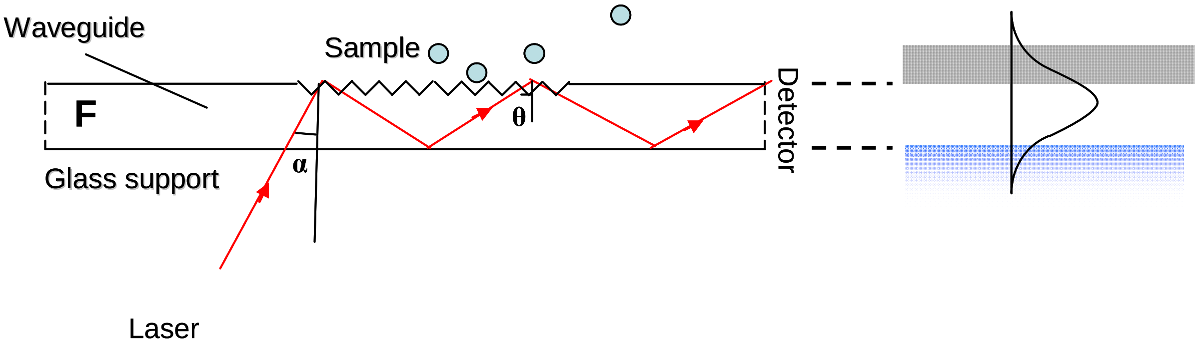

Figure 6.4: Sensor with illustration of light guided in the waveguide. A He–Ne laser beam propagates through the glass support S (refractive index n_S), α is the incoupling angle, F the waveguiding film (refractive index $n_F \approx 1.8$, thickness $d_F \approx$ 200 nm), the intensity of the light being monitored via the detector. The right hand drawing sketches a typical electromagnetic field distribution for a zeroth guided light mode.

The planar waveguide measures the refractive index (RI) of the cover medium and in fact it is a refractometer where it is possible to change the cover medium. Light is coupled into the waveguide at the near end facet of the film over a range of coupling angles, α, guided in the film range of over a equivalent internal incidence angles, θ, and then coupled out at the far end edge, where the detector measures the output light. The effective refractive indices (N) of the waveguide can be calculated from the measured α.

In the other word, N is the average effective refractive index of the different waveguide layers and of the medium above, and can be related to the incoupling angles (Ramsden 1993).

$$N = n\sin\alpha + k\lambda/\Lambda \qquad (1)$$

Where n is the refractive index of air, α the angle of the incoupled light, k the diffraction order, λ the wavelength of the laser and Λ the period of the diffraction grating. If particles deposited, the refractive index changes at the interface and the incoupling angles shift. Monitoring the shift of the incoupling angles of the guided modes allows for the simultaneous determination of the thickness and the refractive index of the adsorbed layer. Therefore this technique enables the direct real time monitoring of any changes on the surface. For more details about the governing equations for this technique see appendix A.

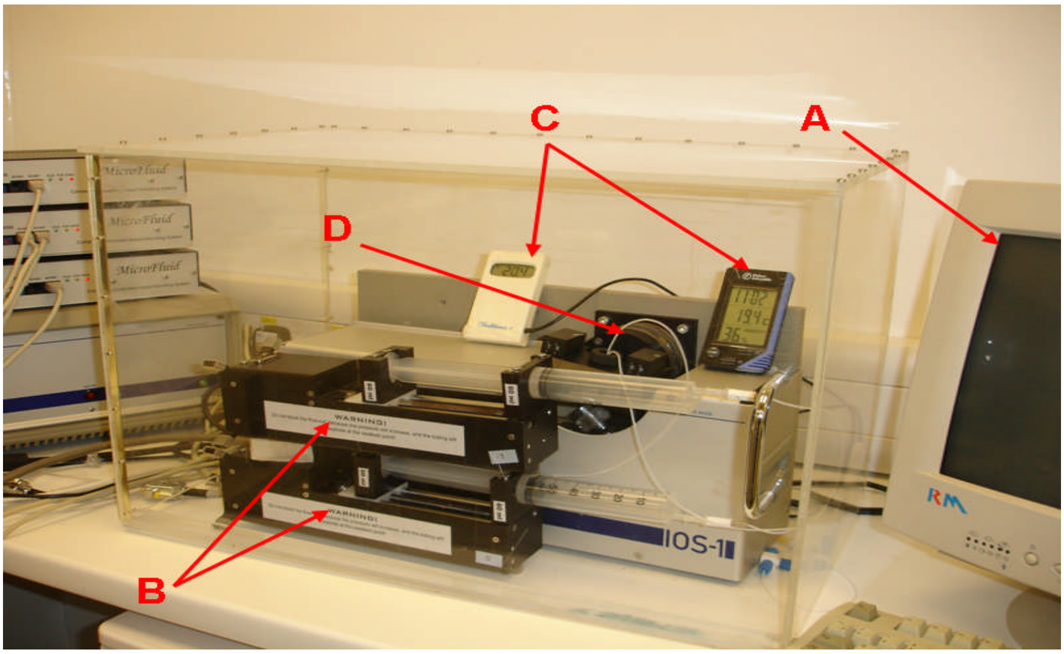

Figure 6.5: Experimental setup of OWLS, BIOS-1 integrated optics scanner (ASI, Switzerland). A, computer, B, injection system, C, temperature control units, D, goniometer and cuvette.

A schematic of the flow through cuvette mounted on the goniometer is presented in Figure 6.6. Before starting the experiment the waveguide is cleaned and inserted into a holder and the cuvette secured on top of the waveguide.

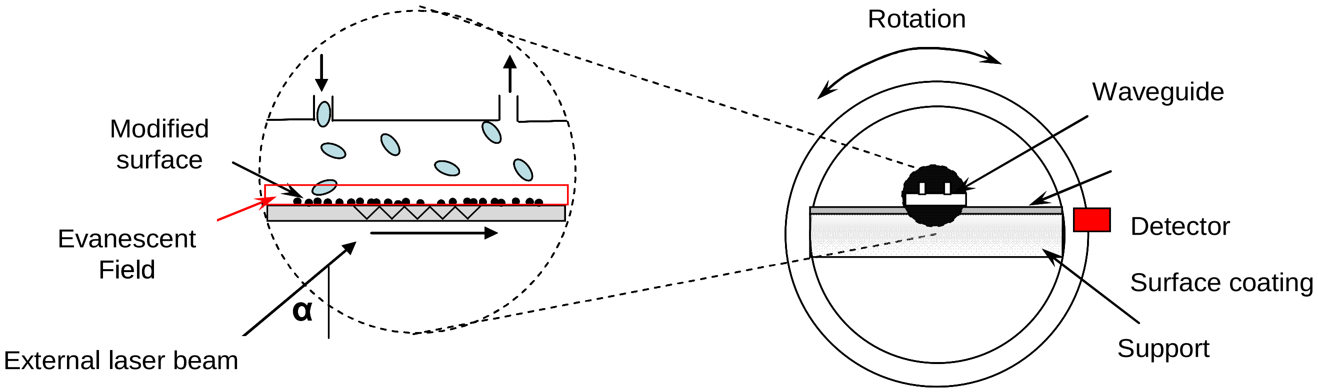

Figure 6.6: ***Goniometer***

OWLS's sensing principle is based on the evanescent electromagnetic field associated with the guided light, which extends a few hundred nanometers above the waveguide. The grating incouples light into a planar optical waveguide in which the light then propagates, generating an evanescent field. This evanescent field is used to probe the optical properties of the solution in the area of the surface zone. This is the basis for the sensitivity of the method to changes in the refractive index when deposition of macromolecules, cells or nanoparticles occurs.

The refractive index of all solutions have been measured by a J357 refractometer (Rudolph Research Analytical, Hackettstown, USA) which has a sapphire prism onto which a 633 nm laser is focused (Fig. 6.7).

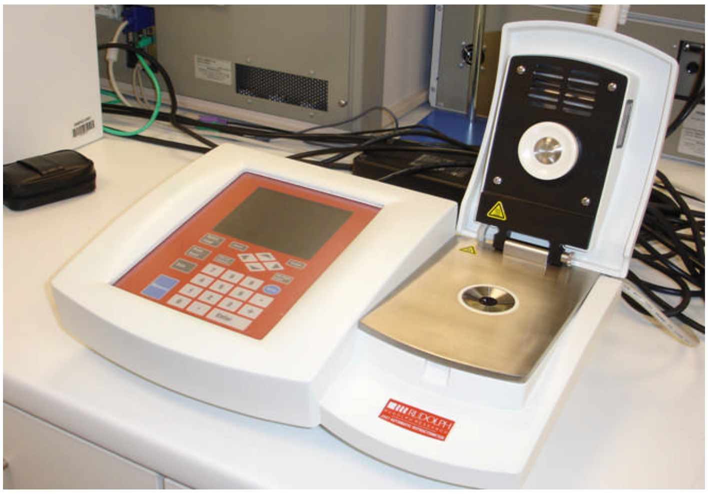

Figure 6.7: Rudolph J537 refractometer

6.7.2 Planar waveguide

A schematic of the waveguide is shown in Figure 6.7. This sensor chip is used to sense the adhesion or adsorption of particles or cells. In order to introduce light into the waveguide, the laser beam could be focused onto one end. Since the waveguide is only 100-200 nm thick, however, this is very difficult. It is more convenient to use a diffraction grating to couple the light into the waveguide as shown in Figure 6.4. A planar waveguide can be used to measure the refractive index of the cover medium and consists of a three-layer dielectric structure (Fig. 6.8):

a. optical glass substrate S

b. waveguide film F supported on the glass substrate

c. cover medium C, which it is possible to change

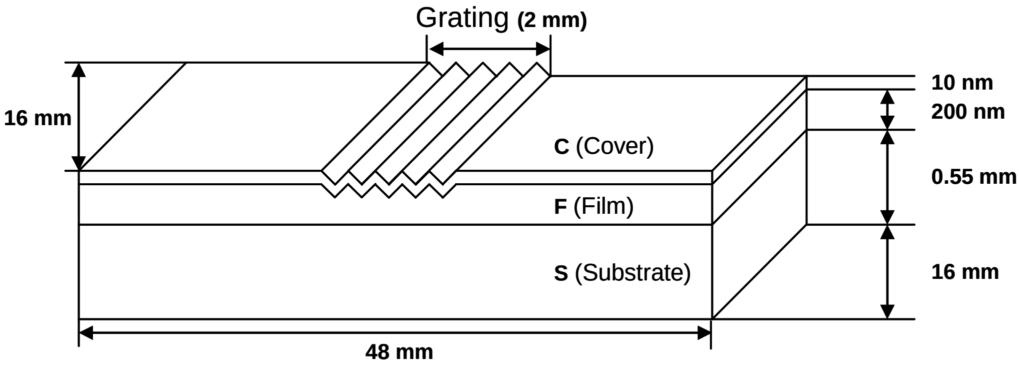

Figure 6.8: Sketch of the optical waveguide grating coupler sensor chip (made by Microvacuum Ltd, Budapest).

6.8 Experimental part of the research

6.8.1 Waveguide sensor chips

Silica-titania sensors $Si_{0.6}Ti_{0.4}O_2$, the original planar waveguide chips used for OWLS measurements, are made from amorphous silica-titania in the ratio of approximately 2:1, with a penetration depth of the evanescent field of the order of 100 nm. These waveguides, obtained from MicroVacuum Ltd (Budapest, Hungary), have a $Si(Ti)O_2$ waveguiding surface layer, with thicknesses $d_F \approx 200$ nm and refractive index $n_F \approx 1.80$, and are provided with an embossed surface relief grating of $1/\Lambda = 2400$ lines per mm (grating constant $\Lambda = 417$ nm). These chips were optimized for a wavelength $\lambda = 633$ nm.

Before starting an experiment, extended soaking is necessary to avoid a drift in the effective refractive index during the experiments. This effect is attributed to the gradual filling of the porous waveguiding film with solvent (Ramsden, 1994a). This is an essential procedural step, which is needed to improve the adhesion of nanoparticles on the surface. Therefore for each experiment the waveguides were pre-equilibrated overnight in ultra pure water at 25 ºC and then inserted into the flow cell assembly which is mounted by a cuvette into the system.

6.8.2 Substratum waveguide cleaning

Cleaning of the waveguide prior to the experiment is an important factor for obtaining reliable results. Waveguides were cleaned after each experiment and could be reused several times to reduce costs. There are a few methods can be used for cleaning depending on the experimental parameters. For example, bacterial cells attached on an uncoated waveguide can be removed easily using a weak acid solution whereas magnetic nanoparticles adhere more strongly and required more aggressive detergent. In this work a number of cleaning methods were used. (The rinse step involves filling the centrifuge tube with fresh water and then it pouring out).

6.8.3 Cleaning off the bacteria

To remove bacteria from the waveguide surfaces Roche “COBAS Integra” cleaning solution was used. The method for cleaning bacterial cells from waveguides was sonication in Roche cleaning solution for 15 min, rinsing with ultrapure water, and treating with O_2 plasma (20mW for 2 min at 0.5 mbar O_2) (Bio-Rad Barrel Asher) (Fig. 6.9).

Figure 6.9: Plasma cleaning apparatus (placed in the clean room).

6.8.4 Cleaning off the magnetic nanoparticles

Magnetic nanoparticles adsorbed on the waveguides are extremely well bonded and cannot be removed by the Roche treatment. The protocol used instead comprises full submersion of waveguides in chromic acid for 3 min at room temperature and then immediate rinsing with KOH (2M) for 1 min and then sonicating in ultra pure water for 30 min to remove the entire residue, rinsing with ultra pure water, and treating with O_2 plasma for 2 min (Fig. 6.10).

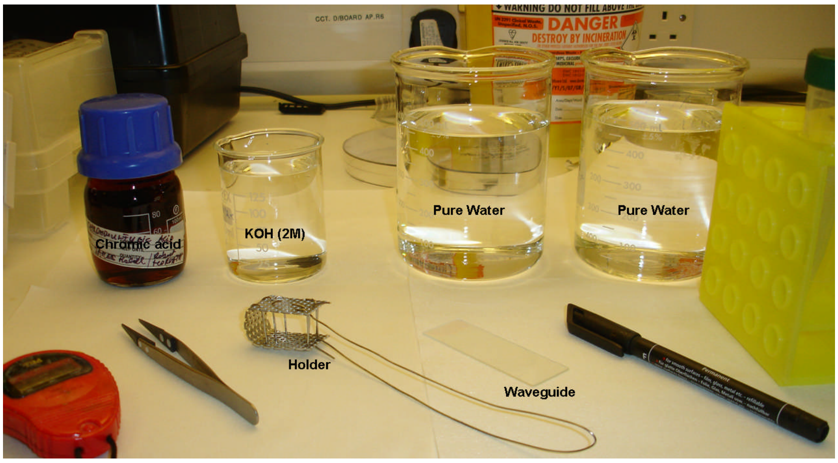

Figure 6.10: Chromic acid cleaning in the clean room.

6.8.5 Determination of surface potential

The zeta potential is the electrostatic potential at the slipping shell, which is a certain distance out from the particle surface into the solution (Somasundaran, 2006). The zeta potentials of the prepared nanoparticles suspended in ultrapure water (100 μg/mL) were measured at room temperature using a Beckman Culture USA Delsa NanoC Particle Analyzer. The pH of the as-prepared particles in suspension was 7.0. To generate zeta potentials versus pH curves, the pH of the suspensions was adjusted using dilute HCl and KOH solutions followed by stirring to equilibrium (Fig. 6.11).

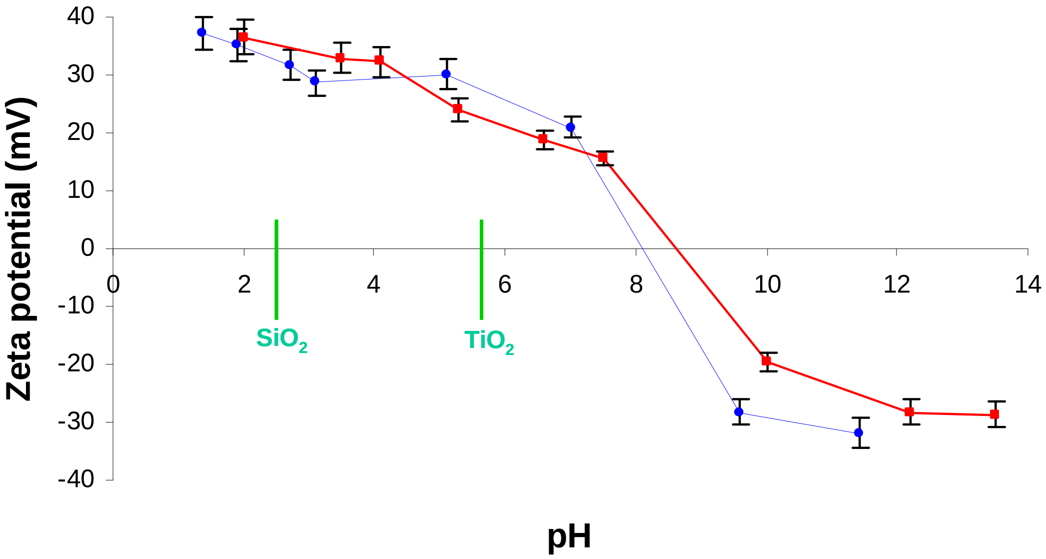

Figure 6.11: Surface charge on Fe_3O_4 magnetic nanoparticles coated with PEG (blue) and without PEG (red), suspended in water at 25 °C as a function of pH, (pH changed by appropriate additions of HCl or NaOH). The isoelectric point is the pH at which the zeta potential is zero. The isoelectric points of the oxides constituting the substratum are also marked (Cacace et al., 1997).

The zeta potentials of bacteria suspended in deionised water (5.6 mg/L) were measured. Bacteria in aqueous suspensions always have a negative charge (Fig. 6.12). For our experiments in order to keep the bacteria alive the pH had to be kept to 7. At pH 7, the bacteria are negatively charged and hence they will electrostatically attract the nanoparticles.

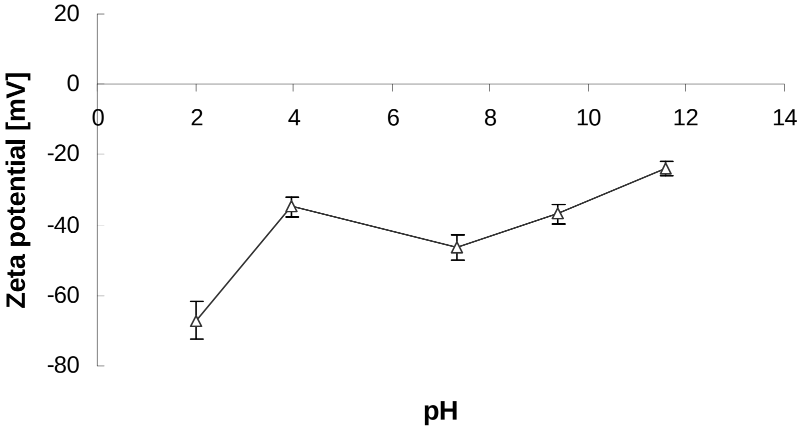

Figure 6.12: Surface charge of *Rhodococcus erythropolis* suspended in water at 25 °C as a function of pH, (pH changed by appropriate additions of HCl or NaOH). Symbols are centred as the mean, with the range marked. The bacteria are expected to be alive at pH ranging from 5.7–7.5 (middle point only).

6.9 Creation of a layer of magnetic nanoparticles on the waveguide (adsorption/desorption)

For my experiments I wanted to investigate the adhesion of magnetic nanoparticles to the surface of bacteria, by depositing a thin layer of Fe_3O_4 magnetic nanoparticles onto a $Si(Ti)O_2$ waveguide surface and firstly the experiments were carried out to reveal the effect of PEG deposition with nonPEG-coated and PEG-coated particles to create the layer. Therefore initial work was to investigate the adsorption/desorption characteristics of magnetic nanoparticles using OWLS. The effective refractive indices N of the transverse magnetic TM_0 and transverse electric TE_0 modes were continuously and repeatedly determined using a flow rate of 0.4 mm^3/s while:

(i) ultrapure water flowed through the cuvette until a stable baseline was achieved and then (ii) a Fe_3O_4 magnetic nanoparticles solution, at a concentration of 50 μg/mL in water, and finally (iii) ultrapure water again drawn into the cuvette to wash out the excess particles which were not adsorbed on the surface of the waveguide for measuring the desorption kinetics. During the entire sequence of flowing water, the effective refractive indices (propagation constants) of the zeroth order transverse magnetic and transverse electric lightmodes were measured. The solution of magnetic nanoparticles was made up and sonicated for 20 minutes before use. The temperature was maintained at 25 ºC and the pH of the solution was 7.0. The refractive index increment (dn/dc) (Ball and Ramsden, 1998) of the nanoparticles in water required for the calculations was determined by use of a refractometer at different concentrations. The determined value of dn/dc was 0.558 cm3/g for bare nanoparticles and 0.244 cm3/g for the coated particles with PEG (Section 4.11).

6.9.1 Experimental results and discussion

The comparison of the total mass surface concentration and refractivity calculated shows that the surface was seeded by aggregates of non PEG coated particles and has reasonable aggregates. This is clearly shown in Figure 6.13 which particles gradually make the aggregates on the surface of waveguide. Since the adsorbed mass kept increasing while the resonant peak intensities reduced (data is not shown), so we could not continue the experiment after around 2000 s. The aggregation could even be seen in an ordinary optical microscope.

Whilst the self–assembly of the uncoated resulted in massive aggregates deposited on the waveguide, which increased the noise relative to the signal (because the aggregates absorb too much light), the measurement had to be discontinued and cannot be used to assemble thin films (Fig. 6.13).

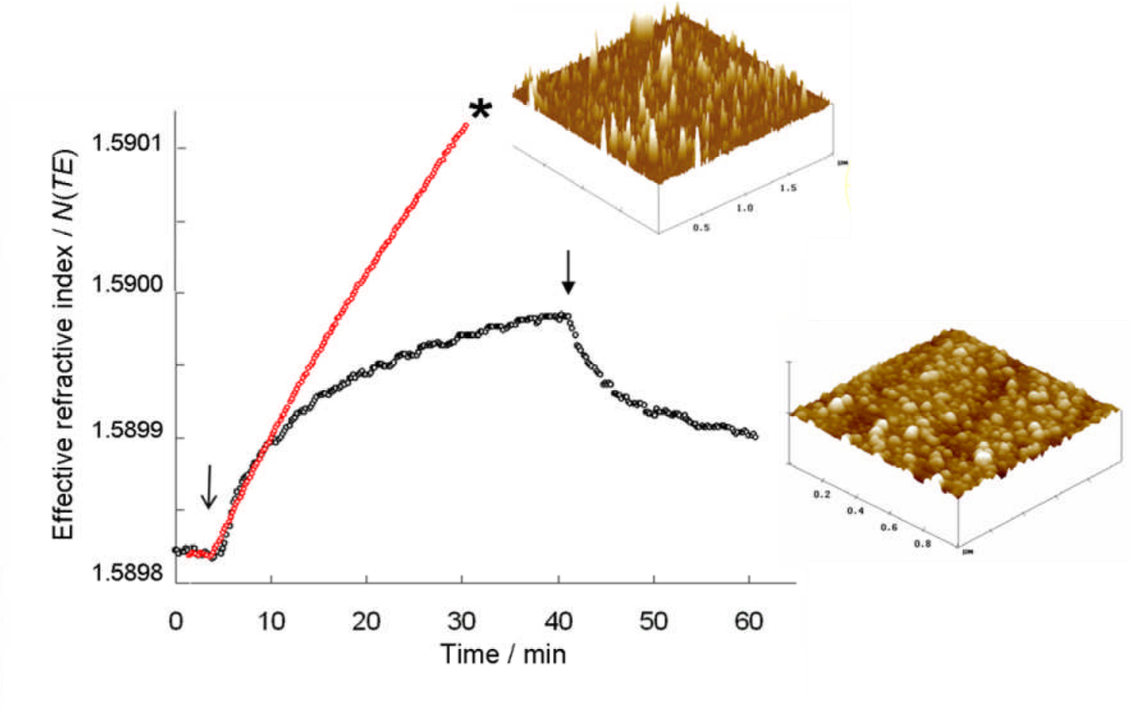

Figure 6.13: Effective refractive index changes during self-assembly of uncoated (red) and PEG-coated (black) nanoparticles at pH=7 on the surface of the waveguide at concentration of 50 µg/mL. The initiation of nanoparticle flow is marked by the open-headed arrow. The replacement of the nanoparticle suspension by ultrapure water is marked by the solid-headed arrow. The asterisk marks where the measurement had to be discontinued due to excessive noise (too much guided light was absorbed by the particles).

Therefore we decided to use coated particles by PEG. Because this polymer does not effect on the surface charge of particles and prevent of agglomeration.

6.9.2 Microscopy of adsorbed nanoparticles on the waveguide

Careful and detailed study of the adsorption desorption behaviour is essential to achieving a deeper understanding of the nanofilm functional behaviour, Atomic force microscopy (AFM) was used to visualize the nanoparticles attached onto the solid/liquid interface. AFM has the ability to obtain topographical information of the waveguide surface coated by nanoparticles and it has several advantages over the electron microscope (Bogue, 2007). Unlike the electron microscope images which are two dimensional, the AFM provides a true three dimensional surface profile. Moreover samples viewed by AFM do not need special preparation that would destroy the sample and can work perfectly in an ambient environment. While the electron microscope needs expensive vacuum environment. Therefore AFM was used to scan the surface of waveguides coated by magnetic nanofilms.

AFM images were collected in tapping mode with a SPM 3000 Dimensions equipped with a silicon cantilever (Nanosensore PPP-NCH) with a sharpened tip (radius < 10 nm). Samples were transferred to the AFM from the OWLS experiments while in contact with. 2μm × 2 μm height images were captured using a scan speed of 0.5 Hz and a maximum resolution of 512 × 512 pixels. Images were flattened to remove background slopes. Each sample was scanned at several randomly chosen locations, but no difference was observed among these locations on a given sample. Figure 6.14 shows a typical example.

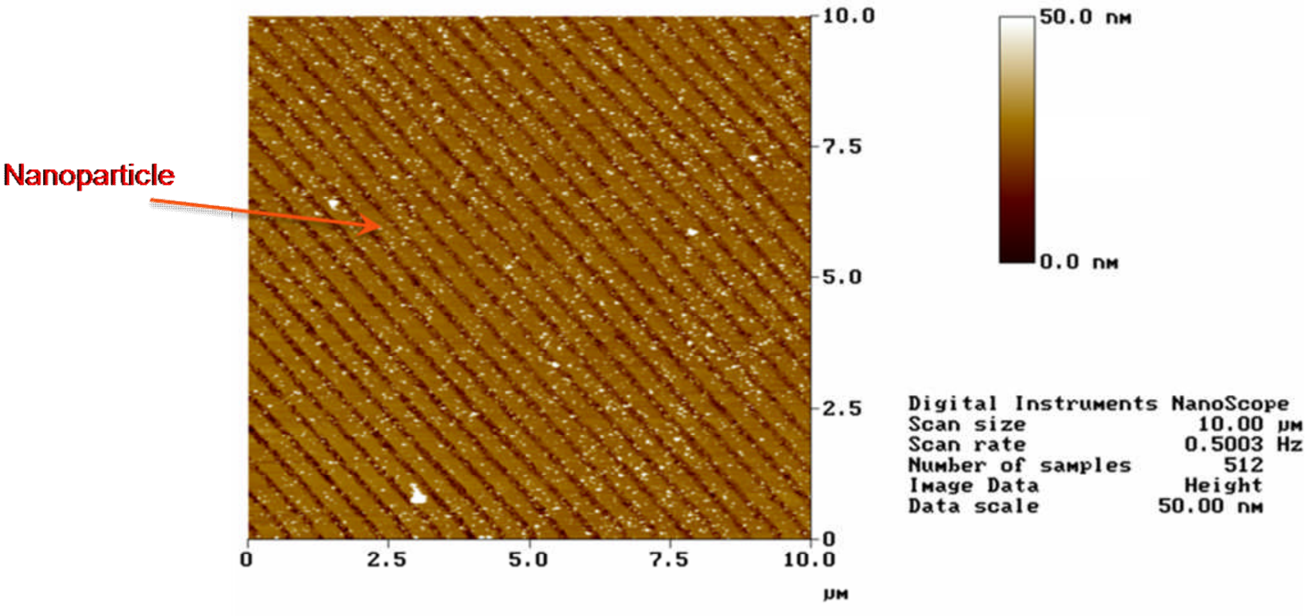

Figure 6.14: AFM image of Fe_3O_4 particles deposited on a waveguide. The diagonal features are the grating. The nanoparticles are the small points and the bigger objects are presumably dust contamination. From the height difference between the substratum and nanoparticle top we deduce that the particles have a diameter of 50 nm.

6.10 pH dependence of nanoparticles adsorption

The zeta potential results illustrated that the surface charge of the nanoparticles is dependent on the pH of the solution. Therefore pH 3 and 7 were chosen for the experiments to demonstrate the different charges of particles. These experiments were similar to the previous work except that the pH of the entire system (water and nanoparticle solution) was maintained at pH 3 and pH 7 whilst (i) water, (ii) nanoparticles solution at the concentration of 50 µg/mL, (iii) pure water again was followed through the cuvette. These experiments were carried out using nanoparticles coated with PEG.

6.10.1 Determination of dn/dc for nanoparticle solutions in water at pH 3 and pH 7

The variation of refractive index with concentration, dn/dc, at pH 3 and pH 7 has been calculated and the results show the same value of 0.0002 for both pH (Fig. 15)

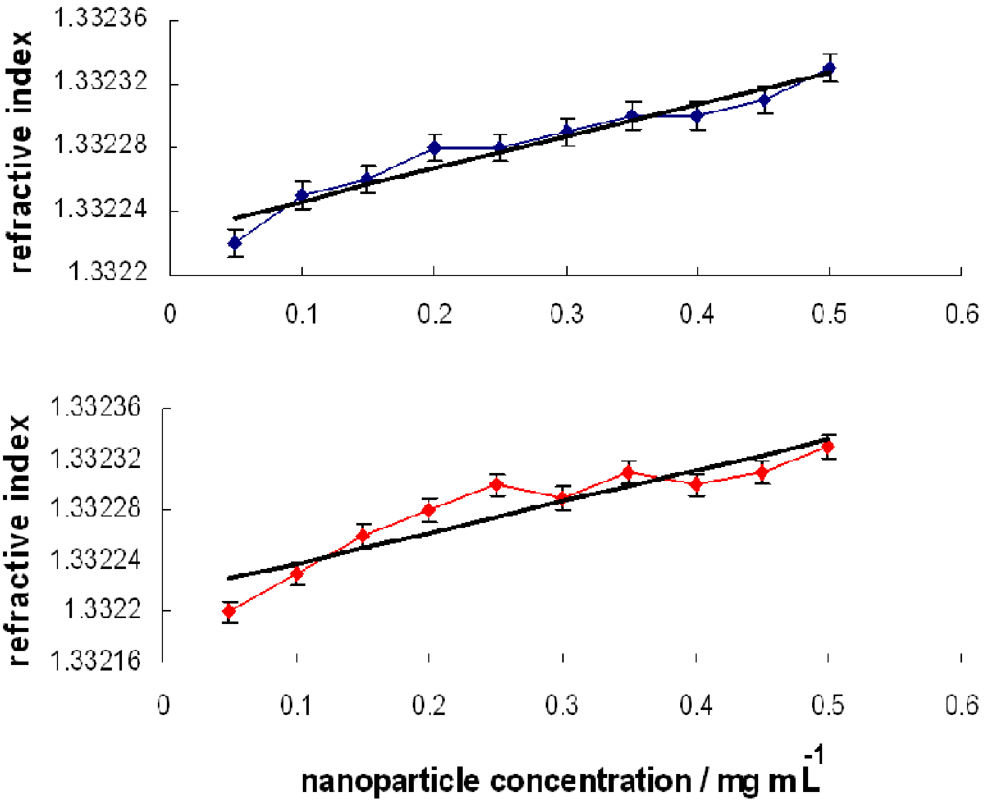

Figure 6.15: Variation of refractive index with concentration of nanoparticles coated with PEG in water at pH 3 (up) and pH 7 (down) at 25 ºC (dn/dc= 0.0038 cm^3/g).

6.10.2 Adsorption/desorption kinetics

Optical waveguide lightmode spectroscopy (OWLS) applied to provide the kinetic adsorption and desorption data. The experimental curves after calculation of the mass is shown in Figure 6.16.

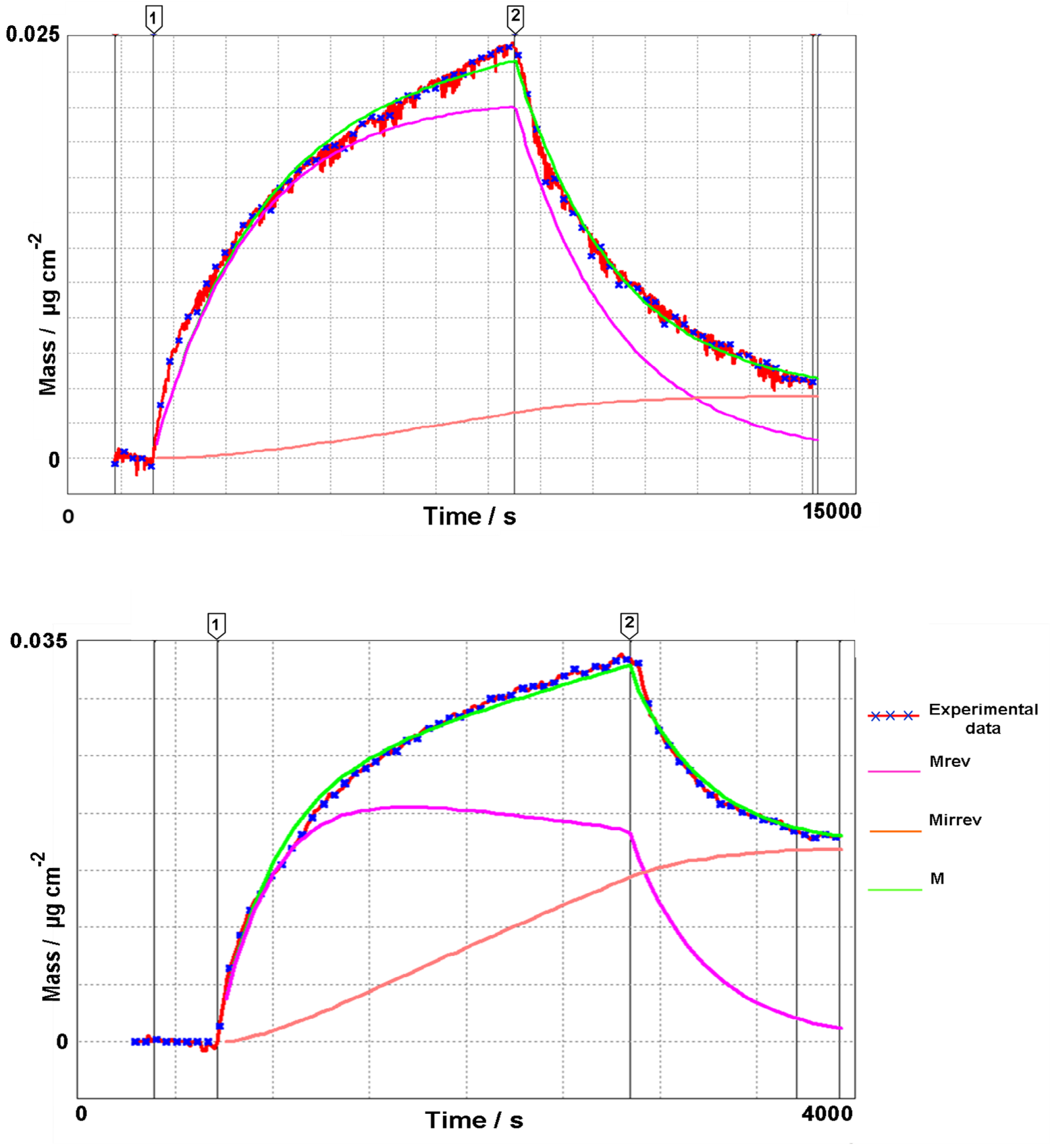

Figure 6.16: Self-assembly of PEG-coated nanoparticles suspended in ultrapure water calculated from the OWLS data, adsorbed on Si(Ti)O_2 in a concentration of 50 µg/mL at pH 3 (up) and pH 7 (down) at temperature 25 °C. See Appendices A.2 and B.2 for details of calculations. The pumping speed was 0.4 mL/h. The smooth lines represent M_{rev}: reversibly adsorbed particles, M_{irrev}: irreversibly adsorbed particles, M: total mass of adsorbed particles obtained by fitting a model to the kinetics (see text). Vertical line 1 marks initiation of nanoparticle adsorption and 2 marks the start of desorption. The peak fractional surface coverage θ = Ma / m = 0.034 / 0.25 = 14% in this experiment.

It is immediately seen that a significant proportion of particles desorbs during the washing step. On the basis of this observation, we have postulated two possible modes of nanoparticle adsorption, reversible and irreversible (Fig 6.17), as has previously been used to interpret protein adsorption (Kurrat et al., 1994).

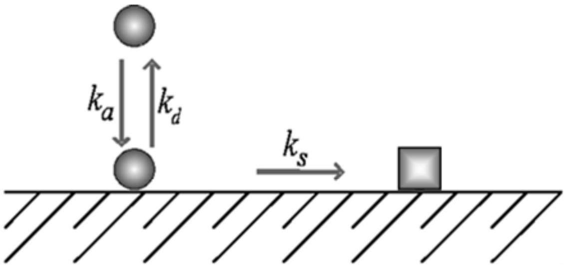

Figure 6.17: Diagram of the processes involved for particle self-assembly at the waveguide surface, with corresponding rate coefficients. Note the change of state undergone by the particle due to its residence on the surface.

The kinetic equations corresponding to Figure 6 are:

$$M = M_{rev} + M_{irrev} \qquad (2)$$

$$\frac{dM_{rev}}{dt} = k_a c_s \phi(M_{irrev} a) - k_d M_{rev} - k_s M_{rev} \qquad (3)$$

$$\frac{dM_{irrev}}{dt} = k_s M_{rev} \qquad (4)$$

where M is the total mass of reversible (M_{rev}) and irreversible (M_{irrev}) mass deposited on the substratum, φ is the available area function, k_d is the desorption and k_a the adsorption rate coefficient, c_s is the effective particle concentration in the vicinity of the adsorbent surface; φ is the available area function k_s is the rate coefficient for transformation from the reversible to the irreversible form and a is the area occupied by one particle, assumed to be the same for the two modes of adsorption.

We used the Schaaf-Talbot interpolation formula for φ (Schaaf and Talbot, 1989). The diffusion coefficient of the nanoparticles was calculated from the Stokes-Einstein equation:

$$D = \frac{k_B T}{6\pi r \eta} \tag{5}$$

where T is the absolute temperature (298.15 K), η the viscosity of the medium (water, 1.0×10^{-3} kg m^{-1} s^{-1}), and k_B is Boltzmann's constant (1.38×10^{-23} J K^{-1}), giving $D = 4.0 \times 10^{-8}$ cm^2 s^{-1} . Eqn. 2 was fitted to the experimental data and the fitted parameters are gathered in Table 1.

The diffusion coefficient for the bacteria in water was calculated as 1.2×10^{-8} cm^2/s using Perrin's formula for prolate ellipsoids approximated as:

$$D = k_B T / [12\eta R(g / h)^{1/3}] \tag{6}$$

where T is the absolute temperature (298.15 K), η the dynamic viscosity of the water (1.0×10^{-3} kg/ms), k_B is Boltzmann's constant (1.38×10^{-23} J/K), r the diameter of the particles (50 nm), R the equivalent radius (0.52 μm), g mean diameter (0.5 μm) and h

mean length (3 μm) of the bacteria.. The fitted parameters or the particularly useful quantities derived from them are gathered in Table 6.1.

Table 6.1: Adsorption parameters calculated from the OWLS data for the nanoparticles solution in a concentration of 50 μg/mL at pH 3 & 7 and temperature 25 °C. The units of *M* are μg cm^{-2}. k_a: reversible adsorption, k_s: Irreversible adsorption, *m/a*: total mass adsorbed particle, k_d: desorption.

Parameter	Units	pH 3	pH 7
k_a	cm/s	$5.83 \times 10^{-7} \pm 0.1 \times 10^{-7}$	$1.98 \times 10^{-6} \pm 0.03 \times 10^{-6}$
k_d	s^{-1}	$5.2 \times 10^{-4} \pm 0.1 \times 10^{-4}$	$2.4 \times 10^{-3} \pm 0.05 \times 10^{-3}$
k_S	s^{-1}	$2.4 \times 10^{-5} \pm 0.5 \times 10^{-5}$	$0.3 \times 10^{-3} \pm 0.01 \times 10^{-3}$
m/a	μg / cm^2	5.7 ± 1	0.25 ± 0.005

The predicted value of *m/a* for spherical nanoparticles from the data in section 2.5 is $m_t / \pi r_t^{\,2} = 10.8$ μg cm^{-2}. Comparison with the fitted value (0.25 μg cm^{-2}) suggest that the particles have a greatly expanded effective radius r_e, due to Lewis acid/base and electrostatic repulsions (Cacace et al., 1997), equal to $\frac{m_t / \pi r_t^{\,2}}{m_t / \pi r_e^{\,2}} = \frac{10.5}{0.25} = 360$ nm.

It is rather remarkable that despite the simplicity of our hybrid nanoparticles, which only contain two types of molecule and four types of atom, they have a complex behaviour with memory that has otherwise been observed only with seemingly incomparably more complex nano-objects, namely proteins, which are constituted from up to twenty different amino acids and at least five different atoms. This suggests that our hybrid could be used as a cheap and robust surrogate for a protein under certain circumstances.

From these results it is clear that nanoparticles adsorbed on the surface of waveguide dependent to the pH of the solution. It seems that the nanoparticles stick more to the surface at lower pH which could be contributed to the surface charges of particles. On the other hand as the pH increases the adsorbed molecule reduces which could be attributed to increase of negatively charged of the particles at higher pH, therefore the molecules would not be sited on the surface of waveguide, hence the charges of the waveguide is negative.

6.10.3 Experimental results and discussion

The adsorption and desorption of the nanoparticles at the solid/liquid (i.e. buried) interface is relatively straightforward and well understood (Mátè and Ramsden, 1998; Ramsden and Mátè, 1998). Here we investigate the adsorption characteristics of spherical magnetic nanoparticles. Irrespective of the composition of the system such as concentration, controlling the adsorption of the minerals is strongly depending on the pH (Fein et al., 1997; Daughney and Fein, 1998). The pH dependence adsorption of the particles to the surfaces is result of electrostatic attraction between them. Figure 6.18 shows mass calculated for magnetic nanoparticles and it is a typical plot of adsorption and desorption of aqueous nanoparticles (The mass calculation is fully described in appendix B). Adsorption of nanoparticles was typically continued until a definite plateau was reached, at which for all practical purposes the amount of adsorbed nanoparticles was no longer increasing. We have seen that the approximation of a layer of PEG coated particles can give reasonable results in the optical analysis of such layers at which the particles have positive charge.

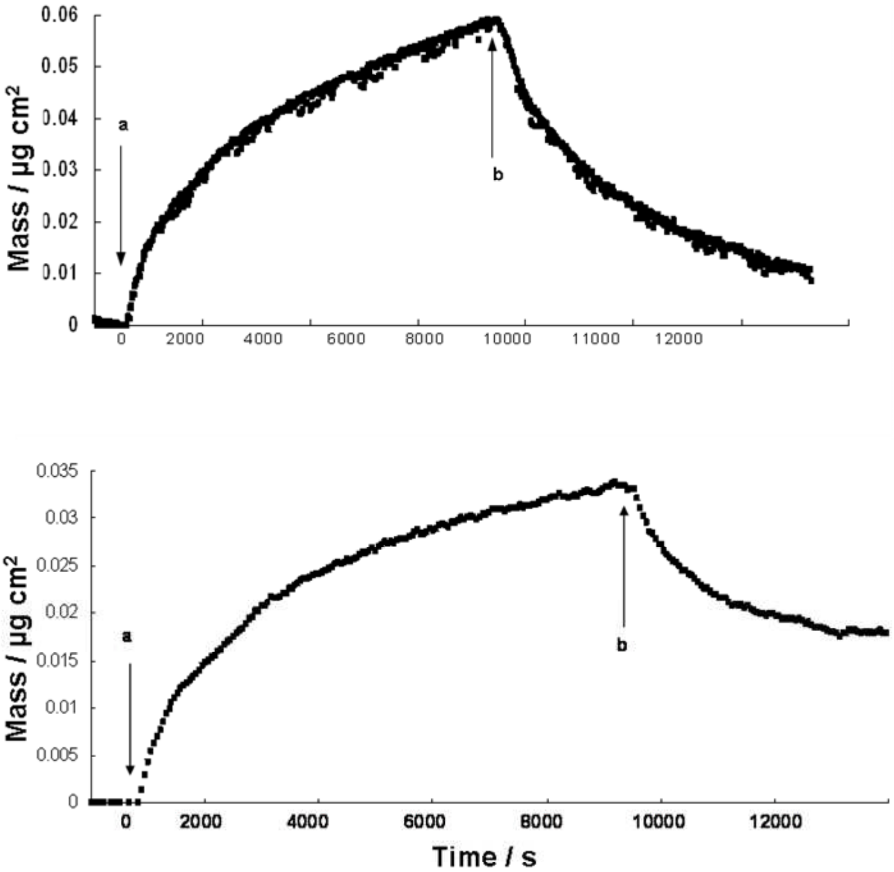

Figure 6.18: Representative plots of the mass of the nanoparticles coated with PEG, calculated from OWLS data, adsorbed onto the waveguide at pH 3 (up) and pH 7 (down) on the surface of the waveguide at the concentration of 50 µg/mL bulk solution against time. The arrow ‘a’ indicates the start of nanoparticle flow (adsorption phase) and ‘b’ the start of water flow (desorption phase).

The most reasonable interpretation of the behaviour of the mass adsorption in our experiments is that at lower pH (3 and 7) the particles are adsorbed. In the higher pH regime interactions between adsorbed particles and the surface of the waveguide prevent the formation of the film and a fairly dense nanoparticles monolayer is formed.

When the pH of the nanoparticle solution is higher than the isoelectric point, the particles are not bound on the negatively charged waveguide and therefore they are not able to form a monolayer. The particles are likely to be close to the surface of the support but due to their negatively charged surfaces, they are readily washed away from the waveguide. The nanoparticles at lower pH form a monolayer structure. The positively charged particles attach to the surface and after washing still remain on the surface (Fig. 6.19) as a monolayer.

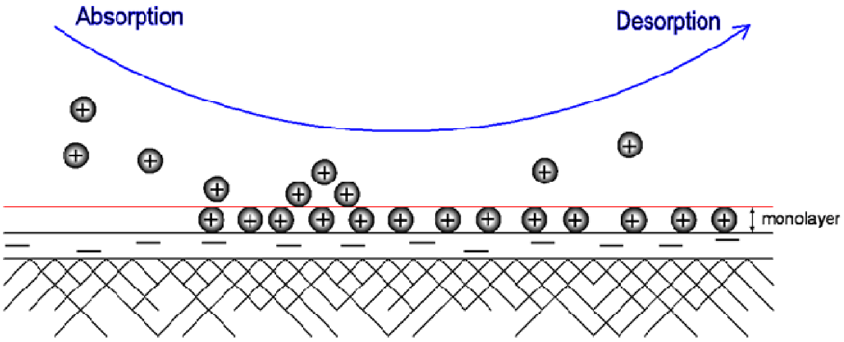

Figure 6.19: Nanoparticles coated with PEG adsorption/desorption model at pH 7 leads to form a monolayer of the particles. Due to their positively charged surface the particles become attached to the negatively charged surface of the waveguide (Fig. 6.11) (Ramsden and Máté 1998) and form a monolayer structure.

6.11 Bacteria adsorption/desorption to nanoparticles layer

R. erythropolis was chosen for further investigation. The experiments with bacteria were undertaken at pH 7 and 25 ºC, because at pH 7 and room temperature are optimal conditions for the growth of aerobic mesophilic bacteria (Finnerty, 1992).

The nanoparticles solution was made up at pH=7 and sonicated for 20 min before use. The bacteria were grown until the mid-exponential growth phase and harvested by centrifugation at 1400 *g* for 10 min. The cell pellets were washed twice with Ringer's solution and resuspended back in the solution. After making a monolayer of magnetic nanoparticles on the OWLS waveguide the adsorption/desorption characteristics of bacteria onto coated waveguides were determined whilst the bacterial solution was drawn into the flow cell and the final step is washing, which provides information about the stability of the formed layer and possible desorption kinetics. The dn/dc was calculated as the best linear fit to be 0.0038 for the bacteria (Figure 6.20). The concentration was determined based on dry weight of bacteria which is 0.00563 g/L.

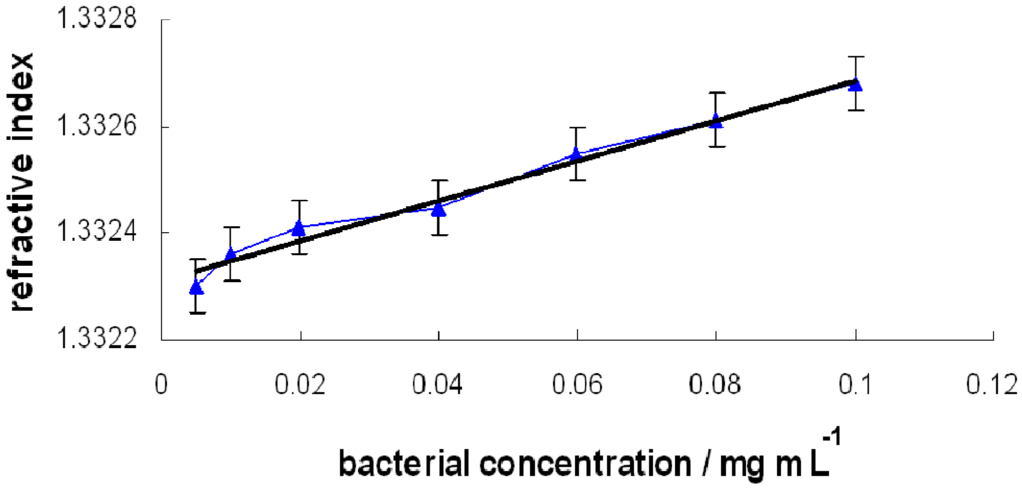

Figure 6.20: Variation of refractive index with concentration of bacteria in water at 25 ºC (dn/dc= 0.0038 cm^3/g).

6.11.1 Experimental results and discussion

The attachment of bacteria was investigated on the bare waveguide and coated waveguide with a monolayer of magnetic nanoparticles and the curves were fitted shown in Figure 6.21.

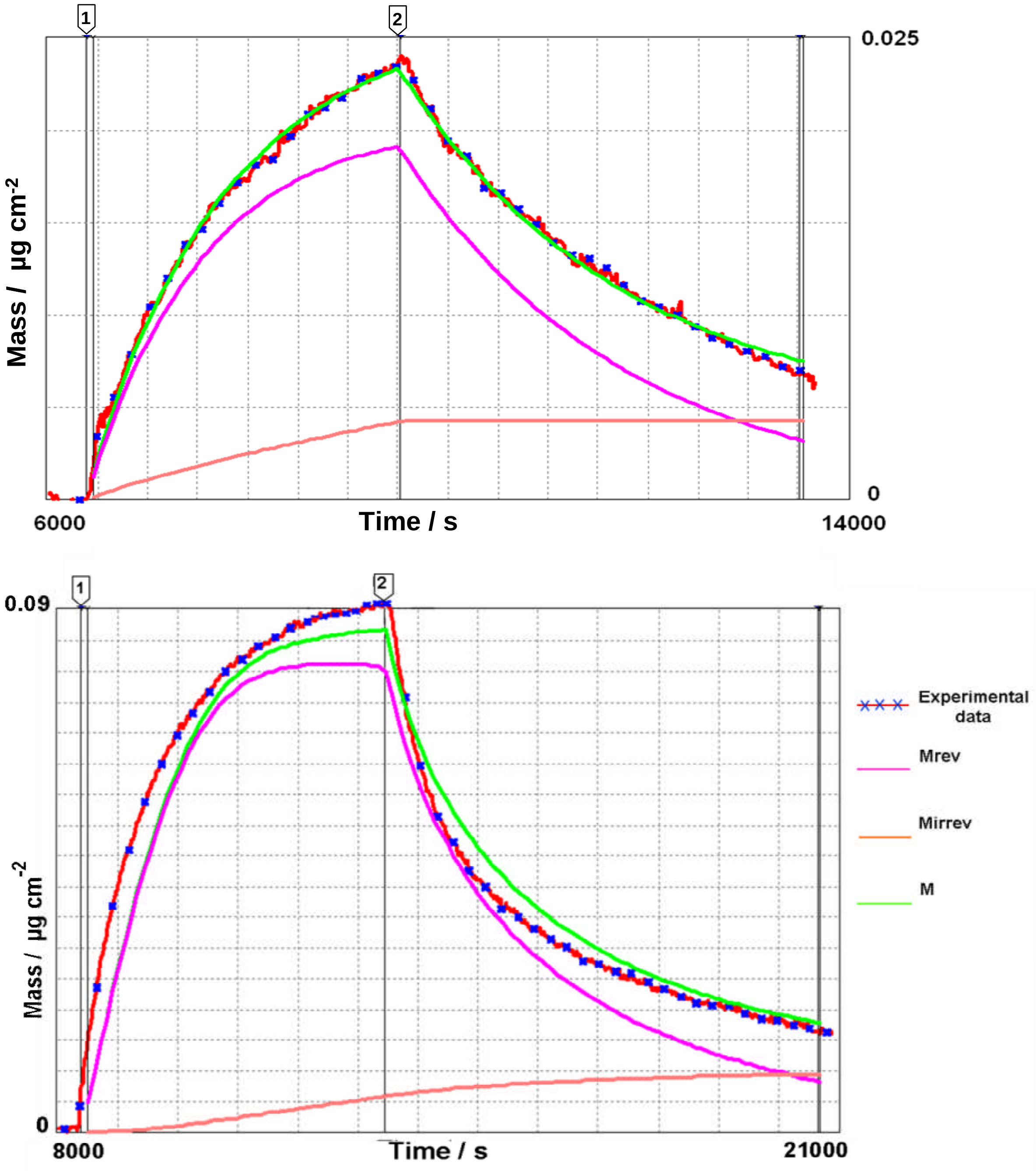

Figure 6.21: Plot of amount of bacteria, calculated from the OWLS data, adsorbed on the waveguide (up) and nanofilm (down) in a concentration of 50 µg/mL at pH 7 and temperature 25 ºC. The pumping speed was 0.4 mL/h. M_{rev}: reversibly adsorbed bacteria, M_{irrev}: Irreversibly adsorbed bacteria, M: total mass adsorbed particles, obtaining by fitting a model for the bacterial attachment. Vertical line 1, initiation of bacterial flow, vertical line 2, washing (see equ. 2).

Table 6.2: Adsorption parameters calculated from the OWLS data for the bacterial solution on the surface of waveguide and nanofilm in a concentration of 50 µg/mL at pH 7 and temperature 25 ºC. The units of *M* are µg cm^{-2}. K_a: reversible adsorption, K_s: Irreversible adsorption, m/a: total mass adsorbed bacteria, K_d: desorption.

Parameters	Units	Bacteria on the waveguide	Bacteria on the nanofilm
k_a	cm/s	$5.93 \times 10^{-7} \pm 0.06 \times 10^{-7}$	$5.23 \times 10^{-5} \pm 0.05 \times 10^{-5}$
k_d	s^{-1}	$0.43 \times 10^{-3} \pm 0.008 \times 10^{-3}$	0.01 ± 0.0002
k_S	s^{-1}	$1.0 \times 10^{-8} \pm 0.03 \times 10^{-8}$	$1.0 \times 10^{-7} \pm 0.03 \times 10^{-7}$
m/a	µg / cm^2	0.13 ± 0.003	0.37 ± 0.01

Our results clearly suggest that the nanofilm facilitates the adsorption of the bacteria (see table 6.2 values).

6.12 Conclusions

The PEG-coated magnetic nanoparticles allow well-defined thin films to be deposited on planar substrata.

The hybrid particles, although ostensibly uniform, morph into two types at the substratum: reversibly adsorbable and irreversibly adsorbable. Thus their behaviour is comparable to that of a very much more complex protein molecule (e.g.) serum albumin, Kurrat et al., 1997).

The PEG coating, which so successfully prevents the 25 nm-radius particles from aggregating, while physically only 30 nm thick, creates a strong interparticle repulsion that increases their effective radius more than tenfold to 360 nm. This may limit their ability to adsorb on bacteria.

The summarized conclusions from this chapter are:

1. Pure magnetic nanoparticles aggregate.
2. PEG prevents the aggregation of particles.
3. Charges of particles can be tuned by pH.
4. Neutral pH results in good nanofilms on silica–titania.
5. The positively charged nanoparticles facilitate the bacterial adsorption

7: Future work

This brief final chapter suggests some possible future areas for research on bacterial attachment for enhancing the biodesulfurization process and highlights the areas that may support this study. It is now clearly demonstrated that bacteria in aqueous environments are mainly associated with surfaces (Costerton et al., 1987) and there are various kinds of dynamical studies on the surfaces of bacteria while they are adhering to the surfaces; they are able to change themselves or drive chemical reactions. Since the attachment of nanoparticles on the surface of bacteria is affected by their environment, more detailed investigations into the implicated physicochemical properties (and the dynamics of the bacterial membrane structure) would be of interest. Moreover membrane fluidity in media with different salt concentrations and at different temperatures would be pertinent here.

The attachment of bacteria to magnetic particles needs further investigation by OWLS to analyse the kinetics of bacterial attachment on the nanomagnetic film in more detail. In order to get more information about the process one could use thicker waveguides capable of supporting additional modes, each are of which enables an additional parameter to be determined.

There are many possibilities to synthesise different kinds of nanoparticles and indeed some of them are easy and inexpensive for industrial proposes. This work has shown that Fe_3O_4 magnetic nanoparticles could enhance the biodesulfurization ability;

therefore following from these experiments is to investigate other kinds of magnetic nanoparticles, to see whether the same or better enhancement is obtained.

Shewanella putrefaciens showed desulfurization activity and detection of HBP in the culture medium confirmed that this strain desulfurised DBT via the 4S pathway. Therefore, *S. putrefaciens* is a potentially useful desulfurizing bacterium. At present, we consider it necessary to confirm the rate-limiting step in DBT desulfurization by *S. putrefaciens*. This is required to determine whether the genes encoding the DBT desulfurizing enzymes of Shewanella are different from those of other desulfurizing bacteria such as *R. erythropolis* IGTS8.

The experiments in this thesis used a model BDS system (organosulfur compound in water). The next step towards making this into an industrial process would be to investigate BDS in actual crude oil.

Appendices

APPENDIX A

Principle of optical waveguide lightmode spectroscopy

A.1 Reflection, refraction and total internal reflection

When light travels across medium of differing refractive indices (for example F and C) some light will be reflected back and some will be refracted. This is commonly known as Snell's law although Herriot had initially discovered it sometime before Snell (Fig. A.1).

$$n_F \sin \theta_F = n_C \sin \theta_C \qquad \text{(C1)}$$

where n_F and n_C are the refractive indices of media F and C respectively where $n_C > n_F$. θ_F is the angle of incidence, θ_C the angle of refraction, and θ_R the angle of reflexion, $\theta_R = \theta_F$.

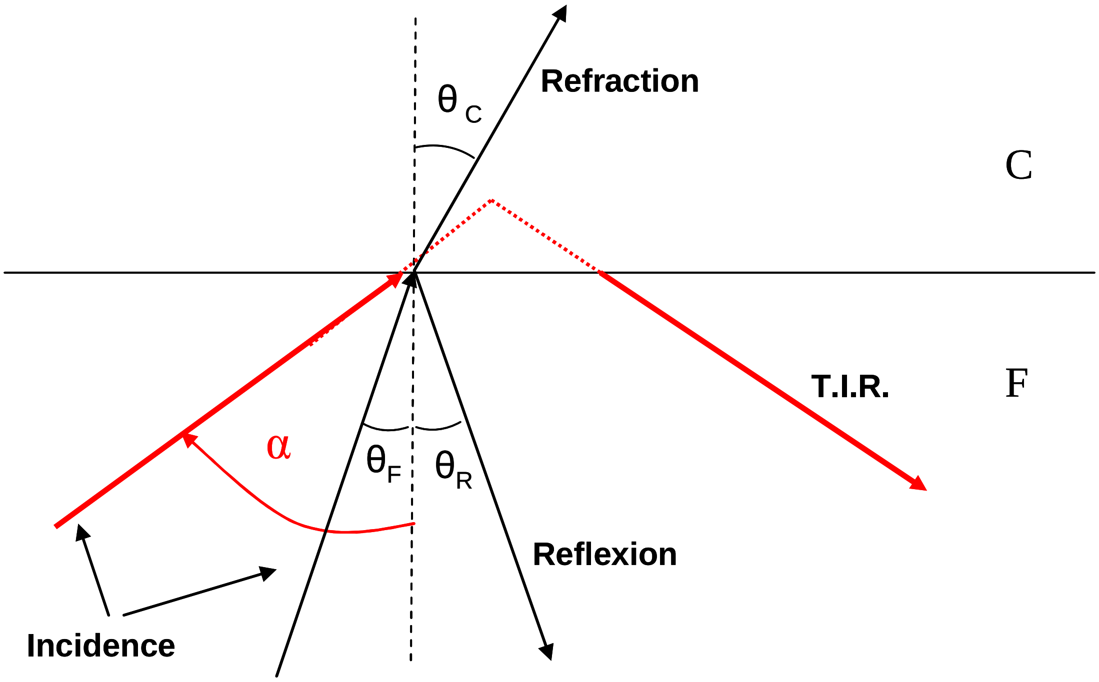

Figure A.1: Refraction, reflection and total internal reflection. Light travelling into media F (dark arrow) will refract into medium C and reflect back into medium F with the C/F relationship dependent on the angle of incidence α_F. Total internal reflection (red arrow) will occur above a critical incidence angle, here no light is refracted. The penetration of the evanescent field is shown as the dotted red lines.

Above a critical angle (α), total internal reflection will occur. This only occurs when the light is travelling from a high to low refractive index material. The light confined within two reflecting interfaces will travel as a standing wave between the surfaces and as an evanescent wave beyond (Fig. A.2). The light penetrates evanescently into C before returning to F, resulting the Goos-Hänchen shift, D (Tien, 1977).

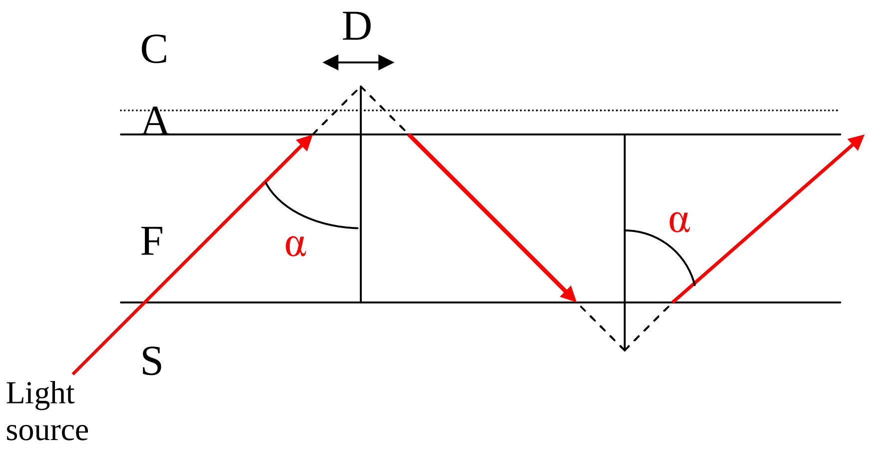

Figure A.2: Laser light travelling through an optical waveguide. Light is confined within a high refractive index film (F) and will penetrate into the surrounding low refractive index material (S and C). A denotes an adsorbed adlayer, D the Goos-Hänchenshift and α the angle of incidence.

A.2 Waveguide and adlayer parameter calculations

A three layer model is used to calculate the waveguide parameters

$$\pi m = \frac{2\pi}{\lambda}\sqrt{n_F^2} - N^2 d_F - \arctan\left[\left(\frac{n_F}{n_S}\right)^{2p}\sqrt{\frac{N^2-n_S^2}{n_F^2-N^2}}\right] - \arctan\left[\left(\frac{n_F}{n_C}\right)^{2p}\sqrt{\frac{N^2-n_C^2}{n_F^2-N^2}}\right] \quad \text{(C 2)}$$

where

p=1 and $N=N_{TM}$ for transverse magnetic (TM) mode p=0 and $N=N_{TE}$ for transverse electric (TE) mode.

Adsorption of material onto the surface will form an adlayer with the parameters characterised using the four layer mode equation (Ramsden, 1995a). The refractive index of the adlayer, n_A is calculated using:

$$n_A = \left(\frac{\frac{FM(N_{TM})}{A(N_{TM})} - d_F}{\frac{FE(N_{TE})}{A(N_{TE})} - d_F} \left(\frac{1}{n_C^2} + \frac{1}{n_F^2} - \frac{1}{N_{TM}^2} \right) - \frac{1}{n_C^2} + \frac{1}{N_{TM}^2} \right)^{-1/2} \qquad \text{(C 3)}$$

and the thickness, d_A calculated using

$$d_A = \left(\frac{FE(N_{TE})}{A(N_{TE})} - d_F \right) \left(\frac{n_F^2 - n_C^2}{n_A^2 - n_C^2} \right) \qquad \text{(C 4)}$$

where

$$A(N) = \frac{2\pi}{\lambda} \sqrt{n_F^2 - N^2} \qquad \text{(C 5)}$$

$$FM(N) = \arctan\left(\frac{n_F^2}{n_S^2} \sqrt{\frac{N^2 - n_S^2}{n_F^2 - N^2}} \right) + \arctan\left(\frac{n_F^2}{n_C^2} \sqrt{\frac{N^2 - n_C^2}{n_F^2 - N^2}} \right) \qquad \text{(C 6)}$$

$$FE(N) = \arctan\left(\sqrt{\frac{N^2 - n_S^2}{n_F^2 - N^2}}\right) + \left(\sqrt{\frac{N^2 - n_C^2}{n_F^2 - N^2}}\right) \quad \text{(C 7)}$$

APPENDIX B

B.1 Random sequential adsorption

As molecules adsorb onto a surface their shape will impact on the available surface for further adsorption. After a time adsorption will stop as the surface becomes jammed– this is the jamming limit (θ_J) (e.g. a sphere has $\theta_J \sim 0.547$). The bacterial available area φ is at first close to one but as the molecules start to adsorb the surface becomes more occupied (Ricci et al., 1992). At a certain point the surface cannot accommodate further adsorption, despite there being apparent space available, and the jamming limit is reached (Ramsden, 1993; Evans, 1993; Ramsden et al., 1994; Lavalle et al., 2000).The equation used for fitting is

$$\phi(M, a) = \left(1 - x^3\right) / \left(1 - 0.812x + 0.2336x^2 + 0.0845x^3\right) \quad \text{(C 8)}$$

where $x = \frac{\theta}{\theta_J}$, θ, the fractional occupied area being related to M by M = θ m/a, where m is the mass per molecule.

B.2 Mass calculation

In the situation where a specific protein with known polarisability adsorbs, forming an isotropic monolayer, the adsorbed mass can be calculated from the refractive indices

(Ramsden, 1993; Tiefenthaler and Lukosz, 1998). The mass of the molecules in the adlayer is then given as:

$$M = \int_0^\infty \left(c_s(z) - c_{bulk}\right) dz \tag{C9}$$

For an adlayer with a uniform concentration c_A and d_A,

$$M = \left(c_A - c_{bulk}\right) d_A \tag{C10}$$

$$M = c_A d_A \tag{C11}$$

Where c_A is the concentration of molecules in the adlayer (molecules per unit area) and c_{bulk} the bulk (liquid) concentration. The refractive index n_A of the adsorbed layer is related to c_A according to this equation:

$$n_A = n_c + c_A \frac{dn}{dc} \tag{C12}$$

where n_c is the refractive index of the medium in which the molecules are dissolved, i.e. the buffer. The coefficient dn/dc depends on the polarisability of the molecules and finally, eliminating c_A, the mass can be calculated as:

$$M = d_A \frac{n_A - n_c}{dn/dc} \tag{C13}$$

References:

Alimi, H., Ertel, T. and Schug, B. Fingerprinting of hydrocarbon fuel contaminants: literature review. *Environ. Forensics.,* **4** (2003) 25-38.

An, Y. H. and Friedman, R. J. Concise review of mechanisms of bacterial adhesion to biomaterial surfaces. *J. Biomed. Mater. Res. (Appl. Biomater.),* **43** (1998) 338-348.

Andrade, J.D., Hlady, V. and Jeon, S.I. Poly(ethylene oxide) and protein resistance principles, problems, and possibilities. *Adv. Chem. Ser.,* **248** (1996) 51-9.

Arensdorf, J.J., Loomis, A.K., DiGrazia, P.M., Monticello, D.J. and Pienkos P.T. Chemostat approach for the direct evolution of biodesulfurization gain-of-function mutants. *Appl. Environ. Microbiol.,* **68** (2002) 691-698.

Angelova, A., Ionov, R., Koch, M.H.J. and Rapp, G. Interaction of the peptide antibiotic alamethicin with bilayer and non-bilayer forming lipids: Influence of increasing alamethicin concentration on the lipids supramolecular structures. *Arch. Biochem. Biophys.,* 378 (2000) 93-106.

Arshady, R. (ed), Microspheres Microcapsules and Liposomes. **3,** London: Citus Books, (2001).

Baumberg, J., Cronin, L., Gee, M., Kearnes, M., Macnaghten, Ph., Makatsoris, H., Ramsden, J., O'Reilly, R., and Webb, M. Where is nano taking us? *Nanotechnology Perceptions,* **3** (2007) 3-14.

Ball, V. and Ramsden, J. J. Buffer dependence of refractive index increments of protein solutions. *Biopolymers*, **46** (1998) 489–492.

Bell, K. S., Philp, J. C., Aw, D. W. J., and Christofi, N. The genus Rhodococcus. *J. Appl. Microbiol.,* **85** (1998) 95-210.

Benz, R., Prab, W. and Ringsdorf, H. Black lipid membrane from polymerizable lipids, *Angew. Chem. Suppl.,* (1982) 869-880.

Beveridge, T. J. The bacteria surface: general considerations towards design and function. *Can. J. Microbiol.,* **34** (1988) 363-372.

Blumberg, K.O., Walsh, M.P. and Pera, Ch. Low-sulfur gasoline & diesel : The key to lower vehicle emissions. *International Council on Clean Transportation (ICCT)* (2003).

Bogue, R. Nanometrology: a critical discipline for the twenty-first century. *Sensor Rev,* **27** (2007) 189-196.

Brash, J.L., Wojciechowski, P.W. Interfacial Phenomena and Bioproducts. New York: Marcel Dekker, (1996).

Brassington, K. J., Hough, R. L., Paton, G. I., Semple, K. T., Risdon, G. C., Crossley, J., Hay, I., Askari, K. and Pollard, S. J. T. Weathered hydrocarbon wastes: a risk management primer. *Critical Reviews in Environmental Science and Technology,* **37** (2007) 199-232.

Bressler, D.C., Norman, J.A. and Fedorak, P.M. Ring cleavage of sulfur heterocycles: how does it happen. *Biodegradation,* **8** (1998) 297-311.

Brusatori, M.A. Protein adsorption kinetics under an applied electric field: an optical waveguide lighmode spectroscopy study. (2001) PhD Thesis, Wayne State University.

Cabeen, M.T. and Jacobs-Wagner, C. Bacterial cell shape. *Nature Reviews Microbiology,* **3** (2005) 601–610.

Cacace, M.G., Landau, E.M. and Ramsden, J.J. The Hofmeister series: salt and solvent effects on interfacial phenomena. *Q. Rev. Biophys.,* **3** (1997) 241-277.

Campbell, I.M. An Orphaned Child Makes Good - The Story of USDOE/PETC's Foray into Fossil Fuel Biodesulfurization. *Prepr. Am. Chem. Soc., Div. Petroleum Chem.,* **38** (1993) 275-278.

Carter , G. R. and Wise, D. Essentials of Veterinary Bacteriology and Mycology, 6th Ed, Oxford: Blackwell, (2003).

Chikazumi, S., Taketomi, S., Ukita, S., Mizukami, M., Miyajima, M., Setogawa, H., and Kurihara, Y. Physics of magnetic fluids. *J. Magn. Magn. Matr.,* **65** (1987) 245-251.

Chouly, C., Pouliquen, D., Lucet, I. Jeune, J. J. and Pellet, P. Development of superparamagnetic nanoparticles for MRI: Effect of particle size, charge and surface nature on biodistribution. *J. Microencapsulation*, **13** (1996) 245–255.

Christy, R., Vestal, Z. and John Zhang. Magnetic spinel ferrite nanoparticles from microemulsions. *Int. J. Nanotech.,* **1** (2004) 1-2.

Coey, J.M.D. Noncollinear spin arrangement in ultrafine ferrimagnetic crystallites. *Phys. Rev. Lett.,* **27** (1971) 1140-1142.

Corcoran, J,A. The production and use of immobilized living microbial cells. In: Wiseman, A. (Ed.) *Topics in Enzyme and Fermentation Biotechnology*, **10**, pp. 12-50 (1985).

Cornell, R. M. and Schwertmann, U. The Iron Oxides- Structures, Properties, Reactions, Occurrence and Uses. Weinheim: VCH (1996).

Costerton, J.W., Cheng, K-J., Geesey, G.G., Ladd, T.I., Nickel, J.C., Dasgupta, M. and Marrie, T.J., Bacterial biofilms in nature and disease, *A. Rev. Microbiol.*, **41**(1987) 435-464.

Cullity, B. D. Introduction to Magnetic Materials. New York: Addison-Wesley, (1972).

Cyr, J.D. Hydrodesulfurization: A catalytic process. (2000) http://www.che.lsu.edu/COURSES/4205/1999/cyr/paper.htm

Dahlberg, M. D., Rohrer, R. L., Fauth, D. J., Sprecher, R. and Olson, G. J. Biodesulfurization of dibenzothiophene sulfone by *Arthrobacter* sp. and studies with oxidized Illinois No. 6 coal. *Fuel,* **72** (1993) 1645-1649.

Dankert, J., Hogt, A. H. and Feijen, J. Biomedical polymers: bacterial adhesion, colonization, and infection. *CRC Crit. Rev. Biocompatibility,* **2** (1986) 219–301.

Daughney, C.J. and Fein, J.B. The effect of ionic strength on the adsorption of $H^{+,}$ Cd^{2+}, Pb^{2+} and Cu^{2+} by *Bacillus subtilis and Bacillus licheniformis*: a surface complexation model. *J. Colloid Interface Sci.,* **198** (1998) 53-77.

Dean, J. A. Analytical Chemistry Handbook. New York: McGraw-Hill, (1995).

Denis-Larose, C., Labbe, D., Nergeron, H., Jones, A.M., Greer, C.W., Al-Hawari, J., Grossman, M.J., Sankey, B.M. and Lau, P.C.K. Conservation of plasmid-encoded dibenzothiophene desulphurisation genes in several rhodococci. *App. Environ. Microbiol.,* **63** (1997) 2915-2919.

Drexler, K. E. Molecular engineering: An approach to the development of general capabilities for molecular manipulation. *Proc. Natl Acad. Sci. U.S.A.,* **78** (1981) 5275-5278.

Dubertret, B., Skourides, P., Norris, D. J., Noireaux, V., Brivanlou, A. H., and Libchaber, A. In vivo imaging of quantum dots encapsulated in phospholipid micelles. *Science,* **298** (2002) 1759-1762.

Elliott, D. W. and Zhang, W.-X. Field assessment of nanoscale biometallic particles for groundwater treatment. *Environ. Sci. Technol.,* **35** (2001) 4922-4926.

EPA report, EPA proposes effective date for diesel fuel sulfur control requirements in rural Alaska. U.S. Environmental Protection Agency (2005) Report on EPA420-F-05-028.

Evans, J. W. Random and cooperative sequential adsorption. *Rev. Mod. Phys.,* 65 (1993) 1281-1329.

Fang, X. X., Zhang, Y. L., Luo, L. L., Xu, P., Chen, Y. L., Zhou, H. and Hai, L. Organic sulfur removal from catalytic diesel oil by hydrodesulfurization combined with biodesulfurization. *Mod. Chem. Ind.,* **26** (2006) 234-238.

Fein, J.B., Daughney, C.J., Yee, N. and Davis, T.A. A chemical equilibrium model for metal adsorption onto bacterial surfaces. *Geochim. Cosmochim. Acta,* **61** (1997) 3319-3328.

Finnerty, W.M. The biology and genetics of the genus *Rhodococcus*. *A. Rev. Microbiol.,* **46** (1992) 193-218.

Fletcher, M. (ed), Bacterial adhesion. New York: Wiley (1996).

Folsom, B.R., Schieche, D.R., DiGrazia, P.M., Werner, J. and Palmer, S. Microbial desulfurization of alkylated dibenzothiophenes from a hydrodesulfurized middle distillate by *Rhodococcus erythropolis* I19. *Appl. Environ. Microbiol.,* **65** (1999) 4967-4972.

Fried, T., Shemer, G. and Markovich, G. Ordered two-dimensional arrays of ferrite nanoparticles. *Adv. Mater.,* **13** (2001) 1158-1161.

Gallagher, J. R., Olson, E. S. and Stanley, D. C. Microbial desulfurization of dibenzothiophene: a sulfur-specific pathway. *FEMS Microbiol. Lett.,* **107** (1993) 31-36.

Gao, X. H., Cui, Y. Y., Levenson, R. M., Chung, L. W. K. and Nie, S. M. In vivo cancer targeting and imaging with semiconductor quantum dots. *Nat.Biotechnol.,* **22** (2004) 969-976.

Gary, J.H. and Handwerk, G.E. Petroleum Refining: Technology and Economics.4th edn, New York: Marcel Dekker, (2001).

Gee, S. H., Hong, Y. K., Erickson, D. W., Park, M. H. and Sur, J. C. Synthesis and Aging Effect of Spherical Magnetite (Fe3O4) Nanoparticles for Biosensor Applications. *J. Appl. Phys.,* **93** (2003) 7560-7562.

Gill, I. S., and Ballesteros, A. Bioencapsulation within synthetic polymers (part 1): sol-gel encapsulation of biologicals. *Trends Biotechnol*., **18** (2000) 282-296.

Golander, C.G., Herron, J.N., Lim, K., Claesson, P., Stenius, P. and Andrade, J.D. Properties of immobilizated PEG films and the interaction with proteins. In: Harris JM, editor. Poly(ethylene glycol) chemistry, biotechnical and biomedical applications. New York: Plenum Press, (1992) pp. 221-45.

Goodsell, D. S. Bionanotechnology: Lessons from Nature. 1th edn. New Jersey: Wiley-Liss, (2004).

Grabar, K.C., Brown, K.R., Keating, C.D., Stranick, S.J., Tang, S.L. and Natan, M.J. Nanoscale characterization of gold colloid monolayers: a comparison of four techniques, *Anal. Chem.,* **69** (1997) 471-477.

Gray, K. A., Pogrebinsky, O. S., Mrachko, G. T., Xi, L., Moticello, D. J., and Squires, C. H. Molecular mechanisms of biocatalytic desulfurization of fossil fuels. *Nature Biotechnol.,* **14** (1996) 1705-1709.

Gray, K.A., Marchco, G.T. and Squires, CH.H. Biodesulfurization of fossil fuels. *J. Curr. Opin. Microbiol.,* **6** (2003) 229-235.

Grigoriev, P. Unified carrier-channel model of ion transfer across lipid bilayer membranes. *J. Biol. Phys. Chem.,* **2** (2002) 77-79.

Grossman, M.J., Lee, M.K., Prince, R.C., Garrett, K.K., George, G.N. and Pickering, I.J. Microbial desulfurization of a crude oil middle-distillate fraction: analysis of the extent of sulfur removal and the effect of removal on remaining sulfur. *Appl. Environ. Microbiol.,* **65** (1999) 181-188.

Guarnaccia, S.P. and Schnaar, R.L. Hepatocyte adhesion to immobilized carbohydrates. I. Sugar recognition is followed by energy-dependent strengthening. *J. Biol. Chem.,* **257** (1982) 14288-14292.

Guidelli, R., Aloisi, G., Becucci, L., Dolfi, A., Moncelli M.R. and Buoninsegni, F T. New Directions and Challenges in Electrochemistry. Bioelectrochemistry at metal/water interfaces *J. Electroanal. Chem.,* **504** (2001) 1-28.

Gupta, A. K. and Curtis, A. G. Surface modified superparamagnetic nanoparticles for drug delivery: interaction studies with human fibroblasts in culture. *J. Mater. Sci.: Mater. Med.,* **15** (2004) 493-496.

Gupta, A. K., and Gupta, M. Synthesis and surface engineering of iron oxide nanoparticles for biomedical applications. *Biomater.,* **26** (2004) 3995-4021.

Harris, L. A., Goff, J. D., Carmichael, A. Y., Riffle, J.S., Harburn, J.J., St. Pierre, T.G. and Saunders, M. Magnetite nanoparticle dispersions stabilzed with triblock copolymers. *Chem. Mater*., **15** (2003) 1367-1377.

Hartdegen, F.J., Coburn, J.M. and Roberts, R.L. Microbial desulfurization of petroleum. *Chem. Eng. Prog.,* **80** (1984) 63-67.

Haynes, C. A. and Norde, W. Globular proteins at solid/liquid interfaces. *Colloids Surf. B: Biointerfaces,* **2** (1994) 517-566.

Hirasawa, K., Ishii, Y., Kobayashi, M., Koizumi, K. and Maruhashi, K. Improvement of desulfurization activity in Rhodococcus erythropolis KA2-5-1 by genetic engineering. *Biosci. Biotech. Biochem*., **65** (2001) 239-246.

Holland, I.B. Translocation of bacterial proteins – an overview. *Biochem. Biophys. Acta*, **1694** (2004) 5-16.

Horvath, R., Pederson, H. C., Skivesen, N., Selmeczi, D. and Larsen, N. B. Monitoring of living cell attachment and spreading using reverse symmetry waveguide sensing. *Appl. Phys. Lett.,* **86** (2005).

.

Horvath, R., Voros, J., Graf, R., Fricsovszky, G., Textor, M., Lindvold, L.R. Spencer, N.D., Papp, E. Effect of patterns and inhomogeneities on the surface of waveguides used for optical waveguide lightmode spectroscopy applications. *Appl. Phys. B: Lasers Opt.,***72** (2001) 441-447.

Hyeon, T. Chemical synthesis of magnetic nanoparticles. *Chem. Commun.,* **8** (2003) 927-935.

Hug, T. S., Prenosil, J. E. and Morbidelli, M. Optical waveguide lightmode spectroscopy (OWLS) to monitor cell proliferation quantitatively. *Biotechnol. Bioeng.,* **80** (2002) 213-221.

Hulst, A.C., Tramper, J. A new technique for the production of immobilized biocatalyst in large quantities. *Enzyme Microbial Technol.,* **11** (1989) 546-556.

Kayser, K.J., Bielaga-Jones, B.A., Jackowski, K., Odusan, O. and Kilbane, J.J. Utilization of organosulfur compounds by axenic and mixed cultures of *Rhodococcus rhodochrous* IGTS8. *J. Gen. Microbiol.*, **139** (1993) 3123-3129.

Keaveney, T., Ultra low sulfur diesel update. (2008), available at: http://www.northeastdiesel.org/pdf/nhriworkshops08/ULSD-Update-Sprague-Energy.pdf (accessed 10th July 2008).

Kertesz, M.A. and Wietek C. Desulfurization and desulfonation: applications of sulfurcontrolled gene expression in bacteria. *Appl. Microbiol. Biotechnol.*, **57** (2001) 460-466.

Kiessling V, Tamm LK. Measuring distances in supported bilayers by fluorescence interference-contrast microscopy: polymer supports and SNARE proteins. *Biophys. J.*, **84** (2003) 408-418.

Kilbane, J.J. Microbial biocatalyst development to upgrade fossil fuels, *Curr. Opin. Microbiol.*, **17** (2006) 305-314.

Kilbane, J.J. and Bielaga, B.A. Toward sulfur-free fuels. *Chemtech.* **20** (1990) 747-751.

Kilbaine, J.J. and Jackowski, K. Biodesulfurization of Water-Soluble Coal-Derived Material by *Rhodococcus rhodochous* IGTS8. *Biotechnol. Bioeng.*, **40** (1992) 1107-1114.

Kilbane, J.J. Sulfur-specific microbial metabolism of organic compounds. *Resource Conservation Recycling,* **3** (1990) 69-79.

Kim, D. K., Zhang, Y., Viot, W., Rao, K. V. and Muhammed. M. *J. Magn. Magn. Mater.,* **225** (2001) 30-36.

Kirimura, K., Furuya, T., Sato, R., Ishii, Y., Kino, K. and Usami S. Biodesulfurization of naphthothiophene and benzothiophene through selective cleavage of carbon-sulfur bonds by Rhodococcus sp. Strain WU-K2R. *Appl. Environ. Microbiol.*, **68** (2002) 3867-3872.

Kirshenbaum I. Bacteriological desulfurization of petroleum. (1961) US Patent 2,975,103.

Kobayashi, M., Horiuchi, K., Yoshikawa, O., Hirasawa, K., Ishii, Y., Fujino, K., Sugiyama, H. and Maruhashi, K. Kinetic analysis of microbial desulfurization of model and light gas oil containing multiple alkyl dibenzothiophenes. *Biosci. Biotech. Biochem.,* **65** (2001) 298-304.

Kobayashi, M., Onaka, T., Ishii, Y., Konishi, J., Takaki, M., Okada, H., Ohta, Y., Koizumi, K. and Suzuki M. Desulfurization of alkylated froms of both dibenzothiophene and benzothiophene by a single bacterial strain. *FEMS Microbiol. Lett.*, **187** (2000) 123-126.

Kodama, K., Umehara, K., Shimizu, K., Nakatanni, S., Minuda, Y. and Yamad, K. Identification of microbial products from dibenzothiophene and its proposed oxidation pathway. *Agr. Biol. Chem.,* **37** (1973) 45-50.

Krekeler, C., Ziehr, H. and Klein, J. Physical methods for characterization of microbial cell surfaces. *Experientia,* **45** (1989) 1047-1054.

Krishna, S. Biodesulphurization of fuels : A tool for petroleum and oil industry. *AIBA Newsletter,* **8** (2001) 1-3.

Kurrat, R., Ramsden, J.J. and Prenosil, J.E. Kinetic model for serum albumin adsorption: experimental verification. *J. Chem. Soc. Faraday Trans.,* **90** (1994) 587-590.

Kurrat, R., Presonil, J. E. and Ramsden, J. J. Kinetics of human and bovine serum albumin adsorption at silica-titania surfaces. *J. Colloid Interface Sci.*, **185** (1997) 1-8.

Kurrat, R., Walivaara, A., Marti, B., Textor, M., Tengvall, P., Ramsden, J. J., and Spencer, N. D. Plasma protein adsorption on titanium: comparative in situ studies using optical waveguide lightmode spectroscopy and ellipsometry. *Colloids and Surfaces,* **11** (1998) 187-201.

Labana, S., Pandey, G. and Jain, R.K. Desulfurization of dibenzothiophene and diesel oils by bacteria. *Lett. Appl. Microbiol*., **40** (2005) 159-163.

Lachlan C.W., MacLean I., Raul E. Martinez, David A. Experimental studies of bacteria–iodide adsorption interactions. *Chem. Geol*., **212** (2004) 229-238.

Larkin, M.J., Kulakov L.A. and Allen, C.C. Biodegradation and *Rhodococcus* — masters of catabolic versatility*, Curr. Opin. Biotechnol.,* **16** (2005) 282-290.

Lasic, D.D. Novel applications of liposomes. *Trends Biotechnol.,* **16** (1998) 307-321.

Lavalle, G., Gergely, A., Lustig, and V. Ball. Critical analysis of the apoferritin adsorption at solid-liquid interfaces in the framework of a particular adsorption model. *J. Chem. Phys*., **113**(2000) 8212-8224.

Lee, K. and Levy, E.M. Bioremediation: Waxy Crude Oils Stranded on Low-Energy Shorelines. In: Proceedings of The 1991 Oil Spill Conference. *American Petroleum Institute,* Washington D. C (1991).

Lee, M.K., Senius, J.D. and Grossman, M.J. Sulfur-specific microbial desulfurization of sterically hindered analogs of dibenzothiophene. *Appl. Environ. Microbiol*., **61** (1995) 4362-4366.

Li, H., Rosario, A. C., Davis, S. V., Glass, T., Holland, T. V., Davis, R. M., Lesko, J. J., Riffle J. S., and Florio, J. Network formation of vinylester-styrene composite matrix resins. *J. Adv. Mater.,* **28** (1997) 55-62.

Li, M.Z., Squires, C.H., Monticello, D.J. and Childs, J.D. Genetic analysis of the dsz promoter and associated regulatory regions of Rhodococcus erythropolis strain IGTS8. *J. Bacteriol.,* **178** (1996) 6409-6418.

Li, S-Y., Ramsden, J. J., Prenosil, J. E., and Heinzle, E. Measurement of adhesion and spreding kinetics of baby hamster kidney and hybridoma cells using an integrated optical method. *Biotechnol. Prog.,* **10** (1994) 520-524.

Li, Q.L., Li, H.L., Pol, V.G., Bruckental, I., Koltypin, Y., Nowik, I., Calderón-Moreno, J.M., and Gedanken, A. Sonochemical synthesis, structural and magnetic properties of air-stable Fe/Co alloy nanoparticles. *New J. Chem.,* **27** (2003) 1194-1199.

Li, G. Q., Ma, T., Li, S. S., Li, H., Liang, F. L. and Liu, R. L. Improvement of dibenzothiophene desulfurization activity by removing the gene overlap in the dsz operon. *Biosci. Biotechnol. Biochem*., **71** (2007) 849-854.

Liong, S. A multifunctional approach to development, fabrication, and characterization of Fe_3O_4 composites. (2005) PhD Thesis, Georgia Institute of Technology.

Lu, A.H., Salabas, E. L. and Schult, F. Magnetic nanoparticles: synthesis, protechtion, functionalization, and application. *Angew. Chem. Int. Ed.,* **46** (2007) 1222-1244.

Lu, A.-H., Schmidt, W., Matoussevitch, N., Pnnermann, H., BSpliethoff, B., Tesche, B., Bill, E., Kiefer, W., SchVth, F. *Angew. Chem. Int. Ed.*, **43** (2004) 4303-4305.

Luo, R.G., Sirkar, K.K. Method and apparatus for isolation purification of biomolecules. (2000) US Patent 6,022,477.

Luo, M. F., Xing, J. M., Gou, Z. X., Li, S., Liu, H. Z. and Chen., J. Y. Desulfurization of dibenzothiophene by lyophilized cells of Pseudomonas delafieldii R-8 in the presence of dodecane. *Biochem. Eng. J.,* **13** (2003) 1-6.

Ma, T., Li, G., Li, J., Liang, F. & Liu, R. Desulfurization of dibenzothiophene by Bacillus subtilis recombinants carrying dszABC and dszD genes. *Biotechnol. Lett.,* **28** (2006) 1095-1100.

Maghsoudi, S., Kheirolomoom, A., Vossoughi, M., Tanaka, E. and Katoh, S. Selective desulfurization of dibenzothiophene by newly isolated *Corynebacterium* sp. Strain P32C1. *Biochem. Eng. J.,* **5** (2000) 11-16.

Malik KA. Microbial removal of organic sulfur from crude oil and the environment: some new prospectives. *Process Biochem.,* **13** (1980) 10-2.

Maliyantz, A. A., Bakteriologische Methode der Entschwefelung von Erdel. *Azerbaidzhanskoe Neftyanoe Khoz.,* **6** (1935) 89-93.

Malmsten, M., Biopolymers at Interfaces, Revised and Expanded. New York: Marcel Dekker (2003).

Marcelis, C.L.M. Anaerobic biodesulfurization of thiophenes. PhD Thesis, University of Wageningen (2003).

Marshall, K. C. and Rogers, F.J. Interaction between colloidal montmorillonite and cells of Rhizobium sp. with different inorganic surfaces. *Biochim. Biophys. Acta,* **198** (1941) 410-422.

Marshall, K. C. Mechanism of the initial events in the sorption of marine bacteria to surfaces. *Biochim. Biophys. Acta,* **156** (1948)179-184.

Marshall, K. C. Mechanisms of bacterial adhesion at solid water interfaces. New York: Plenum Press (1985) pp. 133-161.

Máté, M. and Ramsden, J. J. Addition of particles of alternating charge. *J. Chem. Soc. Faraday Trans.,* **94** (1998) 2813-2816.

Matsubara, T., Ohshiro, T., Nishina, Y. & Izumi, Y. Purification, characterization, and overexpression of flavin reductase involved in dibenzothiophene desulfurization by Rhodococcus erythropolis D-1. *Appl. Environ. Microbiol.,* **67** (2001) 1179-1184.

Matsui, T., Hirasawa, K., Konishi, J., Tanaka, Y., Maruhashi, K. and Kurane, R. Microbial desulfurization of alkylated dibenzothiophene and alkylated benzothiophene by recombinant Rhodococcus sp. strain T09. *Appl. Microbiol. Biotechnol.,* **56** (2001) 196-200.

Matsui, T., Onaka, T., Tanaka, Y., Tezuka, T., Suzuki, M. and Kurane, R. Alkylated benzothiophene desulfurization by Rhodococcus sp. Strain T09. *Biosci. Biotechnol. Biochem.,* **64** (2000) 596-599.

McFarland, B.L. Biodesulfurization. *J. Curr. Opin. Microbiol.*, **2** (1999) 257-264.

Mc Farland, B.L., Boron, D.J., Deever, W., Meyer, J.A., Johnson, A.R. and Atlas, R.M. Biocatalytic sulfur removal from fuels: applicability for producing low sulfur gasoline. *Crit. Rev. Microbiol.,* **24** (1998) 99-147.

McColl, J., Horvath, R., Aref, A., Larcombe, L., Morgan, S., Chianella, I., Yakubov, G., and Ramsden, J. Polyphenol control of cell spreading on glycoprotein substrates. *J. Biomater. Sci., Polym Ed*., **20** (2009) 841-51.

Melo, L.F., Bott, T. R., Fletcher, M., Capdeville (ed), B. Biofilms – Science and Technology, *Dordrecht Kluwer Academic* (1992).

Meza, M. Application of magnetic particles in immunoassays. *Scientific and Clinical Appl. Magn. Carriers*, Ch. 22 eds Häfeli E., et al., New York: Plenum Press (1997) pp. 303-309.

Mohebali, G., Ball, A. S. Biocatalytic desulfurization (BDS) of petrodiesel fuels. *Microbiol.,* **154** (2008) 2169-2183.

Moller, W., Nemoto, I. and Heyder, J. Effect of magnetic beads aggromeration on cytomagnetometric measurements. *IEEE Transactions on Nanobioscience,* **2** (2003) 247-254.

Monticello, D.J. Biodesulfurization and the upgrading of petroleum distillates. *Curr. Opin. Biotechnol.*, **11** (2000) 540-546.

Monticello, D.J., Bakker, D. and Finnerty, W.R. Plasmid-mediated degradation of dibenzothiophene by *Pseudomonas* species, *Appl. Environ. Microbiol.,* **49** (1985) 756-760.

Monticello, D.J. Continuous process for biologic desulfurization of sulfur-bearing heterocyclic molecules. Energy BioSystem Corporation, The Woodlands, Texas: US Patent (1995) 5,472,875.

Monticello, D.J. Riding the fossil fuel biodesulfurization wave. *Chemtech.,* **28** (1998) 38 - 45.

Mornet, S. Vasseur, S., Grasset, F., Verveka, P., Goglio, G., Demourgues, A. Portier, J., Pollert, E. and Duguet, E. Prog. *Solid State Chem*., **34** (2006) 237-247.

Morrish, A. H. and Yu, S. P. Magnetic measurements on individual microscopic ferrite particles near the single-domain. *Phys. Rev*., **102** (1956) 670-673.

Mueller, P., Rudin, D.O., Tien, H. and Wescott, W. Reconstitution of cell membrane structure in vitro and its transformation into an excitable system. *Nature,* **194** (1962) 979-980.

Naito, M., Kawamoto, T., Fujino, K., Kobayashi, M., Maruhashi, K. and Tanaka A. Long-term repeated biodesulfurization by immobilized Rhodococcus erythropolis KA2-5-1 cells. *Appl. Microbiol. Biotechnol.*, **55** (2001) 374–378.

Naser, W., CEO Energy biosystems corporation the woodlands, texas before the senate environment and public works subcommittee on clean air, wetlands, private property and nuclear safety, (1999).
http://epw.senate.gov/107th/nas_5-18.htm

Neuberger, T., Schopf, B., Hofman, H., Hofman, M. and Rechenberg, B. Superparamagnetic nanoparticles for biomedical applications: Possibilities and limitations of a new drug delivery system. *J. Magn. Magn. Mater.,* **293** (2005) 483-496.

Ohshiro, T., and Y. Izumi. Microbial desulfurization of organic sulfur compounds in petroleum. *Biosci. Biotechnol. Biochem.,* **63** (1999) 1-9.

Olsvik, O., Popovic, T., Skjerve, E., Cudjoe, K.S., Horns, E., Ugelstad, J. and Uhlen, M. Magnetic separation techniques in diagnostic microbiology. *Clin. Microbial. Rev.,* 7 (1994) 43-54.

Omori, T., Monna, L., Saiki, Y. and Kodama, T. Desulfurization of dibenzothiophene by Corynebacterium sp. Strain SY1 *Appl. Environ. Microbiol.,* **58** (1992) 911-915.

Pakula, R., and A. Freeman. A new continuous biofilm bioreactor for immobilized, oil degrading filamentous fungi. *Biotechnol. Bioeng.,* **49** (1996) 20-25.

Pankhurst, Q. A., Connolly, J., Jones, J, S. K. and Dobson, J. Applications of magnetic nanoparticles in biomedicine. *J. Phys. D: Appl. Phys*., **36** (2003) 167-181.

Papazoglou, E. S., Parthasarathy, A. Bionanotechnology. 1th edn. London: Morgan & Claypool, (2007).

Park, J. N., An, K., Hwang, Y., Park, J.-G., Noh, H.-J., Kim, J.-Y., Park, J.-H., Hwang, N.-M. and Hyeon, T. Ultra-large-scale syntheses of monodisperse nanocrystals. *Nature Materials,* **3** (2004) 381-385.

Patel, S.B., Kilbane, J.J. and Webster, D.A. Biodesulphurisation of dibenzothiophene in hydrophobic media by Rhodococcus sp strain IGTS8. *J. Chem. Technol. Biotechnol.,* **69** (1997) 100-106.

Pellegrino, T., Manna, L., Kudera, S., Liedl, T., Koktysh, D., Rogach, A. L., Keller, S., Radler, J., Natile, G., and Parak, W. J. *Nano Lett*., **4** (2004) 703-707.

Phillips, R., Purohit, P. K. and Kondev, J. Mechanics of Biological Nanotechnology. Springer Berlin: Heidelberg (2006) pp. 693-729.

Pivnick, H. *Pseudomonas rubescens*, a new species from soluble oil emulsions. *J. Bacteriology,* **70** (1955) 1-6.

Potyrailo, R.A., Hobbs, S.E., Hieftje, G.M.Optical waveguide sensors in analytical chemistry: today’s instrumentation, applications and trends for future development. *Fresen. J. Anal. Chem*., **362** (1998) 349-373.

Prayuenyong, P. Biodesulphurization, (2001) Thesis, Cranfield University.

Prestvik, W. S., Berge, Mork, P.C., Stenstad, P.M. and Ugelstad, J. Preparation and application of monosized magnetic particles in selective cell separation. In: Häfeli U., Schütt W., Teller J., Zborowski M. (Eds.), Scientific and Clinical Applications of Magnetic Carriers. New York, Plenum Press (1997) pp. 11-36.

Pankhurst, Q. A., Connolly, J., Jones, S. K. and Dobson, J. Applications of magnetic nanoparticles in biomedicine. *J. Phys.,* **36** (2003) 167-181.

Purrucker, O., Hillebrandt, H., Adlkofer, K. and Tanaka, M. Deposition of highly resistive lipid bilayer on silicon - silicon dioxide electrode and incorporation of gramicidin studied by AC impedance spectroscopy. *Eletrochim., Acta* **47** (2001) 791-798.

Raguse, B., Braach-Maksvytis, V., Cornell, B.A., King, L.G., Osman, P.D.J.,Pace, R.J. Wieczorek, L., Tethered lipid bilayer membranes: formation and ionic reservoir characterization. Langmuir, **14** (1998) 648-659.

Rajendran, M., Pullar, R. C., Bhattacharya, A. K., Das, D., Chintalapudi, S. N. and Majumdar, C.K. Magnetic properties of nanocrystalline $CoFe_2O_4$ powders prepared at room temperature: variation with crystallite size. *J. Magn. Magn. Mater*., **232** (2001) 71-83.

Rall, H. T., Thompson, C. J., Coleman, H. J. and Hopkins, R. L. Sulfur compounds in crude oil. Bulletin 659, U.S. Dept Interior, Bureau of Mines. (1972).

Ramsden, J.J. Experimental methods for investigating protein adsorption kinetics at surfaces. Q. Rev. Biophys., **27** (1993) 41-105.

Ramsden, J. J. Porosity of Pyrolyzed Sol-Gel Wave-Guides. *J. Mater. Chem.,* **4** (1994a) 1263-1265.

Ramsden, J. J., Li, S. Y., Prenosil, J. E. And Heinzle, E. Kinetics of adhesion and spreading of animal cells. *Biotechnol. Bioeng.,* **43** (1994b) 939-945.

Ramsden, J. J. Dynamics of protein adsorption at the solid/liquid interface. *Recent Res. Dev. Phys. Chem.,* **1** (1997) 133-142.

Ramsden, J.J. and Máté, M., Kinetics of monolayer particle deposition. *J. Chem. Soc., Faraday T rans.,* **94** (1998), 783-788.

Ramsden, J.J., OWLS: A versatile technique for sensing with bioarrays. *Chimia,* **53** (1999) 67-71.

Ramsden, J.J. What is nanotechnology? *Nanotechnol. Percep.,* **1** (2005a) 3-17.

Ramsden, J.J., Li, S.Y., Heinzle, J.E., Prenosil, Optical method for measurement of number and shape of attached cell in real time. *Cytometry,* **19** (1995b) 97-102.

Ricci, S. M., Talbot, J., Tarjus, G. and Viot, P. Random sequential adsorption of anisotropic particles. II. Low coverage kinetics. *J. Chem. Phys*., **97** (1992) 5219-5228.

Rodriguez, V., Busscher, H. J., Norde, W., De Vries, J. and Van der Mei, H. C. On relations between microscopic and macroscopic physicochemical properties of bacterial cell surfaces: an AFM study on *Streptococcus mitis* strains. *Langmuir,* **19** (2003) 2372-2377.

Ruiz, N., Kahne, D. and Silhavy, T.J. Advances in understanding bacterial outer-membrane biogenesis. *Nature Rev. Microbiol.,* **4** (2006) 57–66.

Safarik, I. and Safarikova, M., Magnetic nanoparticles and biosciences. *Monatshefte fuer chemie,* **133** (2002)737-759.

Schmidt, H. Nanoparticles by chemical synthesis, processing to materials and innovative applications. *Appl. Organometal. Chem.*, **15** (2001) 331-343.

Schulz, H., Bohringer, W., Ousmanov, F. and Waller, P., Refractory sulfur compounds in gas oils. *Fuel Process. Technol.*, **61** (1999) 5-41.

Setti, L., Farinelli, P., Di Martino, S., Frassinetti, S., Lanzarini, G. and Pifferi, P. Developments in destructive and non-destructive pathways for selective desulfurizations in oil biorefining processes. *Appl. Microbiol. Biotechnol***.,** **52** (1999) 111–117.

Shafi, R. and Hutchings, G.J. Hydrodesulfurization of hindered dibenzothiophenes: an overview. *Catal. Today***,** **59** (2000) 423-442.

Shah, P.S., Hanrath, T., Johnston, K.P. and Korgel, B.A. Nanocrystal and nanowire synthesis and dispersibility in supercritical fluids *J. Phys. Chem.,* B **108** (2004) 9574-9587.

Shennan, J.L. Microbial attack on sulphur-containing hydrocarbons: Implications for the biodesulphurisation of oils and coals. *J. Chem. Technol. Biotechnol.,* **67** (1996) 109-123.

Shi, Y., Superparamagnetic nanoparticles for magnetic resonance imaging (MRI) diagnosis. (2006) PhD Thesis, University of South Australia.

Singh, A., Magnetic Nanoparticles fabrication, analysis and application. (2006). http://www.engr.sjsu.edu/MatE297/Singh_Magnetic_NanoPaticles.doc

Slaten, L. E. Precipitation of dispersed fine-particle magnetite. *J. Appl. Phys.*, **31** (1960) 74-75.

Solano, S.F., Marchal, R., Ropars, M., Lebeault, J., Vandecasteele, J. Biodegradation of gasoline: kinetics, mass balance and fate of individual hydrocarbons. *J. Appl. Microbiol.*, **86** (1999) 1008-1016.

Somasundaran, P. (Editor) Surface and colloid science. New York: Taylor & Francis, (2006).

Speight, J. G. Handbook of Petroleum Product Analysis. Hoboken: Wiley, (2002).

Squires, C. H., Ji, W., Xi, L., Ortego, B. C., Pogrebinsky, O. C., Gray, K. A. & Childs, J. D. Method of desulfurization of fossil fuel with flavoprotein. (1999) US Patent 5,985, 650.

Stenberg, F., Chovanec, P., Maslen, S.L., Robinson, C.V., Ilag, L.L., von Heijne, G. and Daley, D.O. Protein complexes of the *Escherichia coli* envelopes. *J. Biol. Chem.*, **41** (2005) 34409-34419.

Stumm, W. and Morgan, J. J. Aquatic Chemistry, 3rd Ed. New York: Wiley, (1996).

Sun, S., Zeng, H., Robinson, D. B., Raoux, S., Rice, P. M., Wang, S. X. and Li, G. Monodisperse MFe_2O_4 (M = Fe, Co, Mn) nanoparticles *J. Am. Chemi. Soc.*, **126** (2003) 273-279.

Swallow, K.C., Shrifin, N.S., and Doherty, P.J. Hazardous organic compound analysis. *Environ. Sci. Technol.*, **22** (1988)136-142.

Takafuji, M., Ide, S., Ihara, H. and Xu, Z. Preparation of poly(1-vinylimidazole)-grafted magnetic nanoparticles and their application for removal of metal ions. *Chem. Mater.*, **16** (2004) 1977-1983.

Tang, B. Z., Geng, Y. H., Lam, J. W. Y., Li, B. S., Jing, X. B., Wang, X. H., Wang, F. S., Pakhomov, A. B., and Zhang, X. X. Processible nanostructured materials with electrical conductivity and magnetic susceptibility:preparation and properties of maghemite/polyaniline nanocomposite films. *Chem. Mater.*, **11** (1999) 1581-1589.

Taylor, J. M. New dimensions for manufacturing a UK Strategy for nanotechnology. *Report of the UK Advisory Group on Nanotechnology Applications*, (2002) http://www.innovateuk.org/_assets/pdf/taylor%20report.pdf

Tiefenthaler, K., and W. Lukosz. Sensitivity of grating couplers as integrated-optical chemical sensors. *J. Opt. Soc. Am.*, **B6** (1989) 209-220.

Tien, P. K. Integrated optics and new wave phenomena in optical waveguides. *Rev. Mod. Phys.,* **49** (1977) 361-420.

Tien, H.T. and Ottova-Leitmannova, A., eds. Planar Lipid Bilayers (BLMs) and Their Applications. Amsterdam: Elsevier, (2003).

Tsai, T-H. and You, H-Y. Necrotizing fasciitis caused by *Shewanella putrefaciens* in a uremic patient. *J. Microbiol. Immunol. Infect.,* **39** (2006) 516-518.

Ulman, A,, Fitzpatrick, L.E., Characterization of Organic Thin Films. Greenwich: Manning Publications Co., (1996).

Van Afferden, van M., Schacht, S., Klein, J., Trüper, H.G. Degradation of dibenzothiophene by *Brevibacterium* sp. DO. *Arch. Microbiol.,* **153** (1990) 324-328.

Van Hamme, J.D., Singh, A. and Ward, O.P. Recent advances in petroleum microbiology. *Microbiol. Mol. Biol. Rev.,***67** (2003) 503-549.

Vestal, C.R. and Zhang, Z.J. Synthesis and magnetic characterization of Mn and Co spinel Ferrite-Silica nanoparticles with tunable magnetic core. *Nano Lett.,* **3** (2003) 1739-1743.

Vijaykumar, R., Yu Koltypin, Felner, I., Gedanken. A., Sonochemical synthesis and characterization of pure nanometer-sized Fe_3O_4 particles. *Mat. Sci. Eng. A.,* **286** (2001) 101.

Wang, Z., FingasI, M. and Page, D.S. Oil spill identification. *J. Chromatography*, **843** (1999) 369-411.

Watanabe, K., Noda, K. and Maruhashi, K. Enhanced desulfurization in a transposon-mutation strain of *Rhodococcus erythropolis*. *Biotechnol. Lett.*, **25** (2003) 1299-1304.

Weisman, W. Analysis of petroleum hydrocarbons in environmental media. Total Petroleum Hydrocarbon Criteria Working Group Series, (1998) pp. 1-50.

Welo, L.A. and Baudisch, O. The two-stage transformaiton of magnetite into hematite. *Philos. Mag.*, **50** (1925) 399- 408.

Wilborn, D., R., Goodman, T., G. and Bleiwas, D., I. Technological Advancement - A Factor in Increasing Resource Use. *U.S. Geological Survey Open-File Report*, (2005) pp. 1-197.

Willard, M. A., Kulrihara, L. K., Carpenter, E. E., Calvin, S., and Harris, V.G. Chemically prepared magnetic nanoparticles. *Int. Mater. Rev*., **49** (2004) 3-4.

Worrell, E. and Galitsky, Ch. Energy efficiency improvement and cost saving opportunities for petroleum refineries. LBNL-56183 (2005). http://www.energystar.gov/ia/business/industry/ES_Petroleum_Energy_Guide.pdf

Wu, X. Y., Liu, H. J., Liu, J. Q., Haley, K. N., Treadway, J. A., Larson, J. P., Ge, N., Peale, N. F. and Bruchez, M. P. *Nature Biotechnol*., **21** (2003) 41-46.

Yang, J., Gunn, J., Dave, Sh. R., Zhang, M., Wang, Y. A. and Gao, X. Ultrasensitive detection and molecular imaging with magnetic nanoparticles. *Analyst*, **133** (2008) 154-160.

Yang, J.Z. and Marison, I.W. Two-stage process design for the biodesulfurization of a model diesel by a newly isolated *Rhodococcus globerulus* DAQ3, *Biochem. Eng. J.*, **27** (2005) 77-82.

Yang, S., Albayrak, N. Immobilization of enzyme on a fibrous matrix. (2006) US Patent 102004035803 (2007)

Yeh CS, Cheng FY, Shieh DB, Wu CL. Method for preparation of water-soluble and dispersed iron oxide nanoparticles and application thereof. German Patent 271,593 (2004).

Yeong II Kim, Don Kim, and Choong Sub Lee. Synthesis and characterization of CoFe2O4 magnetic nanoparticles prepared by temperature-controlled coprecipitation method. *Physica B.*, **337** (2003) 42-51.

Zhang, X.Y., Chen, Y.J., Fan, L.N. and Li, Z,Y. Enhancement of low-field magnetoresistance in Fe3O4 particles induced by ball milling. *Solid State Comm.,* **137** (2006) 673-677.

Zhang, L., Dong, Y., Wang, M. and Shi, S. Biodesulfurization of dibenzothiophene and other organic sulfur compound by newly isolated *Micobacterium* strain ZD-M2. *FEMS Microbiol. Lett.,* **247** (2005) 45-50.

Zhang, Y., Kohler, N. and Zhang, M. Surface modi.cation of superparamagnetic magnetite nanoparticles and their intracellular uptake. *Biomaterials,* **23** (2002) 1553-1561.

Zharov, V. P., Kim, J.-W., Curiel, D. T., and Everts, M. Self-assembling nanoclusters in living systems: application for integrated photothermal nanodiagnostics and nanotherapy. *Nanomedical,* **1** (2005) 326-345.